



$\text{div}_2$	two-dimensional divergence $= \frac{\partial}{\partial x} \frac{\partial \cos \phi}{\partial \lambda} + \frac{\partial}{\partial y} \frac{\partial \cos \phi}{\partial \phi}$	$u$	atmosphere, oceans zonal wind component (positive if eastward, called westerlies; negative if westward, called easterlies)
$dm$	mass element $= dx dy \frac{dp}{g} = R \cos \phi d\lambda R d\phi \frac{dp}{g}$	$u_g$	geostrophic part of zonal wind component
$\frac{dp}{g}$	mass element per unit area $= -\rho dz$	$v$	meridional wind component (positive if northward, called southerlies; negative if southward, called northerlies)
$dV$	volume element $= dx dy dz$	$u_g, v_{ag}$	geostrophic, ageostrophic part of meridional wind component
$e$	rate of evaporation	$\mathbf{v}$	two-dimensional wind vector $= (u, v)$
$E$	total energy per unit mass $= c_v T + gz + Lq + \frac{1}{2}(u^2 + v^2)$ or surface evaporation rate	$w$	vertical wind component
$f$	Coriolis parameter $= 2\Omega \sin \phi$	$\mathbf{W}$	vertically integrated transport of water vapor
$F$	frictional force $= (F_\lambda, F_\phi)$	$z$	geopotential height
$F_{BA}$	flux of energy at earth's surface (positive if downward)	$z_E, z_W$	geopotential height at east, west sides of a mountain range
$F_{TA}$	net flux of radiation at top of the atmosphere (positive if downward)	$z_{SA}$	geopotential height in NMC standard atmosphere
$g$	acceleration due to gravity	$\alpha$	specific volume
$G(A)$	generation rate of $A$	$\gamma$	measure of static stability in atmosphere
$IE$	internal energy per unit mass	$\Theta$	potential temperature
$J_q$	energy flux by radiation, pressure work, and subgrid scale terms $= \mathbf{F}_{rad} + p\mathbf{c} + \tau \cdot \mathbf{c}$	$\kappa$	Poisson constant $= R/c_p$
$JJA$	time period June 1 through August 31	$\lambda$	geographic longitude
$K$	horizontal kinetic energy $= K_{TE} + K_{SE} + K_M = K_E + K_M$	$\rho$	density
$K_M, K_{TE}, K_{SE}$	horizontal kinetic energy associated with zonal mean circulations, transient eddies, stationary eddies	$\sigma(A)$	standard deviation of $A$
$L$	heat of condensation	$\tau$	three-dimensional stress tensor
$M$	absolute angular momentum $= M_\Omega + M_r$	$\tau_0$	surface friction stress in the $\lambda$ direction (positive if atmosphere gains westerly momentum)
$M_\Omega, M_r$	$\Omega$ , relative angular momentum	$\phi$	geographic latitude
$p$	pressure	$\psi$	streamfunction for mass in $(\phi, p)$ plane
$p_0$	pressure at ground level (where there are no mountains $p_0 = 1012.5$ mbars)	$\psi_E$	streamfunction for energy in $(\phi, p)$ plane
$p_t$	top level of vertical integration $= 25$ mbars	$\psi_M$	streamfunction for angular momentum in $(\phi, p)$ plane
$P$	available potential energy $= P_{TE} + P_{SE} + P_M = P_E + P_M$	$\psi_q$	streamfunction for water substance in $(\phi, p)$ plane
$P_M, P_{TE}, P_{SE}$	available potential energy associated with zonal mean conditions, transient eddies, stationary eddies	$\omega$	"vertical" pressure velocity (positive if downward) $= dp/dt \approx -\rho gw$
$PE$	potential energy per unit mass	$\Omega$	angular velocity of the earth
$q$	specific humidity		
$Q$	diabatic heating rate per unit mass		
$\mathbf{r}$	position vector		
$R$	mean radius of the earth $= 6371$ km or gas constant for dry air		
$s$	entropy		
$S_A, S_O$	rate of storage of energy in atmosphere, oceans		
$t$	time		
$T$	temperature		
$T_e$	equivalent temperature		
$T_A, T_O$	total meridional energy transport in		

## Mathematic Operators

$$\bar{A} = (t_2 - t_1)^{-1} \int_{t_1}^{t_2} A dt$$

time average of  $A$ 

$$A' = A - \bar{A}$$

departure from time average of  $A$ 

$$[A] = (2\pi)^{-1} \int_0^{2\pi} A d\lambda$$

zonal average of  $A$ 

$$A^* = A - [A]$$

departure from zonal average of  $A$ 

$$\langle A \rangle = (p_0 - p_t)^{-1} \int_{p_t}^{p_0} A dp$$

mass-weighted "vertical" average of  $A$ 

$$\tilde{A} = \int_{-\pi/2}^{\pi/2} [A] \cos \phi d\phi / 2$$

global average of  $A$

## Example of Nomenclature

$\langle [\overline{v\overline{A}}] \rangle$	$= \langle [\overline{v'\overline{A}'}] \rangle + \langle [\overline{v} * \overline{A} *] \rangle + \langle [\overline{v}][\overline{A}] \rangle$
$\langle [\overline{v\overline{A}}] \rangle$	vertical average of meridional (northward) transport of $A$ due to all motions
$\langle [\overline{v'\overline{A}'}] \rangle$	vertical average of meridional transport of $A$ resulting from transient eddies
$\langle [\overline{v} * \overline{A} *] \rangle$	vertical average of meridional transport of $A$ resulting from standing eddies
$\langle [\overline{v}][\overline{A}] \rangle$	vertical average of meridional transport of $A$ resulting from mean meridional circulations

## I. INTRODUCTION

Historically, the study of the atmosphere and oceans, our human environment, together with the study of our broader celestial environment of the sun, moon, and planets provided the initial impetus to develop the field of physics. In more recent times astronomy with its new discoveries has expanded the scope of physics into its modern breadth. However, the earth sciences of meteorology and oceanography have had very little influence on modern developments, and have often been regarded as old, antiquated, and "solved" branches of physics with little intellectual challenge.

Lately, a change in view has taken place, and many physicists have become aware of the new and, in our view, exciting developments in the earth's sciences. For example, the study of simple nonlinear systems first developed by Lorenz (1963,1969) for the study of climate has created a "boom" in this field among applied mathematicians and physicists.

In the present paper we shall try to convey the challenge which questions concerning "the physics of climate" pose to the interested investigator. The climate system, composed of the atmosphere, oceans, cryosphere, lithosphere, and biosphere, forms a highly interactive, complex system with many feedbacks and a great variety of time scales in the individual components. A change in one part of a subsystem may eventually affect all other parts. Feedback processes from the slower subsystems, such as the oceans and glaciers, can initiate quasiperiodicities with a very long time scale in the faster subsystem, i.e., the atmosphere. This leads to what we may call climatic cycles and climatic change, as well as to an increase in predictability of the behavior of the atmosphere.

The systematic study of the atmosphere and oceans has become feasible mainly through the increase of *in situ* observations since World War II. In fact, global observing networks are now available in which satellites play an important role both as collectors of *in situ* data, and also as remote observing platforms in space. Equally important as the increase in data has been the development of the electronic computer, and its application to numerical weather forecasting and climate simulation, first attempt-

ed by von Neumann and his co-workers at the Institute for Advanced Study in Princeton in the early 1950s [see, for example, Smagorinsky (1983)]. The computer has enabled meteorologists to give, for the first time, quantitative forecasts based on the basic laws of physics. As envisioned by von Neumann, a remarkable evolution has taken place where now, thirty years later, numerical models with high spatial and temporal resolutions can provide reasonably accurate simulations of the average climatic conditions in the atmosphere and oceans, their seasonal climatology, their regional structure, and, to some extent, their natural year-to-year variability.

In a sense, this development comes in the nick of time. Man's impact on the local environment is evident all around us, but even globally there is strong evidence of important changes due to human activity. We may mention the measured steady rate of increase in atmospheric CO<sub>2</sub> since the beginning of the industrial revolution, and the first claims that the predicted rise in tropospheric temperature is already detectable above the "climate noise." The numerical general circulation models (GCM's) are giving us tentative answers as to what to expect for regional changes in temperature and precipitation patterns as a function of CO<sub>2</sub> concentration. In the near future, such predictions may affect national and international policy decisions regarding, for instance, the use of coal or thermonuclear fuel as alternative energy sources.

On a more academic level, the GCM's are beginning to clarify the role of geography—for example, the existence of mountains, the particular land-sea distribution, and the presence of the Antarctic and Greenland ice caps—in maintaining the present climate. Active research is also in progress on how much the circulation in the atmosphere (and thus climate) depends on external parameters, such as the rotation rate of the earth, the amount of incoming solar radiation and its seasonal variation, volcanic dust, and aerosols, and on other internal parameters, such as surface albedo, cloudiness, oceanic heat storage, and transports.

Some outstanding works have been published related to certain other aspects of the earth's climate. Among those, we should refer to the monograph *The Nature and Theory of the General Circulation of the Atmosphere* by Edward N. Lorenz (1967), now considered to be a classic, and in dealing with yet larger systems, such as the atmospheres of Jupiter and the sun, we should mention the work *Physics of Negative Viscosity Phenomena* by the late Victor P. Starr (1968).

The present paper is broken down into four major parts.

(1) The first part (Sec. II) contains a general discussion where the global climate system and its subsystems or components—the atmosphere, hydrosphere, cryosphere, lithosphere, and biosphere—are defined. We also discuss here the great variety of possible interactions and feedback loops between the various components, as well as questions concerning the uniqueness of our present climate.

(2) In the second part (Sec. III) we state the basic laws

that describe the behavior of the atmosphere on the rotating earth, proceeding from the fundamental equations of classical physics to the time-averaged and zonally averaged climate equations. Possible simplifications of the basic equations in case of the earth's atmosphere are pointed out.

(3) The third and most extensive part (Secs. IV and V) describes the observational basis for our present conception of the earth's climate. After a discussion of the character of the atmospheric, oceanic, and satellite radiation data sets available, we present, according to our perspective, a description of the "observed" climate. We have chosen to describe the system in terms of how it obeys the fundamental balance equations for radiation, mass, angular momentum, water substance, and, finally, energy. There is some mention of long-period fluctuations in the atmosphere-ocean system, but we will confine the main discussion to climatic conditions during the last 20 to 30 years.

(4) The fourth and last part (Secs. VI and VII) evaluates the theoretical basis, the structure, and present status of the various numerical models used to simulate the climate. From the hierarchy of models, ranging from one- to three-dimensional ones, we will emphasize the large-scale general circulation models of the atmosphere and oceans, since they lead to the most realistic climate simulations. The final discussion will center on the applications of GCM's in investigating the role of various physical factors in shaping climate, and in assessing the possible impact of man's activities on our climate.

## II. NATURE OF THE PROBLEM

### A. Definition of the climate system

In order to discuss the behavior of the climatic system it seems appropriate to present some general thermodynamic concepts, because they will help in putting the nature of the problem of the climate in a proper perspective.

We will define a system within the thermodynamical framework as a finite region in space specified by a set of physical variables  $x_1, x_2, \dots$ . The  $x_i$  symbolize additive or extensive properties. The variables represent, for example, the volume, internal energy, mass of individual components, and angular momentum. A composite system is a conjunction of spatially disjoint simple systems separated by conceptual or real partitions or walls. The amount of the quantity  $x_i$  for the global system is then the sum of  $x_i^\alpha$  for all subsystems, e.g.,  $x_i = \sum_\alpha x_i^\alpha$ . The set of all the quantities  $x_i$  specifies the state of the composite system.

The amount of  $x_i$  transferred from a subsystem  $\alpha$  to an adjacent subsystem  $\beta$  during a given interval of time is denoted by  $x_i^{(\alpha, \beta)}$  and represents a thermodynamic process. The net increase of  $x_i$  for the subsystem  $\alpha$  is such that

$$\Delta x_i^\alpha + \sum_\beta x_i^{(\alpha, \beta)} = \delta x_i^\alpha, \quad (2.1)$$

where  $\delta x_i$  denotes a source term. When  $x_i$  is conserved, it obeys a continuity equation

$$\Delta x_i^\alpha + \sum_\beta x_i^{(\alpha, \beta)} = 0.$$

The summation is extended to all subsystems  $\beta$  that are adjoint to subsystem  $\alpha$ . When  $x_i^{(\alpha, \beta)} \neq 0$  we will call the systems  $\alpha$  and  $\beta$  coupled or interactive by means of  $x_i$  exchange, while if  $x_i^{(\alpha, \beta)} = 0$ , the wall is said to be restrictive for  $x_i$  and the systems are uncoupled.

The systems can be classified in terms of their functions and also in terms of their internal complexity. When the boundary of the system is restrictive for all quantities, it is called an *isolated* system. When the boundary is restrictive only for matter, the system is *closed* (impermeable boundary). An *open* system is one in which the transfer of mass, for instance, is allowed. A cascading system is composed of a chain of open subsystems which are dynamically linked by a cascade of mass or energy in such a way that the output of mass or energy from one subsystem becomes the input for the next subsystem. An open subsystem can be decaying, cyclic, or haphazardly fluctuating.

The state of a system may also be specified by intensive properties which are independent of the total mass of the system and which are defined at a given point of the system and at a given instant. The intensive properties may change in time and so we may consider that they define a field in the domain of the system. As such they are not additive properties. These include temperature, pressure, densities, velocities, etc. The size of a subsystem may be characterized by a scale factor such as the volume or the mass. We will call specific quantities or densities the ratio of the amount of this quantity over the chosen scale factor. The densities are regarded as intensive properties. Besides the thermal properties we must consider the kinematic properties, such as the three-dimensional velocity field, which are also variable in time.

The climate system ( $\mathcal{S}$ ) is a composite system formed by the following five major interactive physical components: the atmosphere ( $\mathcal{A}$ ), the hydrosphere ( $\mathcal{H}$ ) or the oceans ( $\mathcal{O}$ ), the cryosphere ( $\mathcal{C}$ ), the lithosphere ( $\mathcal{L}$ ), and the biosphere ( $\mathcal{B}$ ):

$$\mathcal{S} = \mathcal{A} \cup \mathcal{H} \cup \mathcal{C} \cup \mathcal{L} \cup \mathcal{B}.$$

As shown schematically in Fig. 1, all these subsystems are open systems with a nonuniform distribution of their intensive properties—i.e., they are polythermic, etc. However, the climatic system  $\mathcal{S}$  as a whole may be regarded as a system which is closed for the exchange of matter.

The climatic system is subject to external factors that condition its global behavior. Among these external forces we must consider as a primary factor the solar radiation which provides almost all the energy that drives the climate system. Then we must take into consideration the sphericity of the earth, its rotation, and its orbital

## THE TOTAL CLIMATE SYSTEM AND ITS SUBSYSTEMS

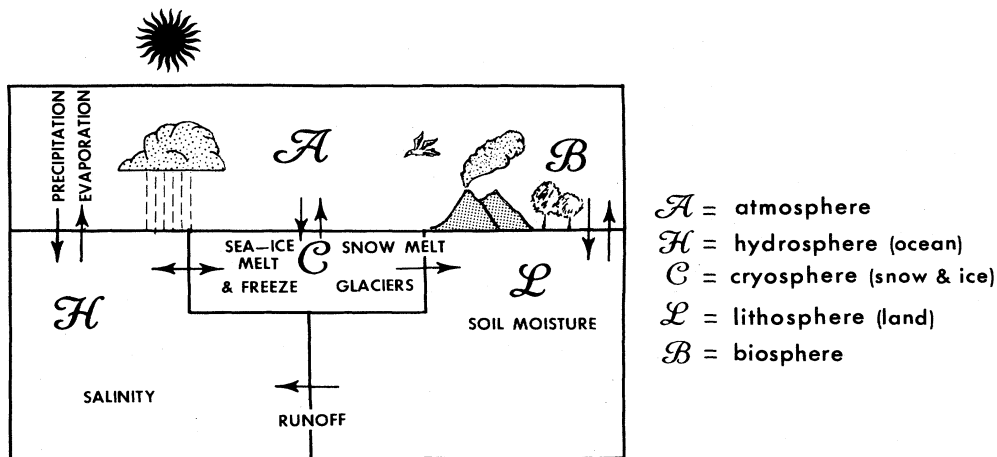


FIG. 1. Schematic diagram of the climate system.

characteristics around the sun. As a consequence, the climate system is subject to two external energy inputs, solar radiation and gravity. However, within the climate system energy occurs in a variety of forms, such as heat, potential energy, kinetic energy, chemical energy, and short- and long-wave radiation. Of all the forms of energy prevailing in the atmosphere, we may disregard the electric and magnetic energies, which are of importance only in the very high atmosphere.

The atmosphere, hydrosphere, cryosphere, lithosphere, and biosphere act as a cascading system connected by flows of energy, momentum, and matter (see also Figs. 7 and 52).

The short-wave solar radiation is unequally distributed over the various parts of the climatic system due to the sphericity of the earth, the orbital motion, and the tilt of the earth's axis. More radiation reaches and is absorbed in the intertropical regions than at polar latitudes. Taken over the globe as a whole, observations show that the system loses about the same amount of energy through infrared radiation as it gains from the incoming solar radiation. However, small, presently unmeasurable imbalances could occur for both short and long periods (Saltzman, 1977).

Due to the observed range of temperature between the equator and the poles the decrease of emitted terrestrial radiation with latitude is much less pronounced than the decrease in absorbed solar radiation, leading to a net excess of energy in the tropics and a net deficit poleward of 40° latitude. This source and sink distribution provides the basic cause for almost all thermodynamic processes occurring inside the climatic system, including the general circulations of the atmosphere and oceans.

The entropy of the incoming solar energy is lower than the entropy exported by the system through long-wave radiation. In fact, the frequency of the solar photons is much higher than the frequency of the terrestrial radiation. Furthermore, we must recognize that the solar radiation originates in a source with a temperature on the or-

der of 6000 K, whereas the terrestrial radiation is emitted at a temperature of about 250 K. Noting that

$$\Delta s = \Delta Q / T,$$

we see that the gross generation of entropy for all internal processes in the climatic system is 20–30 times larger than the amount of imported entropy.

## B. Components of the climate system

The atmosphere comprises the gaseous envelope of the earth, formed by several layers which differ with regard to composition and nature of the energy processes involved. The main layers are, starting from the surface, the troposphere, the stratosphere, the mesosphere, and the thermosphere, separated by conceptual partitions called pauses (e.g., tropopause). The composition of the atmosphere up to the mesosphere is practically uniform for nitrogen, oxygen, and the other inert gases. Among the variable components, water vapor is more predominant in the lower troposphere, and ozone in the middle stratosphere, whereas carbon dioxide, which has been increasing during historical times, is well mixed below the mesopause.

The atmosphere is the component of the climatic system most variable in time and space with a response time on the order of days to weeks. It shows a broad general circulation with less organized eddy motions, such as weather systems, in midlatitudes, and random, turbulent motions (mainly in the planetary boundary layer and near the jet streams). The dimensions of the atmosphere compared with the radius and the mass of the earth show that the atmosphere constitutes a thin viscous film of fluid which adheres to the rotating earth. Due to gravity the density is stratified, decreasing almost exponentially with height.

The hydrosphere consists of all water in the liquid phase distributed on the earth. It includes the oceans, in-

terior seas, lakes, rivers, and subterranean waters. By far the most important for climatic studies are the oceans. They absorb most of the incident solar radiation, and due to their large mass and specific heat they constitute an enormous reservoir to store energy. Due to their thermal inertia the oceans act as buffers and regulators for the temperature. Being fluids more dense than the atmosphere, the oceans have a larger mechanical inertia and a more pronounced stratification. The upper part of the ocean is the most active. It contains a mixed surface layer, with a thickness on the order of 100 m, and is separated from the bulk of the oceans below by a transition partition, the thermocline.

The oceans show much slower circulations than the atmosphere, forming large quasihorizontal circulation gyres with the familiar ocean currents and slow thermohaline overturnings. On a smaller scale the circulation also shows eddies, but turbulence is much less pronounced than in the atmosphere.

The atmosphere and oceans are strongly coupled. Interactions between them through the exchange of energy, matter, and momentum occur on many scales in space and time at their interface. For example, the exchange of water through evaporation and precipitation influences the oceanic salinity. Furthermore, there are internal interactions within each subsystem mainly when and where the gradients of their intensive properties are large. It must be stressed, however, that the oceans and the atmosphere react on a very different time scale to any given perturbation. The relaxation time for the ocean varies within a wide range that stretches from weeks or months in the upper layers to centuries or millenia in the deep ocean.

The lakes, rivers, and subterranean waters are essential elements of the terrestrial branch of the hydrological cycle, which is a crucial factor in the global climate. Furthermore, they influence the climate on a regional or local scale.

The cryosphere includes the extended ice fields of Greenland and the Antarctic, other continental glaciers and snow fields, and sea ice. The cryosphere represents the largest reservoir of fresh water in the hydrosphere. Continental snow cover and sea ice change seasonally, producing large intra-annual and sometimes interannual variations in continental heating and in the upper mixed layer of the ocean due mainly to the high value of their albedo for incoming solar radiation. Due to their lower heat conductivity the ice fields at high latitudes over the oceans act as insulators for the underlying waters, preventing the oceans from losing heat to the atmosphere.

The large continental ice sheets do not vary rapidly enough to influence the climate on a seasonal or interannual basis. However, they play a major role in climatic changes on scales of tens of thousand of years, such as the glacial and interglacial periods that have occurred during the Pleistocene. A glaciation will lower sea level considerably, possibly on the order of 100 m or more, thus changing the configuration of the continents. Due to their large mass and compactness the ice sheets develop a dynamics

of their own with very slow motions. Occasionally breakage may occur, forming icebergs.

The lithosphere includes the continents with their orography, and the bottom of the oceans. Of all the components of the climate system the lithosphere has the longest response time if one excludes the upper active layer, in which temperature and water content can vary in response to atmospheric and oceanic phenomena. For recent geological times, the lithosphere may be regarded as a permanent feature of the climatic system. There is a strong interaction of the lithosphere with the atmosphere through the transfer of mass, angular momentum, and sensible heat, as well as through the dissipation of kinetic energy in the atmospheric boundary layer. The transfer of mass occurs mainly in the form of water vapor or snow, and to a lesser extent by other particles and dust. The volcanoes throw into the atmosphere matter and energy from the lithosphere, thereby increasing the turbidity of the air, leading to spectacular sunrises and sunsets, as seen, for example, during the El Chichon eruption in spring 1982. The added particulate matter, forming what are called aerosols, has an important effect on the radiation balance of the atmosphere, and therefore on the earth's climate. Furthermore, there is a transfer of angular momentum and matter between the lithosphere and the oceans. The exchange of angular momentum is due to the torques between the oceans and the continents.

The biosphere comprises the vegetation cover, the continental fauna, and the flora and fauna of the oceans. The vegetation alters the surface roughness, surface albedo, evaporation, runoff, and field capacity of the soil. Furthermore, the biosphere influences the carbon cycle through photosynthesis and respiration. The biosphere, on the whole, is very sensitive to changes in the atmospheric climate, and it is through the signature of various life forms (fossils, tree rings, pollen, etc.) of past ages that we obtain information on paleoclimates of the earth. At this point we might mention the anthropogenic interaction with the climatic system through human activities, such as agriculture, urbanization, industry, and pollution. Albeit relatively small, the impact of human beings on climate has become important enough to draw the attention of the international community to consider measures to prevent deterioration of the environment.

### C. Interactions among the climate components

The different ranges of relaxation times for the various components of the climatic system can be seen in Fig. 2. The figure also shows the processes that may cause fluctuations in the entire climate system. Thus the whole climate system must be regarded as continuously evolving with parts of the system leading and others lagging in time. The highly nonlinear interactions between the subsystems tend to occur on many time and space scales. Therefore, the subsystems of the climate system are not always in equilibrium with each other, and not even in internal equilibrium. The subsystems have also feedback loops between them, which may amplify or attenuate a

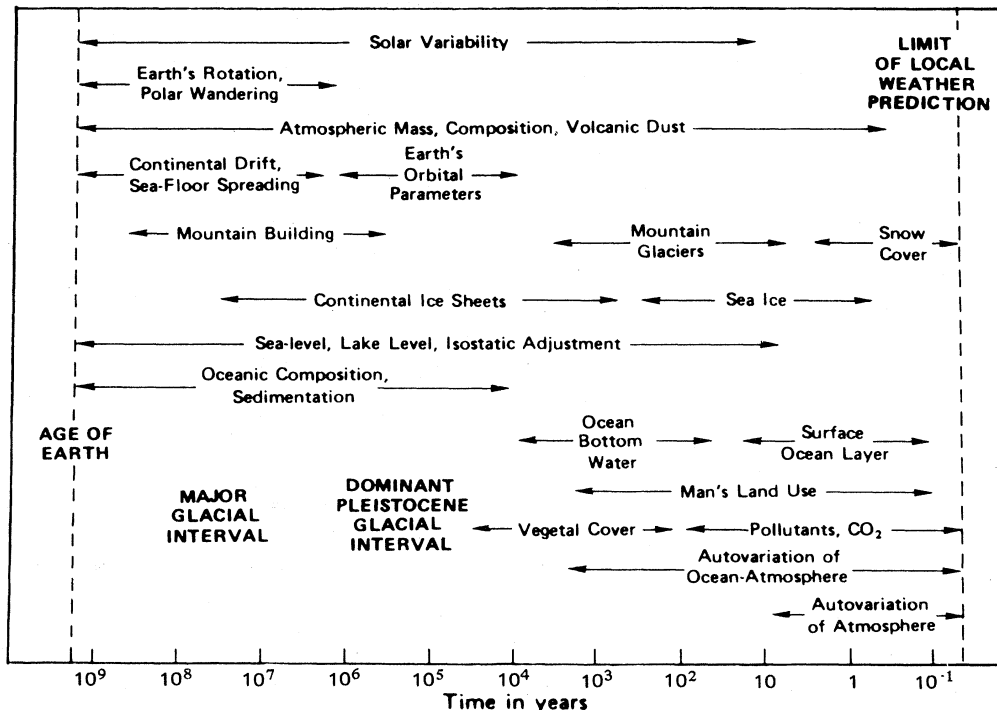


FIG. 2. Characteristic time scales for the various components of the climate system and for certain external forcing factors between  $10^{-1}$  and  $10^9$  years (from National Academy of Sciences, 1975).

perturbation corresponding to a positive or negative feedback, respectively. As an example, let us consider the interaction between the atmosphere and cryosphere. Suppose that for some reason the snow cover increases in extent. Then because of the high reflectivity (albedo) of snow, less solar energy will be available to heat the atmosphere. Thus the temperature will decrease, leading to a further increase in snow cover (a positive feedback). As an example of a negative internal feedback, let us consider the temperature of the atmosphere. If the temperature increases, the atmosphere will lose more long-wave radiation to space, thus cooling the atmosphere and attenuating the initial perturbation.

In nature there are many positive and negative feedback processes. Among them we must mention the so-called greenhouse effect that we will discuss in detail later. It must be noted that a positive feedback process cannot proceed indefinitely, because it would lead to runaway situations that have not been observed. Therefore, a compensation between positive and negative feedback processes must prevail in the mean. However, there is geological evidence (Crowley, 1983) for some catastrophic changes in the climatic state (for example, at the end of the Cretaceous and during the sudden glaciations of the Pleistocene) that could involve some runaway process in which a change to a new and different state occurred.

The interactions among the different subsystems induce modifications in each other, of course, so that they may be regarded as boundary forces. This two-way interaction becomes apparent in the case of air-sea exchange where

sea surface temperatures strongly affect the thermal structure of the atmosphere, while atmospheric wind stresses are largely responsible for generating the general circulation in the oceans. These internal effects are quite different from the external forcing mechanisms which act independently of the climatic system.

The climatic system is highly complex because (1) the atmosphere contains many scales of motion, ranging from turbulence to planetary waves, (2) the climatic subsystems are very different in physical characteristics but are nevertheless coupled through the transfers of energy, momentum, and matter on many different time and space scales, and (3) many classes of perturbations are unstable, grow rapidly, and tend to destroy the mean state. In view of these difficulties in dealing with the global system, we may select certain combinations of its components, and define a hierarchy of internal systems, considering the remaining components as the external system. Because the atmosphere is the most responsive component of the climatic system, it has been common practice in the past to reduce the climatic system to this component alone. However, due to the strong coupling between the atmosphere and the oceans, it was recognized recently that both subsystems should be considered together as a more complete internal system, i.e.,  $\mathcal{A} \cup \mathcal{O}$ .

The study of the variability of climate during the past ages requires also the cryosphere to be included in the internal climate system. This led to the definition of the internal climatic system as given by  $\mathcal{A} \cup \mathcal{O} \cup \mathcal{C}$ , considering then the influence of  $\mathcal{L}$  and  $\mathcal{B}$  as external factors.

In our paper, the main focus will be on the atmosphere and its interactions with the oceans, considering, when necessary, also the influence of the other subsystems.

#### D. The climatic state

We will try to make clear the distinction between weather and climate (Peixóto, 1977). Weather is concerned with detailed instantaneous states of the atmosphere, and the day-to-day evolution of individual synoptic systems. Basically, the study of their evolution requires solving an initial value problem. The initial values of meteorological quantities can only be prescribed at a finite number of points, while the individual motions with scales smaller than the grid scale cannot be prescribed at all. Furthermore, there are random errors in measuring the meteorological quantities, and in the interpolation and smoothing involved in analyzing the meteorological fields. Even if the dynamic equations could be solved exactly, a future predicted state will unavoidably contain errors due to these limitations in the initial conditions. Furthermore, the dynamic equations have to be adjusted before they can be transformed into difference equations and solved numerically. This will lead to a new source of limitations, such as truncation and roundoff errors.

Because of the accumulation of all these errors the predictions will degrade in time, leading to limited predictability. Thus the limits of predictability will depend on the size and nature of the initial errors, on the spatial sampling, on the type of meteorological processes and motions involved, and, finally, on the quality of the prognostic methodology. Therefore, two similar initial states of the atmosphere may lead to widely different later states not only because of the movement and development of individual weather systems but also because of the other limitations of predictability. Estimates for the limit of predictability of weather systems range between a few days (Lorenz, 1969) and two to three weeks (e.g., Leith, 1978, and Miyakoda *et al.*, 1983).

The climate is concerned not with individual weather systems but rather with an ensemble average of these internal states. It is more than an initial value problem, because we have to consider the boundary conditions which define the external forces that modulate the mean conditions. In some cases, for long time scales the internal system behaves as if it has forgotten its past, and responds mainly to the external boundary conditions. The internal climate system on these time scales seems to be almost in a state of equilibrium. In general terms we can then define climate as the ensemble average of climate states of the internal system, together with some measure of its variability for a specified interval of time and with a description of the interactions between the internal and external systems. The variability could, in principle, be separated into a deterministic part, the signal, and a random part associated with weather fluctuations, the noise, following the nomenclature used in communication theory (Leith, 1978).

Let us consider the atmosphere as the internal system. Then the interval of time must, at least, exceed the average life span of the synoptic weather systems in the atmosphere. We can then define climatic states for a month, a season, a year, a decade, and so on. The traditional thirty-year averaging interval (determined by the International Meteorological Organization) to define the climate through its mean values and the higher moments is a particular case for the atmosphere.

To further illustrate the large variability in time for the atmosphere we will present two spectra for the temperature (internal energy) and the wind speed (kinetic energy) near the earth's surface. Thus in Fig. 3 we show an idealized variance spectrum of the atmospheric temperature during its past history as evaluated by Mitchell (1976). The analysis of the spectrum shows several spikes and broader peaks. The spikes are astronomically dictated, strictly periodic components of climate variation, such as the diurnal and annual variations and their harmonics, whereas the peaks represent variations that are, according to Mitchell, either quasiperiodic or aperiodic—however, with a preferred time scale of energization. The peak at 3–7 days is associated with the synoptic disturbances mainly at middle latitudes. The slightly raised region of the spectrum at 100–400 years is associated with the “little ice age” that began near the early 17th century with rapid expansion of the mountain glaciers in Europe. The peak near 2500 years is perhaps due to the cooling observed after the “climatic optimum,” about 5000 years ago, which predominated during the great ancient civilizations. The next three peaks are related to deterministic astronomical variations of the orbital parameters of the earth, which are supposed to be responsible for the ice ages (Milankovitch, 1941): (a) the eccentricity of the orbit of the earth, with a cycle of about 100 000 years, (b) the axial precession, with a cycle of around 22 000 years, and (c) the change in the obliquity of the ecliptic or the axial tilt with a period of about 41 000 years. Finally, the peaks near 45 and 350 million years may, according to Mitchell (1976), be related to glaciations due to orogenic and tectonic effects and to continental drift.

The kinetic energy spectrum in Fig. 4 illustrates the relative importance of the various motions in the atmosphere for periods between seconds and several years. (We should mention that in contrast to the earlier presentation in Fig. 3 of the spectrum of temperature, it was found convenient to use in Fig. 4 as the ordinate scale the relative variance multiplied by the frequency in order to conserve the variance under the curve.) Most of the kinetic energy is concentrated in the low frequencies, namely, at  $10^0$ , around  $10^{-1}$ , and between  $10^{-2}$  and  $10^{-3}$  day $^{-1}$ . The first and third peaks are associated with the diurnal and annual cycles, whereas the second maximum (days-weeks) is associated with large-scale disturbances that occur in middle latitudes along the polar front. The relative maximum around  $10^3$  day $^{-1}$  is due to small-scale turbulent motions, which, combined with molecular friction, are included in the internal energy. We will not regard them as part of the kinetic energy of the circulation,



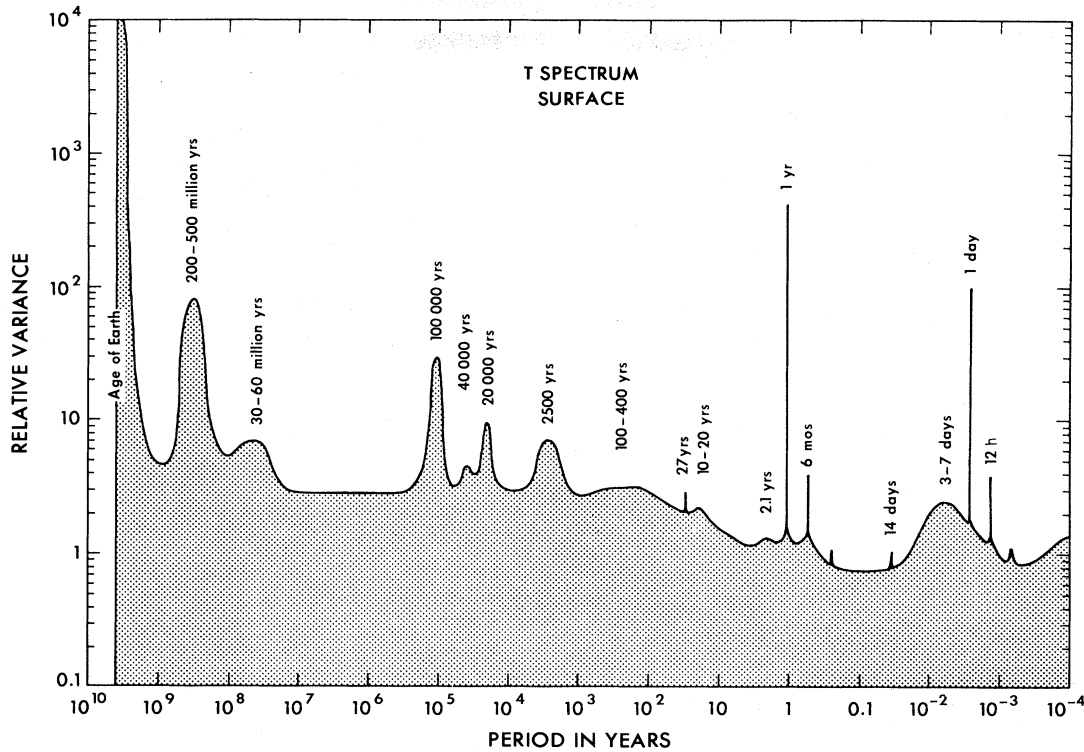


FIG. 3. Idealized, schematic spectrum of atmospheric temperature between  $10^{-4}$  and  $10^{10}$  years, from Mitchell (1976).

although they are very important in the boundary layers of the atmosphere and oceans.

Returning to our general discussion of weather and climate, we find that the physical laws that govern their evolution are basically the same. However, the applications of the equations to these problems are very different. In climate studies it is necessary to average the equations in time, and to consider not only the internal effects but

also the complex interactions between the atmosphere and its external system. For weather prediction the atmosphere behaves almost inertially, so that slowly acting boundary conditions can be ignored. For example, the fluctuations of the sea surface temperatures and snow and ice cover can be disregarded in weather forecasts up to several weeks. Nevertheless, these changes gradually affect the lower atmosphere, and become important when we want to predict the changes of the atmosphere from one month or season to another. At the other extreme, variations in the orbital parameters of the earth must be considered when climatic changes on the order of millenia are studied but are obviously negligible when considering seasonal climatic changes.

If in the integration of the basic equations all initial states lead to the same set of statistical properties, the system is said to be ergodic or transitive. If instead there are two or more different sets of statistical properties, where some initial states lead to one set while the other initial states lead to another, the system is called intransitive. If there are different sets of statistics which a transitive system may assume in its evolution from different initial states through a long, but finite, period of time, the system is called almost intransitive (Lorenz, 1969). In the transitive case, the equilibrium climatic statistics are both stable and unique, whereas in the almost-intransitive case the system in the course of its evolution will show finite periods during which distinctly different climatic regimes prevail. This may be due to internal feedbacks involving the different components of the climatic system. It is now accepted that the glacial and interglacial periods

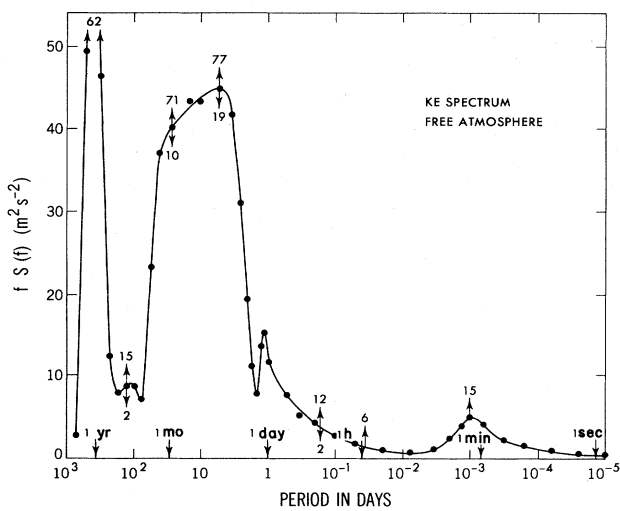


FIG. 4. Spectrum of atmospheric kinetic energy between  $10^{-5}$  and  $10^3$  days, after Vinnichenko (1970). The kinetic energy spectrum is tentative and somewhat schematic, since it is patched together using limited data from a few stations only.

in the earth's history could be manifestations of an almost-intransitive system.

### III. THE BASIC LAWS (MATHEMATICAL FORMULATION)

#### A. Basic equations

Our discussion will be organized around the governing equations of the atmosphere taken as the internal subsystem. These equations express the principles of conservation of mass, momentum (Newton's second law of motion), and energy following the approach advocated by Starr (1951). We will assume that the atmosphere behaves as a homogeneous gaseous system that obeys the ideal gas law when unsaturated. We will further assume conservation of water substance in the various phases for the entire climatic system. Thus we must include also the laws governing evaporation, condensation, and the conversion of cloud droplets into precipitation (raindrops and snow crystals). The radiation laws expressing short-wave absorption, reflection, scattering, and infrared radiative transfer will be mentioned, but we do not consider them explicitly at this point. We will take the fluid components of the climatic system as a continuum and a thermal hydrodynamic system.

#### 1. Complete system of equations

The basic hydrodynamic and thermodynamic laws may be represented by the following equations using the symbols given at the beginning of the paper:

$$\frac{d\rho}{dt} = -\rho \operatorname{div} \mathbf{c}, \quad (3.1)$$

$$\frac{d\mathbf{c}}{dt} = -2\boldsymbol{\Omega}\Lambda\mathbf{c} - (\operatorname{grad} p)/\rho + \mathbf{g} + \mathbf{F}, \quad (3.2)$$

$$c_p \frac{dT}{dt} = Q + \alpha \frac{dp}{dt}, \quad (3.3)$$

$$\frac{dq}{dt} = s(q), \quad (3.4)$$

$$p = \rho R T_e. \quad (3.5)$$

The last equation (3.5) is the equation of state for air considered as an ideal gas. The atmosphere, as any fluid, is called barotropic when the density  $\rho$  is a function of only the pressure  $p$  and otherwise it is called baroclinic. As (3.5) shows, the atmosphere is baroclinic, since, in general, the density depends on temperature as well as on pressure. It is evident that for a barotropic atmosphere, also, the temperature  $T$  is a function of  $p$  only, whereas in baroclinic atmosphere  $T$  is not given solely by the pressure. Therefore, in a barotropic atmosphere  $(\operatorname{grad} T)_{p=\text{const}} = 0$  (isothermal and isobaric surfaces are parallel to each other) and under baroclinic conditions  $(\operatorname{grad} T)_{p=\text{const}} \neq 0$  (isothermal surfaces are inclined with respect to the pressure surfaces).

The time derivatives in these equations are individual

or substantial derivatives expressing the rate of change as a point moves with the flow. Equations (3.1) and (3.2) represent the conservation of mass and Newton's second law of motion written for a frame of reference that rotates with the earth with an angular velocity  $\boldsymbol{\Omega}$ . The apparent acceleration,  $d\mathbf{c}/dt$ , where  $\mathbf{c}$  is the three-dimensional relative velocity differs from the absolute acceleration by the Coriolis term,  $2\boldsymbol{\Omega}\Lambda\mathbf{c}$ , and the centripetal acceleration  $\boldsymbol{\Omega}\Lambda(\boldsymbol{\Omega}\Lambda\mathbf{r})$ . The rotation of the system is then accounted for in Eq. (3.2) by the introduction of the "apparent" Coriolis force,  $-2\boldsymbol{\Omega}\Lambda\mathbf{c}$ , and by the absorption of the centripetal acceleration in the "apparent" gravity  $\mathbf{g}$ . The real applied forces are, besides gravity, the pressure force,  $\alpha \operatorname{grad} p$ , and the friction force,  $\mathbf{F}$ . This last force can be written as the divergence of a stress tensor  $\boldsymbol{\tau}$ , i.e.,  $\mathbf{F} = -\operatorname{div} \boldsymbol{\tau}/\rho$ .

Equation (3.3) represents the first law of thermodynamics, where  $Q$  equals the net heating rate per unit mass. It includes various diabatic effects, namely, radiative heating (solar and infrared), latent heating, frictional and turbulent heating, and boundary layer heating near the earth's surface. In terms of entropy it can be written in the form

$$\frac{ds}{dt} = Q/T. \quad (3.3')$$

If we assume that the atmosphere behaves as an ideal gas, we can use the Poisson equation for the adiabatic expansion and compression  $T p^{-\kappa} = \text{invariant}$ , where  $\kappa = R/c_p$  is the Poisson constant. It is useful to introduce the concept of potential temperature,  $\Theta$ . This is the temperature that a parcel of air would attain if it were displaced adiabatically to a reference level  $p_0$  ( $=1000$  mbars):

$$\Theta = T(p_0/p)^\kappa. \quad (3.6)$$

The potential temperature implicitly takes into account the effects of the compressibility of the air. It is used in order to remove the cooling (warming) effect associated with the adiabatic expansion (compression), allowing the comparison of the temperature of air parcels at various levels in the atmosphere and, thereby, the evaluation of the stability.

Under normal conditions  $\Theta$  increases with height ( $\partial\Theta/\partial z > 0$ ) and the atmosphere is in a statically stable equilibrium. When  $\partial\Theta/\partial z < 0$ , the atmosphere is unstable (cold air on top of warm air), and when  $\partial\Theta/\partial z = 0$ , it is neutral. Actually, we may define the static stability by the quantity  $(T/\Theta)\partial\Theta/\partial z$ . The specific entropy of the air, considered as a perfect gas, can be expressed in terms of  $\Theta$  using (3.3') and (3.6) by the equation

$$s = c_p \ln \Theta. \quad (3.7)$$

Since the slope of the isobaric surfaces,  $p = \text{const}$ , is very small, they may be taken as being almost horizontal. On the other hand, the isentropic surfaces,  $\Theta = \text{const}$ , may have in some regions a pronounced slope and therefore become "inclined" with respect to the isobaric surfaces.

In the regions where the isentropes intersect the isobaric surfaces the atmosphere is obviously baroclinic. On the other hand, when the isentropic surfaces are parallel to the isobaric surfaces (i.e., almost horizontal), the atmosphere is barotropic.

Equation (3.4) expresses the balance of water vapor, with  $s(q)$  representing its sources and sinks. A frequent simplification made is that the water vapor falls out as precipitation as soon as it condenses, releasing its latent heat of condensation and leading to an "equivalent" temperature of a parcel when all the moisture is condensed,  $T_e > T$  as given by

$$T_e = T(1 + Lq/c_p T), \tag{3.8}$$

where  $L$  is the heat of evaporation. Equations (3.1)–(3.4) are evolution or prognostic equations, because they express the time derivatives of dependent variables in terms of their present values. On the other hand, Eq. (3.5) is a diagnostic equation, because it does not contain time derivatives.

The set of Eqs. (3.1)–(3.5) forms a closed system, provided that  $Q$  and  $F$  are known functions or depend on the other variables. With appropriate boundary conditions it is then possible to describe the evolution of the system starting from a given initial state. As shown in Sec. II, knowledge of certain basic parameters, such as the rotation rate of the earth, the orbital characteristics, the chemical composition, and gravity, is, of course, also required. The boundary conditions will specify the mechanical and thermal interactions between the atmosphere and the external system, such as the oceans and continents, the physiography of the land, the incoming and outgoing radiation, and so on.

The equations of motion (3.2) can be rewritten for the three individual components in a spherical coordinate system  $(\lambda, \phi, z, t)$  since we may assume, for our purposes, that the geoid can be approximated by a sphere:

$$\frac{du}{dt} = \frac{\tan\phi}{R} uv - \frac{uv}{R} + fv - f'w - \frac{1}{\rho} \frac{\partial p}{R \cos\phi \partial \lambda} + F_\lambda, \tag{3.9a}$$

$$\frac{dv}{dt} = -\frac{\tan\phi}{R} u^2 - \frac{vw}{R} - fu - \frac{1}{\rho} \frac{\partial p}{R \partial \phi} + F_\phi, \tag{3.9b}$$

$$\frac{dw}{dt} = \frac{u^2}{R} + \frac{v^2}{R} + f'u - \frac{1}{\rho} \frac{\partial p}{\partial z} - g + F_z, \tag{3.9c}$$

where  $u = R \cos\phi d\lambda/dt$ ,  $v = R d\phi/dt$ , and  $w = dz/dt$ . The quantity  $f$  is the so-called Coriolis parameter,  $2\Omega \sin\phi$ , and  $f' = 2\Omega \cos\phi$ .

The first pair of terms on the right-hand side of Eqs. (3.9a)–(3.9c) is of the form  $\xi_i/R$  and shows the influence of the metrics on the motion field. It is interesting to point out that these terms do not "perform work," since  $u\xi_1/R + v\xi_2/R + w\xi_3/R = 0$ . Also, the Coriolis terms involving  $f$  and  $f'$  satisfy a similar invariance relationship.

We shall next show how Eqs. (3.9a)–(3.9c) can be specialized or filtered in order to exclude certain phenomena,

such as sound waves, that are not thought to be important for the large-scale climate in the atmosphere and oceans.

## 2. Filtering of the equations of motion

Because the vertical extent of the atmosphere is small compared with its horizontal dimensions, there is the tendency for the circulations to be predominantly horizontal and in quasihydrostatic equilibrium. These results can be derived from Eqs. (3.9a)–(3.9c) by selecting the dominant terms using, for example, scale analysis (Charney, 1948). Scale analysis is basically a technique for estimating the orders of magnitude of the various terms in the governing equations for a particular class of motions. This technique acts like a filter; it is based on dimensional analysis and on an adequate choice of the characteristic length, depth, and time scales for the fluctuations. These characteristic values are used as basic units to measure the various terms in the governing equations.

For synoptic-scale motions we take the following characteristic values of the variables based upon observations:

- horizontal length scale  $L \approx 10^6$  m,
- depth scale  $H \approx 10^4$  m,
- horizontal velocity scale  $u \approx 10$  m s<sup>-1</sup>,
- vertical velocity scale  $w \approx 10^{-2}$  m s<sup>-1</sup>,
- horizontal pressure scale  $\Delta p \approx 10$  mbars,
- time scale  $L/u \approx 10^5$  s.

Since  $\Omega = 7.29 \times 10^{-5}$  s<sup>-1</sup>, the Coriolis parameter  $f = 2\Omega \sin\phi$  will be  $\approx 10^{-4}$  s<sup>-1</sup> in middle latitudes. Using these values, we can filter the previous equations, since

$$\mathcal{O} \left[ \frac{du}{dt}, \frac{dv}{dt} \right] \approx \frac{u^2}{L} = 10^{-4} \text{ m s}^{-2},$$

$$\mathcal{O} \left[ \frac{dw}{dt} \right] = \frac{uw}{L} = 10^{-7} \text{ m s}^{-2},$$

$$\mathcal{O}(fu, fv) = 10^{-3} \text{ m s}^{-2},$$

$$\mathcal{O}(f'w) = 10^{-6} \text{ m s}^{-2},$$

$$\mathcal{O} \left[ \frac{uv}{R}, \dots \right] = 10^{-5} \text{ m s}^{-2},$$

$$\mathcal{O} \left[ \frac{\partial p}{\rho R \partial \phi}, \dots \right] = 10^{-3} \text{ m s}^{-2},$$

$$\mathcal{O} \left[ \frac{1}{\rho} \frac{\partial p}{\partial z} \right] = 10 \text{ m s}^{-2},$$

and

$$\mathcal{O}(g) = 10 \text{ m s}^{-2}.$$

Frictional effects can be generally neglected for synoptic-scale motions above the planetary boundary layer.

The filtering of the third equation of motion (3.9c) leads to a quasibalance between the vertical pressure gra-

dient force and gravity:

$$\frac{\partial p}{\partial z} \approx -\rho g \tag{3.10}$$

which is the condition of hydrostatic equilibrium. We may mention here that, since pressure and height are related through Eq. (3.10), it is convenient, at times, to use pressure as the vertical coordinate leading to the so-called  $(x, y, p, t)$  system.

In small-scale turbulence and mesoscale phenomena, such as cumulus convection, the vertical velocities may be of the same order of magnitude as the horizontal velocities, and hydrostatic equilibrium conditions are not observed. However, the departures from hydrostatic equilibrium are of short duration and confined to small regions.

If we apply a filter of  $10^{-3} \text{ m s}^{-2}$  to the horizontal equations of motion (3.9a) and (3.9b), we find an approximate balance between the horizontal pressure gradient and the Coriolis force, the so-called geostrophic balance:

$$\begin{aligned} f v_g &= \frac{1}{\rho} \partial p / R \cos \phi \partial \lambda, \\ f u_g &= -\frac{1}{\rho} \partial p / R \partial \phi, \end{aligned} \tag{3.11}$$

where  $v_g$  and  $u_g$  indicate the horizontal components of the geostrophic wind. The geostrophic solutions show that the winds tend to blow parallel to the isobars with high pressure on the right in the northern hemisphere.

The geostrophic approximation applies when the acceleration is much smaller than the Coriolis force. The nondimensional quantity  $Ro \approx (dv/dt)/fu = u/fL$ , the so-called Rossby number, sets a criterion for the validity of the geostrophic approximation. In the atmosphere  $Ro \approx 10^{-1}$  whereas for the oceans  $Ro \approx 10^{-3}$  implying a very strong geostrophic constraint for the ocean circulations.

The complete solutions  $u$  and  $v$  of Eqs. (3.9a) and (3.9b) can then be regarded as the sum of the geostrophic solutions,  $u_g$  and  $v_g$ , and an ageostrophic component, e.g.,  $u = u_g + u_{ag}$ . The horizontal divergence of mass is almost completely due to the ageostrophic component of the flow. Of course, the geostrophic conditions are not valid near the equator, where  $f$  becomes very small. Also, close to the earth's surface, frictional effects have to be included leading to a cross-isobaric flow and a reduction in intensity. As in the case of the hydrostatic equation, the geostrophic approximation is not valid for small-scale circulations.

If we use a filter of  $10^{-4} \text{ m s}^{-2}$ , the horizontal equations (3.9a) and (3.9b) can be written

$$\begin{aligned} \frac{du}{dt} &= f v - \frac{1}{\rho} \frac{\partial p}{R \cos \phi \partial \lambda}, \\ \frac{dv}{dt} &= -f u - \frac{1}{\rho} \frac{\partial p}{R \partial \phi}. \end{aligned}$$

These equations are more general than the geostrophic equations, because they include the accelerations. They

therefore become prognostic equations, whereas the geostrophic equations are only condition equations.

### B. Balance equations

#### 1. Balance equations for angular momentum and energy

Besides the basic quantities used so far we will consider some other quantities that are important in understanding the workings of our climate. Because the sphericity of the earth and its rotation are primary factors in determining the atmospheric and oceanic circulations, it is more useful to consider angular momentum with respect to the earth's axis of rotation than linear momentum. This approach will allow us to analyze the ways through which the circulations fulfill some of the dynamical constraints.

The absolute angular momentum per unit mass about the earth's axis is given by

$$M = \Omega R^2 \cos^2 \phi + u R \cos \phi, \tag{3.12}$$

where the first term may be called  $\Omega$ -angular momentum and the second one relative angular momentum, as shown in Fig. 5. In our rotating coordinate system, the time rate change of total angular momentum for a unit volume equals the sum of all torques acting on it. From Eq. (3.9a) we obtain

$$\rho \frac{dM}{dt} = -\frac{\partial p}{R \cos \phi \partial \lambda} R \cos \phi + F_\lambda R \cos \phi + \dots, \tag{3.13}$$

where the ellipses represent tidal and other extraterrestrial torques. For the atmosphere and oceans only pressure and friction torques are important to generate absolute angular momentum. Therefore, the sources and sinks are to be found near the earth's surface. The friction force,  $F_\lambda$ , is given by  $-\text{div}_\lambda \tau$ , where  $\tau$  represents the stress tensor due to friction. Since the surface stress  $\tau_0$  is directed against the surface winds,  $\tau_0$  will be counted positive when the winds are from the east and negative when they are from the west. In other words, in the regions of east-

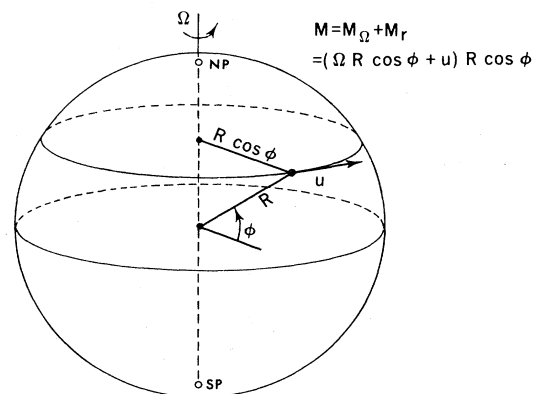


FIG. 5. Schematic diagram of the angular momentum around the earth's axis of rotation. SP, South Pole; NP, North Pole.

terly (or westward) surface winds westerly momentum is transferred from the earth to the atmosphere, and vice versa in the regions of westerly surface winds. As a result, the tropics act as the main source of absolute angular momentum for the atmosphere, and the midlatitudes, where westerlies predominate, as the principle sink. The pressure torque terms will be discussed at a later stage.

In the case of energy, we must define its various forms in order to study how the energy balance requirements are met in the climatic system.

The main source of energy for the climatic system is, of course, the sun. The direct effect of the sun is to heat the atmosphere and the underlying ground and oceans by the absorption of the short-wave incoming radiation. We may ignore geothermal energy, since it is negligible except in very localized regions. Thus the forms of energy that determine the energetics of the climatic system are the solar and terrestrial radiant energy, the potential energy  $\Phi$ , the internal energy  $I$ , the latent heat LH, and the kinetic energy  $K$  per unit mass,

$$\begin{aligned} \Phi &= gz, \\ I &= c_v T, \\ LH &= Lq, \\ K &= \frac{1}{2} \mathbf{c} \cdot \mathbf{c} = (u^2 + v^2 + w^2)/2, \\ E &= K + \Phi + I + LH, \end{aligned} \tag{3.14}$$

where  $E$  is the "total" energy. Although other forms of energy, such as electrical, chemical, and thermonuclear energies, may be important on the local scale, they do not play a significant role in the global energetics of the climatic system.

It is obvious for potential energy that

$$\frac{d\Phi}{dt} = gw \tag{3.15}$$

and for internal energy from Eqs. (3.1) and (3.3) that

$$\frac{dI}{dt} = Q - p\alpha \operatorname{div} \mathbf{c}. \tag{3.16}$$

In an atmosphere in hydrostatic equilibrium the internal energy for a unit-area column is proportional to its potential energy ( $\langle I \rangle / \langle \Phi \rangle = c_v / R$ , in the absence of topography), and the generation and destruction of internal and potential energy occur simultaneously. Since  $c_v + R = c_p$ , the potential plus internal energy integrated over a column is equivalent to the enthalpy in the column. Therefore, we will consider the two forms of energy together in a single form, the so-called total potential energy. The corresponding balance equation is then

$$\frac{d}{dt} (\Phi + I) = gw + Q - p\alpha \operatorname{div} \mathbf{c}, \tag{3.17a}$$

or

$$\frac{d}{dt} (\Phi + I) = gw + Q + \alpha \mathbf{c} \cdot \operatorname{grad} p - \alpha \operatorname{div} p \mathbf{c}. \tag{3.17b}$$

The second-to-last term in Eq. (3.17b) denotes the conversion from kinetic energy.

Furthermore, we obtain for the kinetic energy from Eq. (3.2) after taking the scalar product with  $\mathbf{c}$

$$\frac{dK}{dt} = -gw - \alpha \mathbf{c} \cdot \operatorname{grad} p - \alpha \mathbf{c} \cdot \operatorname{div} \boldsymbol{\tau}, \tag{3.18a}$$

or in an alternative form

$$\frac{dK}{dt} = -gw + p\alpha \operatorname{div} \mathbf{c} - \alpha \operatorname{div} (p \mathbf{c} + \boldsymbol{\tau} \cdot \mathbf{c}) + \alpha \boldsymbol{\tau} \cdot \operatorname{grad} \mathbf{c}. \tag{3.18b}$$

In hydrostatic equilibrium we have.

$$gw + \alpha \mathbf{c} \cdot \operatorname{grad} p = \alpha \boldsymbol{\nu} \cdot \operatorname{grad} p,$$

where  $\boldsymbol{\nu}$  is the horizontal, two-dimensional wind vector.

Inspection of the previous energy equations shows that they are not independent of each other, since they are linked by common terms. In fact, Eq. (3.15) shows that the rate of change of potential energy comes from the work done against the force of gravity,  $gw$ . This same term appears with the opposite sign in Eq. (3.18), proving that there is a conversion of potential into kinetic energy, or vice versa.

As shown by Eq. (3.16) the sources or sinks of internal energy are the rate of heating,  $Q$ , which includes besides radiational and latent heating also frictional heating, namely,  $\alpha \boldsymbol{\tau} \cdot \operatorname{grad} \mathbf{c}$ , and the rate of work performed by compression or expansion against the pressure field,  $p\alpha \operatorname{div} \mathbf{c}$ . These last two terms occur also in Eq. (3.18b) with the opposite sign, showing the link between the kinetic and internal energy.

The term  $-\alpha \operatorname{div} (p \mathbf{c} + \boldsymbol{\tau} \cdot \mathbf{c})$  in Eq. (3.18b) indicates the work at the boundaries by pressure and friction forces. This term plays an important role in transferring energy from the atmosphere into the oceans and generates the wind-driven ocean currents.

For the latent heat we have

$$L \frac{dq}{dt} = L(e - c). \tag{3.19}$$

To illustrate our interpretation of the previous energy equations (3.15)–(3.19), and to show the meaning of the various source, conversion and sink terms of energy we give a schematic diagram of the energy cycle in Fig. 6.

Let us consider next the total energy of the atmosphere. We must then take into account explicitly the radiation balance which results from the incoming solar radiation and the outgoing infrared radiation emitted by the earth. Thus for total energy  $E$  we obtain

$$\frac{dE}{dt} = -\alpha \operatorname{div} p \mathbf{c} - \alpha \mathbf{c} \cdot \operatorname{div} \boldsymbol{\tau} + L(e - c) + Q. \tag{3.20a}$$

Noting that  $Q = -\alpha \operatorname{div} \mathbf{F}_{\text{rad}} - L(e - c) - \alpha \boldsymbol{\tau} \cdot \operatorname{grad} \mathbf{c}$ , we can rewrite Eq. (3.20a) in the form

$$\begin{aligned} \frac{dE}{dt} &= -\alpha \operatorname{div} p \mathbf{c} - \alpha \operatorname{div} \mathbf{F}_{\text{rad}} \\ &\quad - \alpha \operatorname{div} \boldsymbol{\tau} \cdot \mathbf{c}. \end{aligned} \tag{3.20b}$$

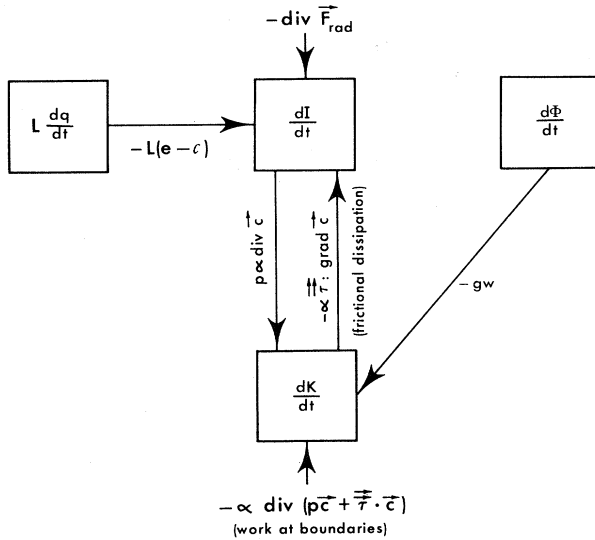


FIG. 6. Schematic box diagram showing the terms which connect the various forms of energy in the atmosphere. Sometimes the conversion from internal into kinetic energy,  $p \propto \text{div } c$ , is written in an alternate form as  $-\alpha c \cdot \text{grad } p$ , which includes the pressure work at the boundaries,  $-\alpha \text{ div } p c$ .

In Fig. 7 we present an integrated picture of how the global radiation and energy balances are achieved in the climatic system. The incoming solar radiation is not all used by the climatic system. A substantial fraction (30%) of the incident solar radiation is reflected (albedo = 0.30) by clouds and to a lesser extent by the earth's surface, and, therefore, does not participate in the atmospheric heat engine. Out of the remaining 70%, 20% is absorbed by the atmosphere and 50% by the oceans and land. This last amount will be used partly to maintain the hydrological cycle through evaporation (24%), heating the atmosphere indirectly when the water is condensed, and partly to heat the atmosphere directly through the flux of sensible heat (6%). The remaining 20% is used to heat the underlying surface, and will be lost later as infrared radiation to the atmosphere (14%) and to outer space (6%).

The heat absorbed by the atmosphere is used to increase the internal and potential energy which will partially (about 1%) be converted into kinetic energy to maintain the atmospheric and oceanic general circulations against friction. Finally, the atmosphere will radiate out to space around 64% as infrared radiation, thereby closing the radiation cycle.

### THE ATMOSPHERIC HEAT ENGINE

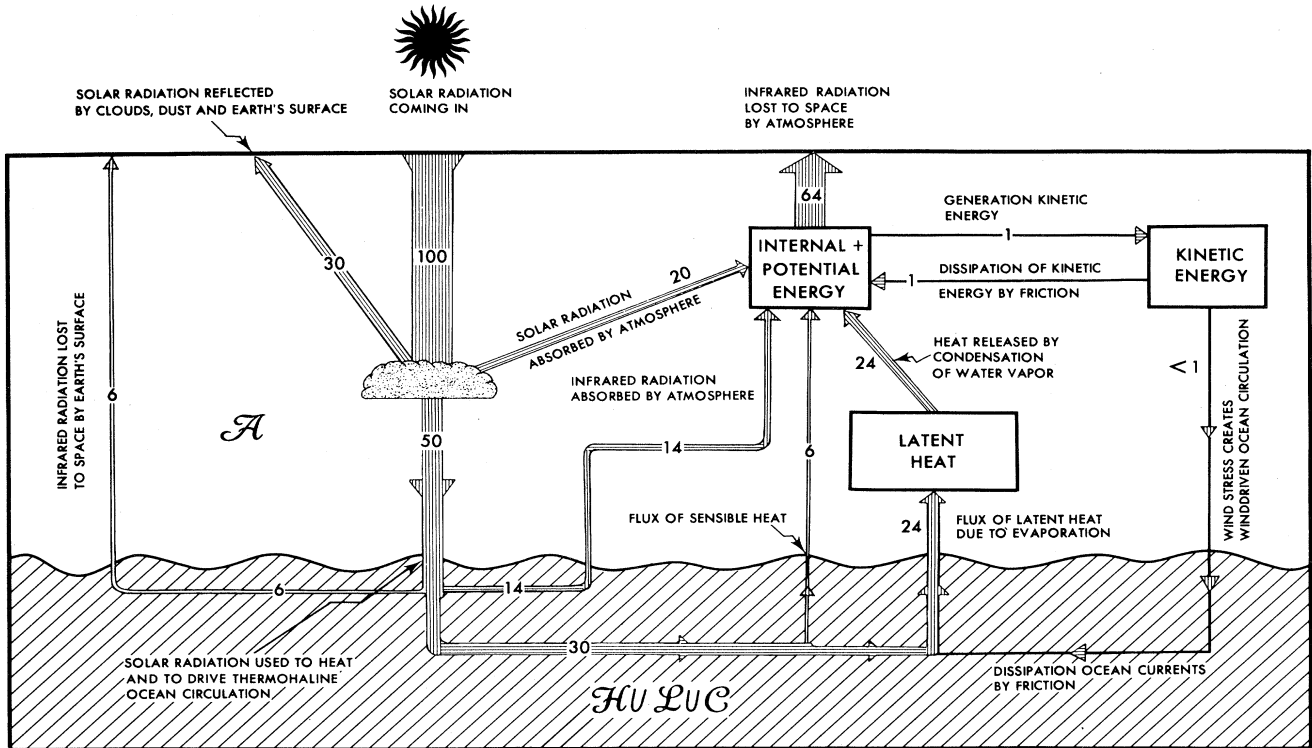


FIG. 7. Schematic diagram of the flow of energy in the climatic system. A value of 100 units is assigned to the incoming flux of solar energy. All values represent annual averages for the entire atmosphere. For simplicity no separate energy boxes have been drawn for the other subsystems.

## 2. General balance equations

Most previous equations are of the general form

$$dY/dt = F(Y, x, y, z, t),$$

where  $Y$  denotes a climatic variable, and the function  $F$  the source and sink terms.

Due to the difficulties involved we usually do not study the properties of a fluid following the motions of the individual particles according to a Lagrangian scheme. Instead, it is more convenient to use an Eulerian approach and to study the behavior of the fluid in a fixed point in space and time. This can be accomplished through the use of the following expansion:

$$\frac{dY}{dt} = \frac{\partial Y}{\partial t} + (\mathbf{c} \cdot \text{grad})Y. \tag{3.21}$$

This expression, combined with the equation of continuity (3.1), leads to the general balance equation:

$$\frac{\partial \rho Y}{\partial t} = \rho \frac{dY}{dt} - \text{div} \rho Y \mathbf{c}. \tag{3.22}$$

From Eq. (3.22) we see that the local rate of change of  $Y$  per unit volume results from the generation or destruction of  $Y$ , and the net inflow across the boundaries into the volume. It is worth noting that Eq. (3.22) is a particular case of our general balance equation (2.1).

Using Eq. (3.22), we can immediately write the balance equations for the angular momentum and the various energy components in a local, Eulerian framework.

### C. Time-averaged balance or climate equations

As mentioned before, the fields that characterize the state of the atmosphere are quite variable in time, leading, when considered over a certain time interval, to an ensemble of states. Thus it is important to determine the mean state of the atmosphere and its temporal fluctuations in order to describe the climate.

If we introduce the time-average operator  $\bar{A} = (1/\tau) \int_0^\tau A dt$  and  $A'$  its departure,

$$A = \bar{A} + A',$$

$$\bar{A}' = 0,$$

and for two arbitrary quantities  $A$  and  $B$ ,

$$\overline{AB} = \bar{A} \bar{B} + \overline{A'B'}.$$

With this formulation we can rewrite the balance equations for the time-averaged conditions in the following manner.

For angular momentum we obtain from Eq. (3.13)

$$\begin{aligned} \frac{\partial \rho \bar{M}}{\partial t} = & -\text{div} \bar{M} \rho \bar{\mathbf{c}} - \text{div} \overline{M'(\rho \mathbf{c})'} - \bar{p} / \partial \lambda \\ & - R \cos \phi \partial \bar{\tau}_{zx} / \partial z, \end{aligned} \tag{3.23}$$

for potential energy from Eq. (3.15)

$$\frac{\partial \rho \bar{\phi}}{\partial t} = -\text{div} \bar{\phi} \rho \bar{\mathbf{c}} + g \bar{\rho} \bar{w}, \tag{3.24}$$

for internal energy from Eq. (3.16)

$$\frac{\partial \rho \bar{I}}{\partial t} = -\text{div} \bar{I} \rho \bar{\mathbf{c}} - \text{div} \overline{I'(\rho \mathbf{c})'} + \bar{\rho} \bar{Q} - \bar{p} \text{div} \bar{\mathbf{c}}, \tag{3.25}$$

for kinetic energy from Eq. (3.18a)

$$\frac{\partial \rho \bar{K}}{\partial t} = -\text{div} \bar{K} \rho \bar{\mathbf{c}} - \text{div} \overline{K'(\rho \mathbf{c})'} - \bar{\mathbf{c}} \cdot \text{grad} \bar{p} - \bar{\mathbf{c}} \cdot \text{div} \bar{\boldsymbol{\tau}} - g \bar{\rho} \bar{w}, \tag{3.26}$$

for total energy from Eq. (3.20b)

$$\frac{\partial \rho \bar{E}}{\partial t} = -\text{div} \bar{E} \rho \bar{\mathbf{c}} - \text{div} \overline{E'(\rho \mathbf{c})'} - \text{div} \bar{\mathbf{J}}_q, \tag{3.27}$$

and for water vapor from Eq. (3.4)

$$\frac{\partial \rho \bar{q}}{\partial t} = -\text{div} \bar{q} \rho \bar{\mathbf{c}} - \text{div} \overline{q'(\rho \mathbf{c})'} + (\bar{e} - \bar{c}), \tag{3.28}$$

where

$$\mathbf{J}_q = \mathbf{F}_{\text{rad}} + p \mathbf{c} + \boldsymbol{\tau} \cdot \mathbf{c} \tag{3.29}$$

represents the sum of the radiation flux and the mechanical energy fluxes by pressure work and frictional stresses. The terms involving products of primed variables are the so-called transient eddy terms. These terms can be very important in the overall balances.

### D. Zonally averaged climate equations

Analogous to the previous results in the time domain, the fields are also not uniform in space, showing variability both as a function of latitude and longitude. However, meteorological conditions are generally more uniform along a latitude circle than in the north-south direction. To a first approximation, we may assume a ‘‘zonally’’ symmetric distribution with respect to the poles, as would be expected from the distribution of incoming solar radiation. Thus it is convenient to define mean zonal values at each latitude circle in order to assess the north-south variability. This can be achieved by introducing a zonal average operator defined by

$$[A] = \int_0^{2\pi} A d\lambda / 2\pi$$

and its departure  $A^*$ , so that

$$A = [A] + A^*$$

and, of course,  $[A^*] = 0$ .

The balance equations for the zonal and time mean conditions can be obtained from the time mean equations in Sec. III.C by an analogous procedure involving now the zonal averaging operator. This breakdown is useful to elucidate the dominant mechanisms responsible for achieving the balances. Thus, for example, for absolute angular momentum we may write, using Eq. (3.23),

$$\begin{aligned} \frac{\partial}{\partial t} [\overline{\rho M}] = & -\partial[\overline{M}][\overline{\rho v}] \cos\phi / R \cos\phi \partial\phi - \partial[\overline{M}][\overline{\rho w}] / \partial z - \partial[\overline{M}^*(\overline{\rho v})^*] \cos\phi / R \cos\phi \partial\phi - \partial[\overline{M}^*(\overline{\rho w})^*] / \partial z \\ & - \partial[\overline{M}'(\overline{\rho v})'] \cos\phi / R \cos\phi \partial\phi - \partial[\overline{M}'(\overline{\rho w})'] / \partial z - [\partial\overline{p} / \partial\lambda] - R \cos\phi \partial[\overline{\tau_{zx}}] / \partial z . \end{aligned} \quad (3.30)$$

The first set of two terms on the right-hand side of Eq. (3.30) involves the transport of angular momentum by the mean meridional circulations, i.e., the overturnings of the  $(\phi, z)$  plane, the second set the transports by stationary or standing eddies, and the third set the transport by transient eddies. The second-to-last term, the pressure gradient term, will vanish only for a smooth earth without mountains. The last two terms, the mountain and friction torque terms, represent the interaction between the earth and the atmosphere [see discussion accompanying Eq. (3.13)].

### E. Globally averaged climate equations

Let us consider now the global atmosphere. Integration of Eqs. (3.23)–(3.28) over the entire volume of the atmosphere will bring out more clearly the internal sources and sinks, as well as the interactions with the external system through the boundaries at the top of the atmosphere and at the earth's surface. Thus we find the following for the various quantities.

#### (1) Angular momentum

$$\frac{\partial}{\partial t} \int_V \int \overline{\rho M} dV = \mathcal{P} + \mathcal{T} , \quad (3.31)$$

where

$$\mathcal{P} = \int_0^\infty \int_{-\pi/2}^{\pi/2} \sum_i (\overline{p}_E^i - \overline{p}_W^i) R \cos\phi dy dz$$

represents the torque on the atmosphere due to mountains, and

$$\mathcal{T} = \int_{\text{surface}} \int \tau_{zx} R \cos\phi dx dy$$

the friction torque on the atmosphere. The summation  $\sum_i$  is taken over the pressure differences,  $\overline{p}_E^i - \overline{p}_W^i$ , at the east and west sides of all major mountain ranges. The sign convention used here is that the pressure and friction torques,  $\mathcal{P}$  and  $\mathcal{T}$ , are counted positive when they tend to increase the eastward angular momentum of the atmosphere.

#### (2) Kinetic energy

$$\begin{aligned} \frac{\partial}{\partial t} \int_V \int \overline{\rho K} dV = & - \int_V \int \overline{\mathfrak{K} \cdot \text{grad} p} dV \\ & + \mathcal{D} + \mathcal{K} , \end{aligned} \quad (3.32)$$

where

$$\mathcal{D} = \int_V \int \overline{\tau \cdot \text{grad} c} dV$$

represents the rate of dissipation of kinetic energy from

the large-scale flow into turbulent motions and, finally, into internal energy;

$$\mathcal{K} = \int_{\text{surface}} \int \overline{\tau_0 \cdot \mathfrak{K}} dx dy$$

the transfer of kinetic energy across the boundary, and  $\overline{\tau_0} = \rho \overline{w \mathfrak{K}} \approx -\rho K_M \partial \mathfrak{K} / \partial z$  the flux of momentum across the boundary. According to these definitions,  $\mathcal{D}$  and  $\mathcal{K}$  are counted positive when they tend to increase the kinetic energy.

It may be shown (e.g., Peixóto and Oort, 1974) that for the entire atmosphere

$$- \int_V \int \overline{\mathfrak{K} \cdot \text{grad} p} dV = - \int_M \int \overline{\omega \alpha} dx dy dp / g .$$

Since the work done by the geostrophic wind is identically zero, the net work results from the ageostrophic flow against the pressure gradient force. This is associated with horizontal divergence or convergence mainly near the earth's surface and at jet stream levels. Moreover, in order to have a generation of kinetic energy, the resulting vertical motions are such that there must be an expansion (rising) of lighter air and a compression (sinking) of denser air, as shown by the right-hand side of the last equation.

#### (3) Energy

$$\begin{aligned} \frac{\partial}{\partial t} \int_V \int \overline{\rho E} dV = & \int_{\text{top}} \int \overline{F_{\text{rad}}} dx dy \\ & + \int_{\text{surface}} \int (-\overline{F_{\text{rad}}} + \overline{F_{\text{SH}}} + \overline{F_{\text{LH}}}) dx dy \\ & + \int_{\text{surface}} \int p \mathbf{c} \cdot \mathbf{n} dx dy + \mathcal{K} , \end{aligned} \quad (3.33)$$

where  $\mathbf{n}$  is the unit vector normal to the surface directed into  $V$ . Further  $F_{\text{SH}} = \rho c_p \overline{w T} \approx -\rho K_H \partial \overline{T} / \partial z$  represents the flux of sensible heat into the atmosphere, and  $F_{\text{LH}} = \rho L \overline{w q} \approx -\rho L K_w \partial \overline{q} / \partial z$  the flux of latent heat into the atmosphere. From these definitions it is clear that  $F_{\text{rad}}$  is counted positive when downward, and the surface fluxes  $F_{\text{SH}}$  and  $F_{\text{LH}}$  are counted positive when upward into the atmosphere.

#### (4) Water vapor

$$\frac{\partial}{\partial t} \int_V \int \overline{\rho q} dV = \int_{\text{surface}} (\overline{E} - \overline{P}) dx dy , \quad (3.34)$$

where  $\overline{E} = \rho \overline{w q} = -\rho K_w \partial \overline{q} / \partial z$  is the evaporation rate, and  $\overline{P}$  the precipitation rate at the earth's surface. Thus the surface evaporation and precipitation rates,  $\overline{E}$  and  $\overline{P}$ , are counted positive when they are directed upward and downward, respectively.

The previous climate equations demonstrate the impor-



tance of the interactions between the atmosphere and the other subsystems through the  $F_{\text{rad}}$ ,  $F_{\text{SH}}$ ,  $F_{\text{LH}}$  and pressure work terms in the energy equation, the  $\mathcal{P}$  and  $\mathcal{T}$  terms in the angular momentum equation, the  $\mathcal{K}$  and pressure work terms in the kinetic energy equation, and the  $\bar{E}$  and  $\bar{P}$  terms in the water vapor equation.

#### IV. THE OBSERVED CLIMATE

In order to get a deeper understanding of such a complex system as the climate we must rely on observations, theory, and experiments.

Using the observations together with the balance equations, we can investigate the mechanisms by which the various processes, such as the fluxes, occur in the atmosphere and oceans. Through such diagnostic techniques we will be able to describe not only the processes that maintain the climatic state, but also to infer the magnitude of some of the external constraints. Furthermore, the insertion of the observations in the climatic equations may lead to results for other parts of the climatic system. This entire methodology may be called the “observational” approach.

At times it may be more illuminating to use regional studies to investigate in greater depth how the atmosphere works. In fact, the use of global means will sometimes obscure through compensation some important mechanisms that occur at favored selected regions on the globe. For example, the eastern parts of the continents and the neighboring oceans behave quite differently from their western counterparts. Furthermore, with global studies it is difficult to assess the influence of land-sea contrast and orography on the maintenance of the general circulation (see, for example, Lau and Wallace, 1979, and the review paper by Held, 1982).

We will confine ourselves to the actual climate during recent times. For a review of climatic variations over geological times see Crowley (1983). Since we are using mainly aerological observations for the last decade or so, we will not be able to consider long-term changes in the climate.

Because the behavior of the atmosphere-ocean system is largely determined by the radiational forcing of the sun, we will begin our discussion with an analysis of this principal external forcing factor. Next we will study the response of the atmosphere and oceans by analyzing their three-dimensional structure and general circulation.

The analysis will be done within the physical-dynamical framework of the basic balance equations presented in Sec. III.C. Thus we will discuss, in order, the global cycles of radiation, angular momentum, water, and energy. For each element we will try to describe how it passes from the atmosphere to the oceans and solid earth, how it is transported in the terrestrial branch, how it returns to the atmosphere, and how, after passing through the atmospheric branch, it will start again on its unending journey. Through a careful study of the usually better known atmospheric branch, we will be able for each

element to infer new, unexpected properties of the terrestrial branch. The highly interactive nature of the processes in the atmosphere—ocean—solid earth system will become evident for each of the elements. Thus for a wide range of time scales we have to consider the various climate components together. An integrated view of the various disciplines in geophysics is essential before we can begin to understand the earth’s climate.

We should add as a final note that the rotation of the earth is, of course, also of great importance for the prevailing climatic regime. In fact, Williams and Holloway (1982) have found in a series of numerical model experiments that the circulations on Jupiter and Saturn with their numerous zonal jets resemble a larger, faster spinning earth, whereas the circulation on Venus resembles a more slowly rotating earth with strong diurnal variations. However, for our present climate on earth the historical variations in the rotation rate have been so small that they have not affected the circulation to any measurable degree.

#### A. Observational network

It appears appropriate to mention the various types of observations needed to define the state of the climatic system. Most of our present knowledge of the physical and dynamical structure of the atmosphere and oceans is based on the *in situ* observations described below.

##### 1. Atmospheric data

After World War II an international effort was begun to launch rawinsondes<sup>1</sup> twice daily at the major airports of the world for general aviation and weather forecasting purposes. The number of reporting stations has grown from a few hundred in the early 1950s to about 2000 in the 1980s. The data coverage over the inhabited regions of the continents is now sufficient for the purpose of large-scale climate research. However, extensive data-void regions are found over the oceans except where there are island stations, and in the North Atlantic where there are a number of weather ships. The station coverage during the 1963–1973 decade is indicated in Fig. 8. During each rawinsonde ascent temperature  $T$ , pressure  $p$ , and humidity  $q$  are measured between the ground and about 20–30 km height. In addition, by tracking the displacements of the balloon, one can obtain the horizontal wind components,  $u$  and  $v$ .

<sup>1</sup>A rawinsonde is “a method of upper-air observation consisting of an evaluation of the wind speed and direction, temperature, pressure, and relative humidity aloft by means of a balloon-borne radiosonde tracked by a radar or radio direction-finder. Height data pertaining to [pressure] levels aloft are computed from the radiosonde data, while wind data are derived by trigonometric computations” (Huschke, 1959, p. 470).

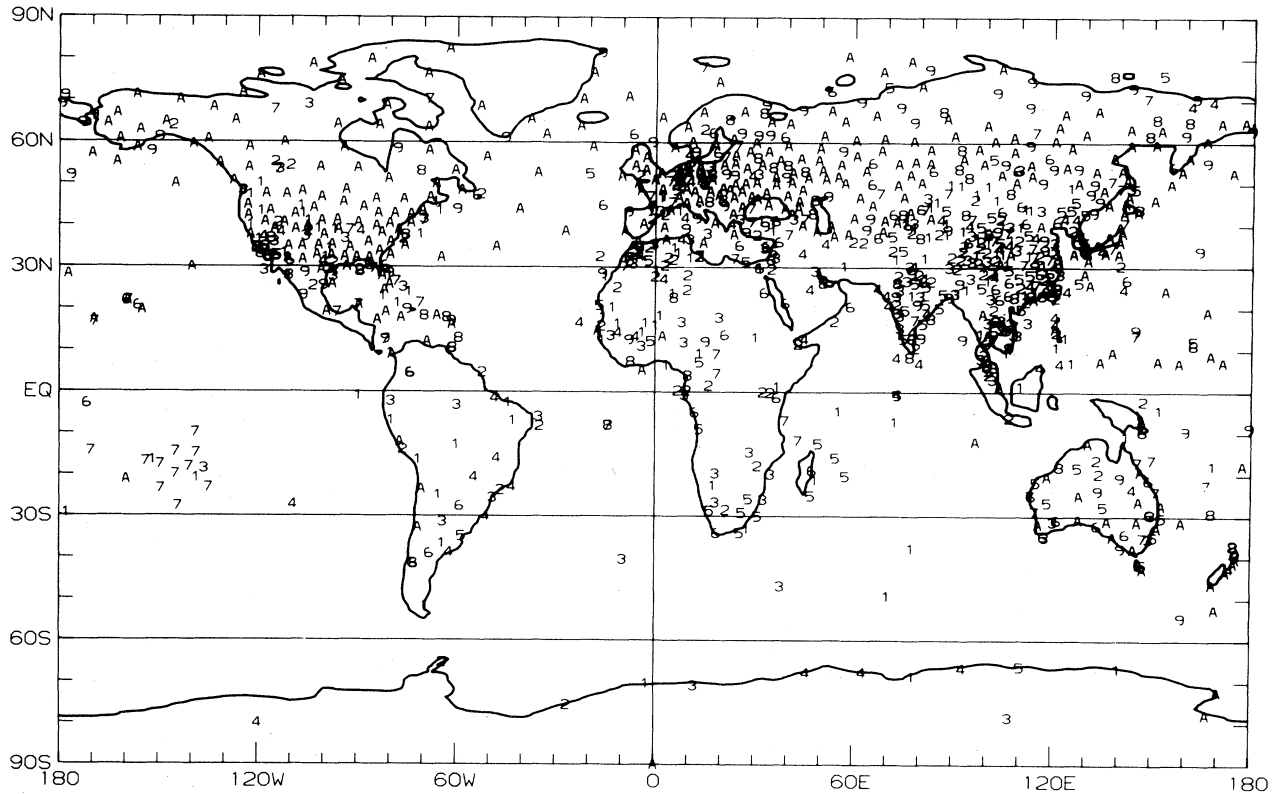


FIG. 8. Network of (daily reporting) rawinsonde stations used in our atmospheric analyses, showing the number of years of observations available. The plotted values range between 1 and 10 (=  $A$ ) years for our present sample, which covers the period May 1963 through April 1973.

The accuracy of the basic data is subject to some uncertainties not only due to instrumental limitations but also to the processing and transmitting of the observations. It seems reasonable to assume that these errors are random in character and uncorrelated. This implies that statistics evaluated for a given station would become progressively more reliable as longer averaging periods are used (" $1/\sqrt{N}$ " rule) for linear quantities. For further discussion see Oort (1978).

Following the same mathematical techniques used previously in several of our projects (Starr, 1968; Oort and Rasmusson, 1971), we computed the desired monthly mean statistics at each station for various standard pressure levels. Next each statistic was interpolated horizontally by computer onto a global  $2.5^\circ$  latitude  $\times$   $5^\circ$  longitude grid using an objective analysis scheme (see, e.g., Oort, 1983). Obviously, the analysis tends to be less reliable in the data-sparse regions over the oceans, especially in the southern hemisphere. In those regions the analyzed field is strongly influenced by the initial guess field, i.e., in our case the zonal average of the basic data in the corresponding latitude belt.

## 2. Oceanic data

Below-surface oceanic data have been collected largely from research vessels on a nonoperational basis. The spatial coverage is more uniform than the coverage in the atmosphere, as shown in Fig. 9. However, there are usually

only a few soundings available at the same location, making it difficult to study temporal variability except at the surface, where merchant ships routinely report oceanic conditions. Thus it is practically impossible to study the oceanic heat storage for individual years, except in certain regions of the North Atlantic and North Pacific Oceans. In the standard oceanographic station data, temperature, salinity, oxygen content, and concentrations of various nutrients are measured at many levels in the vertical between the surface and the ocean bottom. Fortunately, most variability is found in the upper 100 m of the oceans, where one can sample more easily and more frequently using bathythermograph data. Because the year-to-year variability is much smaller in the ocean than in the atmosphere, especially below the surface layer, the historical data are sufficient for first estimates of, for instance, the normal oceanic heat storage, one of the crucial factors in climate.

Current velocities are difficult to measure from a ship, since they are usually very small (on the order of a few  $\text{cm s}^{-1}$ ), except in the major ocean currents. This fact limits severely our present knowledge of the dynamical structure of the oceans.

## 3. Satellite data

The role of satellites in climate research has expanded greatly since the early 1960s, when cloud pictures were

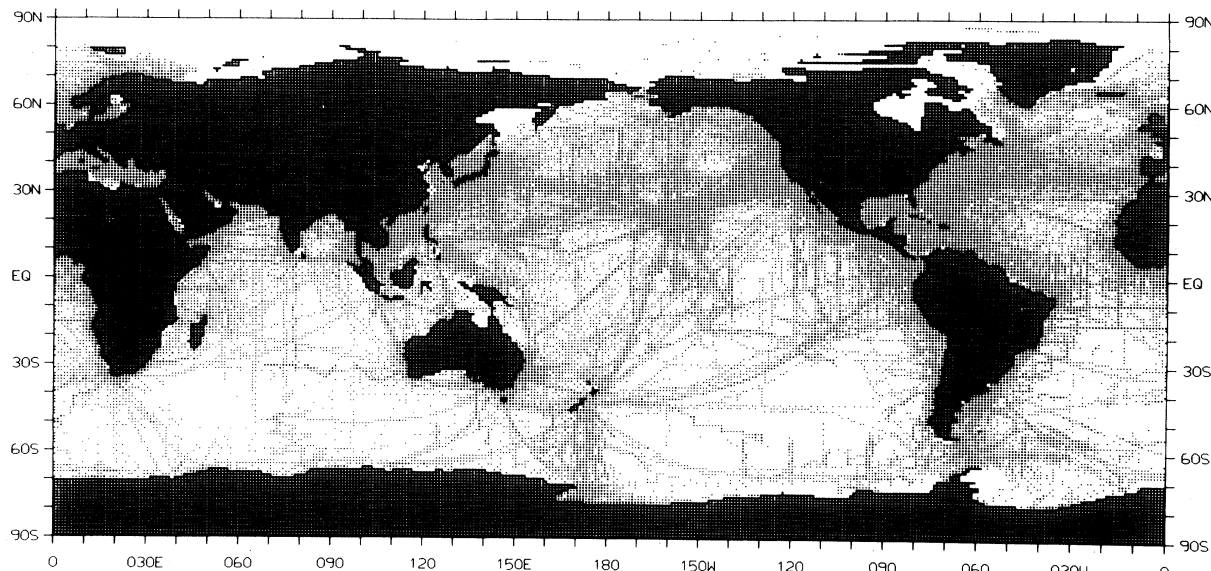


FIG. 9. Network of subsurface ocean data. Shown are those  $1^\circ$  latitude  $\times$   $1^\circ$  longitude squares that contain any historical temperature data taken by oceanographic research vessels during the 3-month period February to April, irrespective of year. A small dot indicates that a square contains 1–4 observations, and a large dot that it contains 5 or more observations (Levitus, 1982).

essentially their only useful product. In fact, recent measurements of net incoming and outgoing radiation fluxes at the “top” of the atmosphere provide the first reliable measurements of the basic driving force of the climatic system.

Further, satellites are providing useful information from other spectral bands besides the ultraviolet, visible, and infrared ones used in the present paper. For example, the microwave band is used to study the precipitable water content of the atmosphere over the oceans, wind stresses at the ocean surface, the distribution and extent of sea ice, and finally the height of sea level. The last quantity is of major importance for getting a handle on the absolute velocity fields in the oceans. Another example is the determination of the nature and concentration of aerosols, e.g., sulfuric acid from volcanic eruptions (such as El Chicon) and dust in the atmosphere using backscattered ultraviolet radiation.

In addition, through inversion techniques in the various absorption bands of  $\text{CO}_2$  and  $\text{H}_2\text{O}$  useful temperature and humidity profiles are now obtained to supplement the rawinsonde network observations over the oceans. However, except for the net radiation balance data, no satellite information was used in our present analysis of the climate. So far, only mean temperatures for relatively thick layers and winds at two cloud levels can be inferred from satellite information. Therefore, the vertical resolution is limited, and the data are, in many cases, not compatible with the observations obtained from rawinsondes at the different levels.

Even without the satellite temperature data, the scope of our present studies of the climate system is quite large. For example, for an average number of 1000 stations taking observations twice a day during a 10-year period for five parameters ( $u$ ,  $v$ ,  $T$ ,  $z$ , and  $q$ ) at 11 levels in the verti-

cal, required handling a minimum of  $1000 \times 2 \times 10 \times 365 \times 5 \times 11 = 4 \times 10^8$  pieces of information. In the oceans, we processed about one million soundings of three parameters at about 30 levels leading to a total of  $10^8$  pieces of information. From these numbers it is clear that it is no small task to handle and ensure quality control of these data collected by countless individuals in many countries by somewhat different instruments.

## B. Radiation balance

As the external factor most important for the earth’s climate we should mention the incoming solar radiation, which is characterized by the so-called solar constant of about  $1360 \text{ W m}^{-2}$ , by the obliquity  $\epsilon$ , by the eccentricity  $e$ , and by the longitude of perihelion  $\pi$  for the earth’s orbit around the sun. Variations in these astronomical factors are probably closely linked to observed variations in the earth’s climate at time scales of thousands of years and longer [see Fig. 3 and Imbrie and Imbrie (1979) for Milankovitch theory of ice ages], but do not seem important at the decadal time scale we are concerned with in the present paper.

The annual mean net (solar minus terrestrial) radiation at the top of the atmosphere is shown in Fig. 10 as obtained from satellites by Campbell and Vonder Haar (1980). There is a clear excess of incoming over outgoing energy on the order of  $60\text{--}70 \text{ W m}^{-2}$  near the equator and a deficit on the order of  $-100 \text{ W m}^{-2}$  near the poles. This equator-to-pole gradient in radiation constitutes the basic driving force for all atmospheric and oceanic motions. Although the net radiation is largely symmetric along each latitude circle, there is a tendency in the tropics for positive anomalies over oceans and negative ones over land. Such anomalies are associated with the differ-

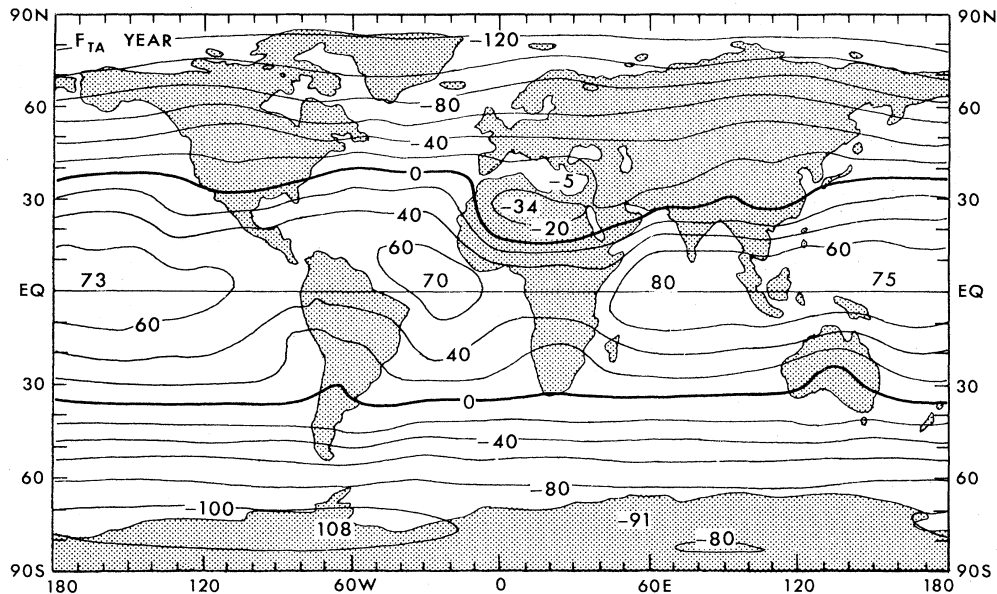


FIG. 10. Global distribution of the net incoming radiation at the top of the atmosphere ( $F_{TA}$ ), after Campbell and Vonder Haar (1980) for annual mean conditions. Units are  $\text{W m}^{-2}$ .

ences in the radiating temperatures between the ocean and land surfaces. These temperature differences are caused by the different heat capacities of the ocean and the land as well as by the possible redistribution of heat in the oceans by currents. The zonal anomaly pattern in Fig. 10 implies the need for some systematic flow of energy in the atmosphere from the tropical oceans to the continents in the annual mean. Especially noteworthy is the large negative anomaly over the North African desert, requiring substantial adiabatic heating through sinking motion of the air.

Of course, the net radiation consists of both incoming short-wave solar radiation that is partly reflected and partly absorbed, and outgoing long-wave terrestrial radiation (see Fig. 7). For zonal mean conditions meridional profiles are drawn in Fig. 11. In addition to the annual mean curves, which are generally symmetric with respect to the equator, we have added curves for the two extreme seasons December 1 through February 28 (DJF) and June 1 through August 31 (JJA). Several factors are worth mentioning. First of all, we find a huge annual variation in the solar forcing between summer and winter conditions in Figs. 11(a) and 11(d). In spite of some reduction by the infrared outgoing flux in Fig. 11(e), the annual variation in net radiation in Fig. 11(f) is still very large. The different values of the albedo at various latitudes in Fig. 11(c) are primarily due to differences in the angle of incidence of the solar radiation and also to differences in cloudiness and in surface conditions—snow, ice cover, vegetation, etc.

The net annual radiation curve in Fig. 11(f) corresponds to the zonal average of the map presented in Fig. 10. Integrated over the globe as a whole the net annual radiation should be near zero, at least in the long run, to

ensure a radiative quasiequilibrium. However, at each latitude a net poleward transport of energy in the atmosphere and oceans is required to keep the system in thermodynamic balance. This required transport is shown in Fig. 12. As is expected for annual mean conditions, the cross-latitude flux is negligible near the equator and maximum [on the order of  $(5-6) \times 10^{15}$  W] in middle latitudes between  $30^\circ$  and  $40^\circ$  latitude. To compute seasonal variations in the required transport, more information is needed, namely, the rate of seasonal heat storage in atmosphere and oceans. We will return to this in the later discussions.

### C. Angular momentum balance

#### 1. Mass and angular momentum in the atmosphere

The mass distribution in the atmosphere can be obtained most readily by measuring the pressure distribution and using the hydrostatic equation (3.10). Thus the surface pressure gives a good measure of the total atmospheric mass in a vertical column. Figure 13 shows a mean annual map of surface pressure reduced to sea level. Although the values in mountainous terrain are extrapolated to sea level, leading to fictitious pressures, this type of analysis has traditionally been used by meteorologists in order to follow the migrating weather systems. Over the oceans and low-level terrain maps accurately represent the mass distribution, but of course not over mountains, where one has to go back to the originally measured surface pressure before reduction to sea level. If one does this the global mean surface pressure turns out to be 985

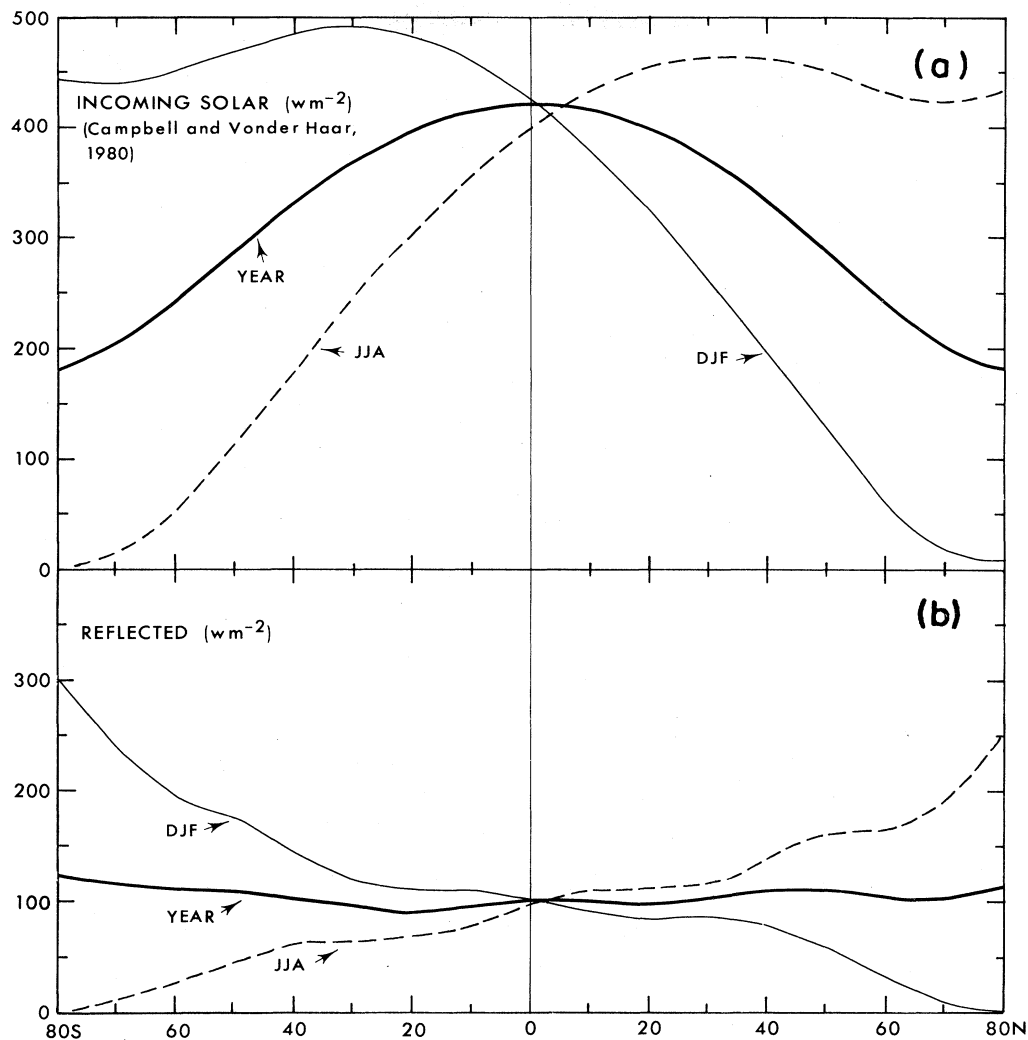


FIG. 11. Zonal mean profile of (a) incoming solar radiation, (b) reflected solar radiation, (c) albedo, (d) absorbed solar radiation, (e) emitted infrared radiation, and (f) net incoming radiation, after Campbell and Vonder Haar (1980). No corrections were made for global radiation balance. Units are  $\text{W m}^{-2}$ , except % for albedo.

mbar, corresponding to a total atmospheric mass of  $514 \times 10^{16}$  kg (Trenberth, 1981). This last value includes  $1.3 \times 10^{16}$  kg water in the vapor form or a global layer of, on the average, 2.5 cm precipitable water. Because of the relatively high evaporation (over the continents) during northern hemisphere summer the total mass of the atmosphere varies annually with an amplitude of about  $0.1 \times 10^{16}$  kg.

The surface winds, shown by arrows in Fig. 13, are associated with the pressure distribution through the geostrophic relation (3.11). These winds therefore tend to parallel the isobars with high pressure on the right-hand side in the northern hemisphere, and on the left-hand side in the southern hemisphere. There is a slight tendency for convergence into the equatorial zone and into the low-pressure belts near 60° latitude, and a tendency for divergence from the subtropical high-pressure cells and the polar regions. Ageostrophic effects in the form of flow into low-pressure areas and out of high-pressure ones are due

to friction and small-scale turbulence in the surface boundary layer. On a zonal mean basis [see Fig. 15(a)] the dominant features of the flow are steady easterly trade winds (from the east,  $u < 0$ ) in the tropics, and westerlies (from the west,  $u > 0$ ) in mid and high latitudes of both hemispheres. The westerlies are especially strong in the southern hemisphere, where they give rise to the strong Antarctic circumpolar current in the ocean near 60°S (see Fig. 19).

Maps of the vertical mean mass flow are presented in Figs. 14(a) and 14(b) for the zonal and meridional components, respectively. The westerlies in middle latitudes now dominate the zonal flow; they actually lead to a superrotation of the atmosphere as a whole on the order of  $+6 \text{ m s}^{-1}$  relative to the solid earth. The meridional component is much weaker than the zonal component, especially in the southern hemisphere with its more homogeneous surface conditions.

In order to describe the behavior of the circulation with

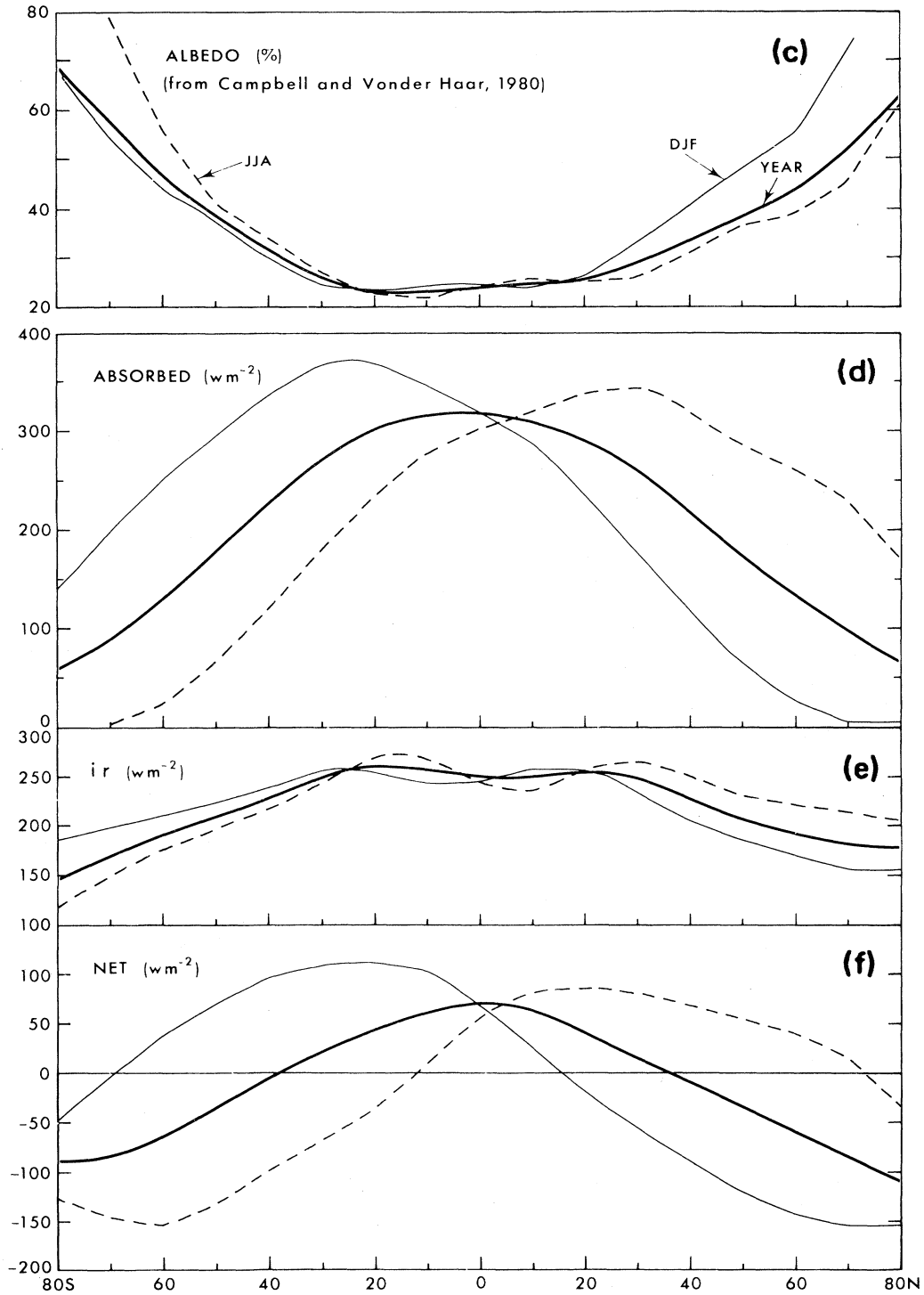


FIG. 11. (Continued).

height and at various latitudes we choose to show the various parameters in zonal mean cross sections. Thus the vertical distribution of the zonal mean flow is presented in Fig. 15(a) in a cross section using the pressure as a

vertical coordinate. The broad maxima near 200 mbars (about 12 km height) are due to the subtropical and polar westerly jet streams and are located just above the region where the baroclinicity of the atmosphere is largest, i.e.,

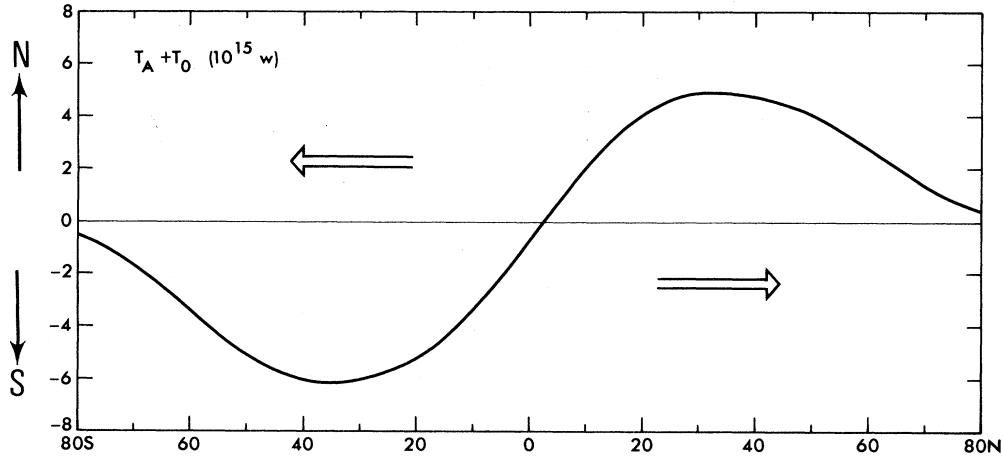


FIG. 12. Zonal mean profile of the required northward transport of energy in the atmosphere-ocean system for annual mean conditions. Units are  $10^{15}$  W.

where the north-south temperature gradient is a maximum. The large observed shear,  $\partial[\bar{u}]/\partial z$ , is determined by the meridional gradient of the mean temperature as shown by the thermal wind equation

$$\partial u_g / \partial z \approx - \frac{g}{fT} \frac{\partial T}{R \partial \phi}$$

This equation can be derived easily by vertical differentiation of the geostrophic equations (3.11) and by using the hydrostatic relation (3.10) and ideal gas law (3.5):

$$\partial u_g / \partial z = - \frac{\partial}{\partial z} \frac{1}{\rho f} \left[ \frac{\partial p}{R \partial \phi} \right]$$

The thermal wind equation shows that the zonal wind increases with height ( $\partial u_g / \partial z > 0$ ) in middle latitudes where the north-south temperature gradient ( $\partial T / \partial \phi < 0$ ) is most pronounced. Of course, in regions where the atmosphere is barotropic, the winds do not change with height ( $\partial v_g / \partial z = 0$ ), because  $(\text{grad } T)_{p=\text{const}} = 0$ . Figure 15(a) further shows that the easterlies ( $u < 0$ ) are the dominant winds in the equatorial zone.

The zonally averaged meridional flow is presented in Fig. 15(b). The values are small, except in the tropics, where they attain values of  $1\text{--}2 \text{ m s}^{-1}$  near the surface and 200 mbars.

For the sake of clarity the  $[\bar{v}]$  data are also used to con-

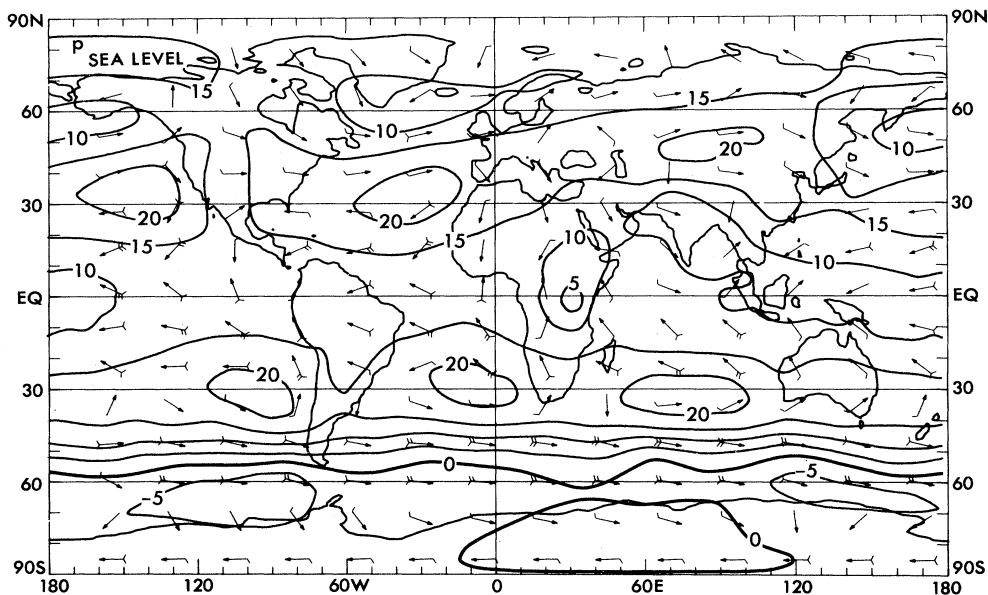


FIG. 13. Global distribution of the surface pressure (in mbars) reduced to sea level. Also shown are vector plots of the surface wind. For geostrophic flow the arrows should parallel the isobars. Each barb on the tail of an arrow represents a wind speed of  $5 \text{ m s}^{-1}$ . (Note that a uniform value of 1000 mbars has been subtracted from the pressure field.)

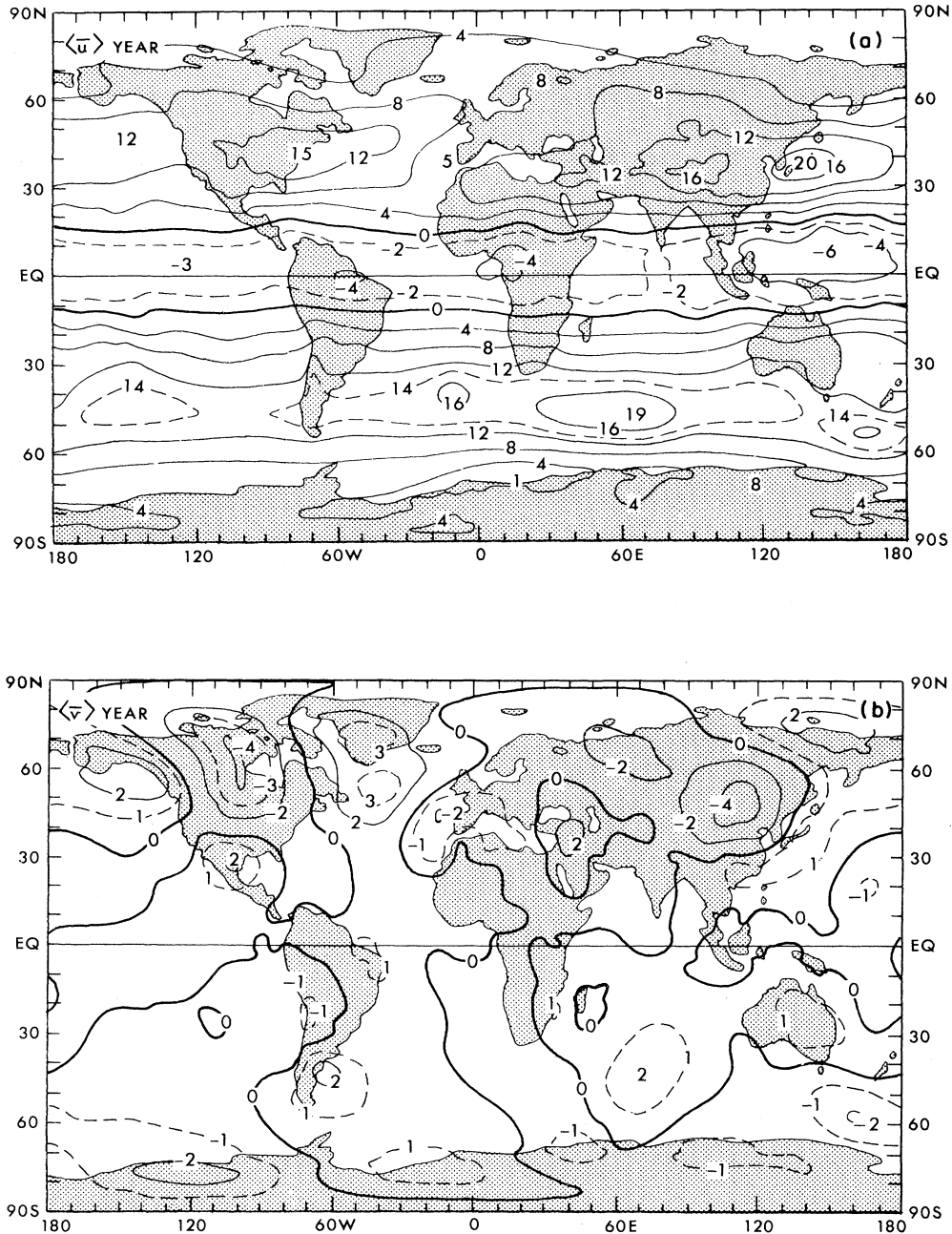


FIG. 14. Global distributions of the vertically averaged (a) zonal and (b) meridional wind components for annual mean conditions. Positive values indicate eastward (or westerly flow) for  $\langle \bar{u} \rangle$  and northward (or southerly) flow for  $\langle \bar{v} \rangle$ . Units are  $\text{m s}^{-1}$  (Oort and Peixóto, 1983).

struct streamlines which indicate the mean overturnings of mass in a north-south cross section. This can be accomplished by introducing the so-called Stokes streamfunction  $\psi$ , given by the equation

$$[\bar{\rho v}] = \partial \psi / 2\pi R \cos \phi \partial z \tag{4.1}$$

or if pressure is used as the vertical coordinate  $[\bar{v}] = g \partial \psi / 2\pi R \cos \phi \partial p$ . Conservation of mass requires in the long-term mean that the flux of mass across any latitudinal wall will vanish:

$$\int \oint \bar{\rho v} d\lambda dz \equiv 2\pi \int_0^{p_{\text{surface}}} [\bar{v}] dp / g = 0 .$$

The annual mean streamlines are shown in Fig. 15(c). These overturnings are often called “mean meridional circulations.” A pattern of three cells can be recognized in each hemisphere, one in the tropical regions (the so-called Hadley cell), another in midlatitudes (the Ferrel cell), and finally a third one in the polar regions (the polar cell). In the Hadley cells there is a rising of warm (light) and moist air in the equatorial region and a descent of colder



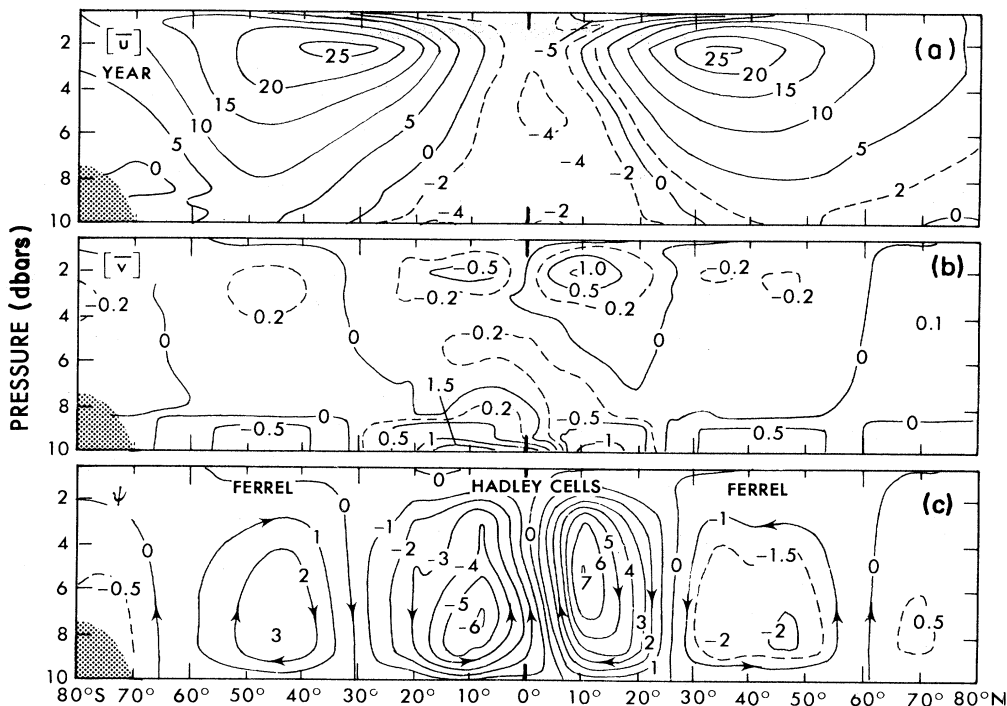


FIG. 15. Zonal mean cross sections of (a) the zonal wind component in  $\text{m s}^{-1}$ , (b) the meridional wind component in  $\text{m s}^{-1}$ , and (c) the inferred flow of atmospheric mass in  $10^{10} \text{ kg s}^{-1}$  for annual-mean and zonally averaged conditions. The (direct) energy-releasing tropical Hadley cells, the (indirect) energy-consuming midlatitude Ferrel cells, and the weak direct polar cells are evident in both hemispheres.

(heavier) air in the subtropics, leading to a thermally driven direct circulation. However, in the Ferrel cell there is a rising of relatively cold air in high latitudes and a sinking of relatively warm air in the lower middle latitudes, leading to a thermally indirect circulation in which the cold air is forced to rise. In a direct circulation with the lowering of the center of mass there is a production of kinetic energy, whereas in an indirect cell with the net rising of the center of mass there is a consumption of kinetic energy [see Eq. (3.18b) and Fig. 6]. The three-cell regime results from the observed pole-to-equator gradient in net radiation combined with the rotation of the earth. Under different conditions, such as lower rotation rates, there could be only one direct cell in each hemisphere, as Hadley proposed in 1735 to explain the trade winds. For a historical review see Lorenz (1967).

Although the circulation in the tropical regions can be largely explained by the Hadley cells, the midlatitude circulation is dominated by almost horizontal, wavelike flows. In fact, the Ferrel cells are only small statistical residues which result after zonal averaging of large, almost compensating, northward and southward flows in the quasi-stationary atmospheric waves [see Fig. 14(b)]. Later in this paper we will show that in midlatitudes these zonal anomalies or “eddies” are the primary transporters of momentum and heat, whereas in the tropics the symmetric Hadley circulations are the important mechanisms in the various transports. The Hadley cells tend to fluctuate in intensity and location with the seasons, being

strongest during winter.

When multiplied by  $R \cos \phi$ , the zonal wind cross section  $[\bar{u}]$  in Fig. 15(a) portrays the vertical structure of the relative angular momentum in the atmosphere. Taken together with the  $\Omega$ -angular momentum, the sum represents the absolute angular momentum of the atmosphere,  $M = \Omega R^2 \cos^2 \phi + uR \cos \phi$ . The behavior of this quantity is described by Eq. (3.30). Since  $\Omega R (=464 \text{ m s}^{-1})$  is much larger than  $u$ , one might expect the required north-south transport of absolute angular momentum to be dominated by the meridional transport of the  $\Omega$  component:

$$[v\bar{M}] = [\bar{v}]\Omega R^2 \cos^2 \phi + [\bar{v}\bar{u}]R \cos \phi . \quad (4.2)$$

However, conservation of mass requires in the long-term mean that the vertical integral of the first term vanish, so that

$$\int_0^{p_{\text{surface}}} [v\bar{M}] dp / g = \int_0^{p_{\text{surface}}} [\bar{v}\bar{u}]R \cos \phi dp / g .$$

Therefore, it is the flux of relative angular momentum that must be responsible for the horizontal transport of absolute angular momentum from the source regions in the tropics to the sink regions in the middle latitudes which is confirmed by our findings in Fig. 16. The streamlines give a good picture of the angular momentum cycle in the atmosphere with sources between 30°S and 30°N latitude, and sinks in midlatitudes. The meridional transport occurs mainly in the upper troposphere with a

strong divergence from the tropics. Figure 16 shows from top to bottom besides the observed streamlines of the flow of relative angular momentum the various modes of horizontal transport. The total meridional transport  $[\bar{v}\bar{u}]$  has been broken down into transient eddy, stationary eddy, and mean meridional circulation contributions according to the scheme

$$[\bar{v}\bar{u}] = [\overline{v'u'}] + [\bar{v}^* \bar{u}^*] + [\bar{v}][\bar{u}]. \quad (4.3)$$

Obviously, as shown in Fig. 16(b), the transient waves in the upper atmosphere dominate by far the transport when compared with the other modes. It is interesting to point out that the transports by the meridional circulations are the dominant mechanism in the lower part of the atmosphere with values of the same order of magnitude as at 200 mbars, whereas the standing eddies are of some importance only in the upper troposphere. The importance of the transient eddies, first predicted by Jeffreys (1926)

and later explained and confirmed by Starr (1948,1953) from observations, has been very important in the development of our present conception of the dynamics of the general circulation. Thus the eddies are found to be an integral part of the circulation, and even to play a primary role in the balance of angular momentum.

Starr (1948) was able to explain how the transport of momentum was achieved by horizontal motions. He showed that for the eddies to transport momentum poleward the streamlines should exhibit a preferential tilt from SW to NE in the northern hemisphere, as sketched in Fig. 17, and from NW to SE in the southern hemisphere. In the northern hemisphere with this configuration the winds from the south have a much larger eastward component than the winds from the north—i.e., the components  $u$  and  $v$  are positively correlated along a given latitude circle. Such a pattern is indeed observed to occur frequently in the upper air flow.

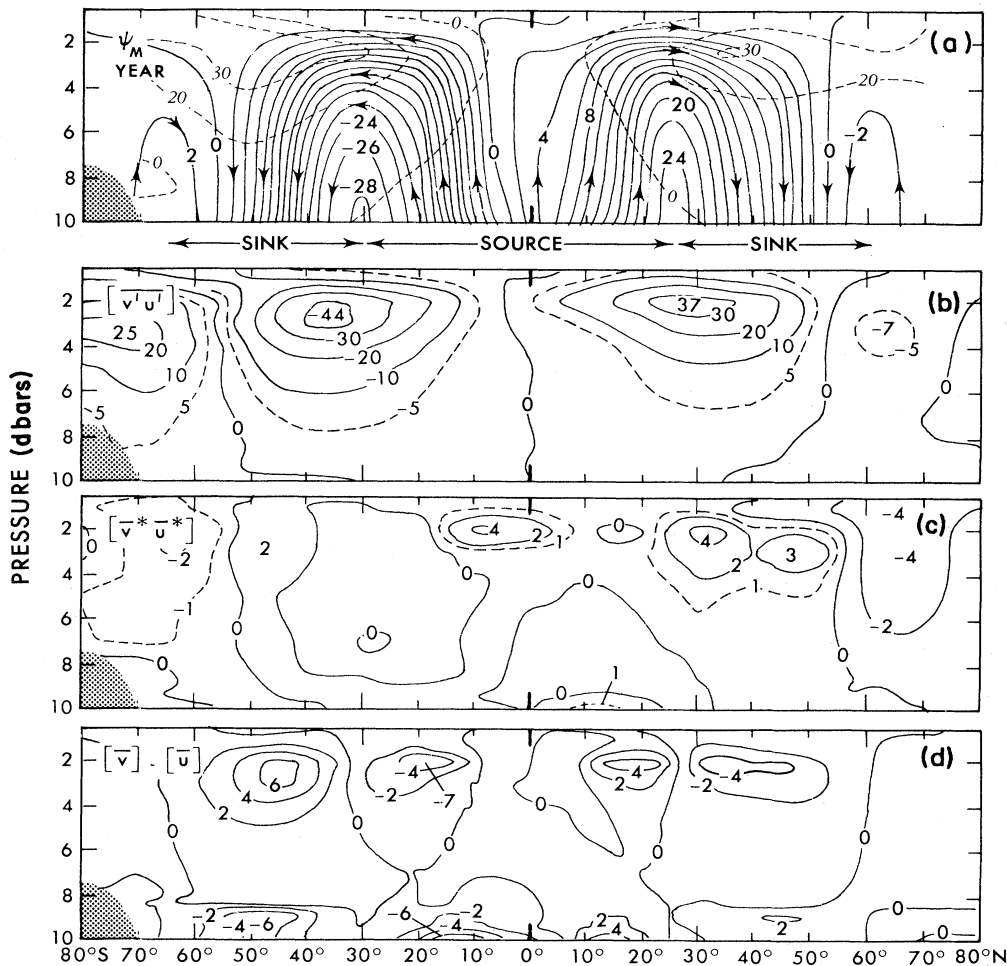


FIG. 16. Zonal mean cross sections of (a) the flow of relative angular momentum in the atmospheric branch of the cycle in units of  $10^{18} \text{ kg m}^2 \text{ s}^{-2}$  (added are some contours of the mean angular velocity  $[\bar{u}]/\cos\phi$  in  $\text{m s}^{-1}$  to show the nature of the eddy transports), (b) the northward flux of momentum by transient eddies, (c) the northward flux of momentum by stationary eddies, and (d) the northward flux of momentum by mean meridional circulations. All data are for annual mean conditions (Oort and Peixóto, 1983). The units in (b), (c), and (d) are  $\text{m}^2 \text{ s}^{-2}$ .

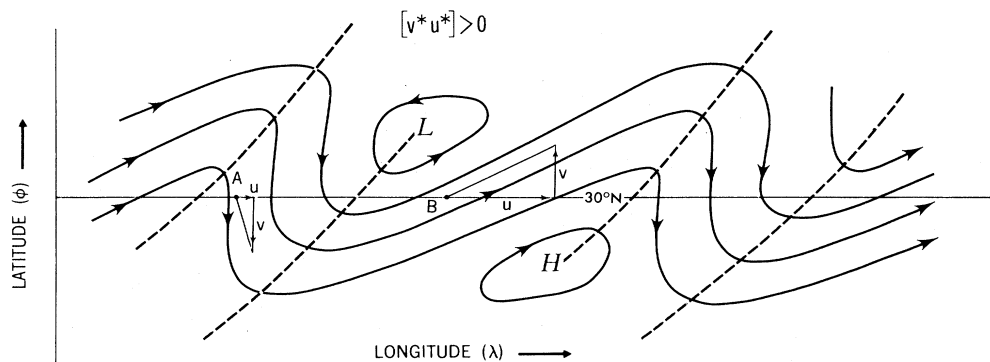


FIG. 17. Schematic picture of the dominant mechanism of northward transport of momentum by eddies in midlatitudes of the northern hemisphere. Note the preferred SW-NE tilt of the streamlines, leading to a positive value of  $[v^*u^*]$ . The transport takes place mainly in the upper troposphere. At point A the  $u$  component is much smaller than at point B, while the  $v$  components are equal in magnitude:  $|v^*u^*|$  at A <  $|v^*u^*|$  at B.

2. Angular momentum exchange with the oceans

As mentioned before (see Fig. 7), the wind stress at the ocean surface is generally thought to be the most important force in driving the general circulation of the oceans. The forces due to horizontal gradients in radiational heating or cooling, and sensible and latent heat exchange with the atmosphere (so-called thermohaline effects) certainly contribute but are believed to be of less importance, at least for the mean circulation in the upper ocean.

The zonal mean surface torque exerted by the atmosphere on the oceans plus land can be computed by using the momentum flux data (Fig. 16) and Eq. (3.30) in vertical mean form. The results obtained are shown in the profiles of Fig. 18(a) for annual, winter, and summer mean conditions. As referred to before in Eq. (3.31), the sign convention is that a positive value of the torque  $\mathcal{T}$  indicates that the atmosphere gains eastward momentum from the underlying surface. Inspection of the profiles in Fig. 18(a) shows that the oceans plus land give angular momentum to the atmosphere in the tropics and gain angular momentum from the atmosphere in middle latitudes, in agreement with the streamline picture shown before in Fig. 16(a). Seasonal changes are particularly strong near 10°N, where the Indian monsoon dominates the circulation.

To close the cycle of angular momentum, it is necessary that the angular momentum return from middle to low latitudes within the oceans and/or continents. The required equatorward transport could conceivably occur in the oceans through fluxes of the kind given in Eq. (4.3). However, since the ocean velocities are very small, it is more likely that most of this transport takes place in the continents. We conjecture that this may happen sporadically through the release of horizontal stresses in fracture zones, such as the San Andreas fault in California.

To balance the oceanic contribution to the gain or loss of angular momentum in each latitude belt, the oceans have to transmit the momentum laterally to the continents. This can be accomplished through east-west pres-

sure torques associated with differences in sea level at the continental margins as observed.

Over land not only surface friction but also mountain torques due to pressure differences across mountain ranges constitute an important mechanism for transferring angular momentum between the land and the atmosphere, as shown by Eq. (3.31). This is confirmed by the meridional profiles of the large-scale mountain torque given in Fig. 18(b). When integrated over entire zonal belts, the mountain torque is of the same sign as the fric-

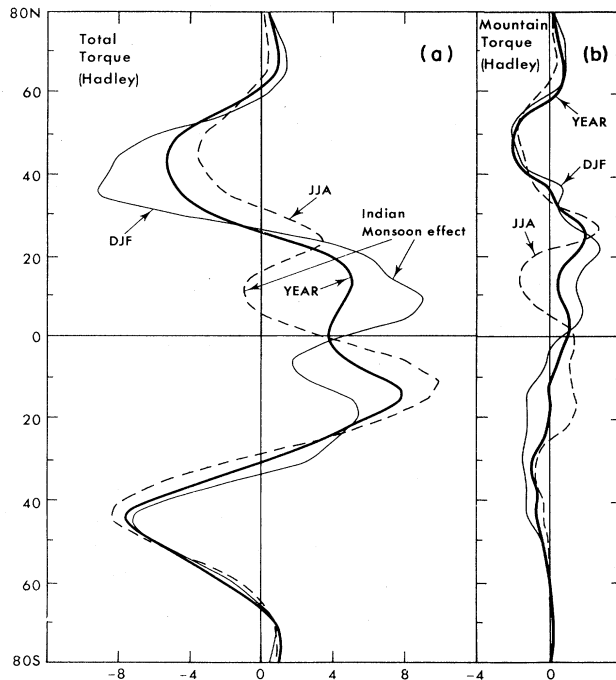


FIG. 18. Zonal mean profiles of (a) the total surface torque due to both friction and pressure differences across mountains, and (b) the mountain torque component alone. The plotted curves represent integrals over belts 5° latitude wide in Hadley ( $10^{18}$  kg m<sup>2</sup> s<sup>-2</sup>) units. The mountain torque data are from Newton (1971).

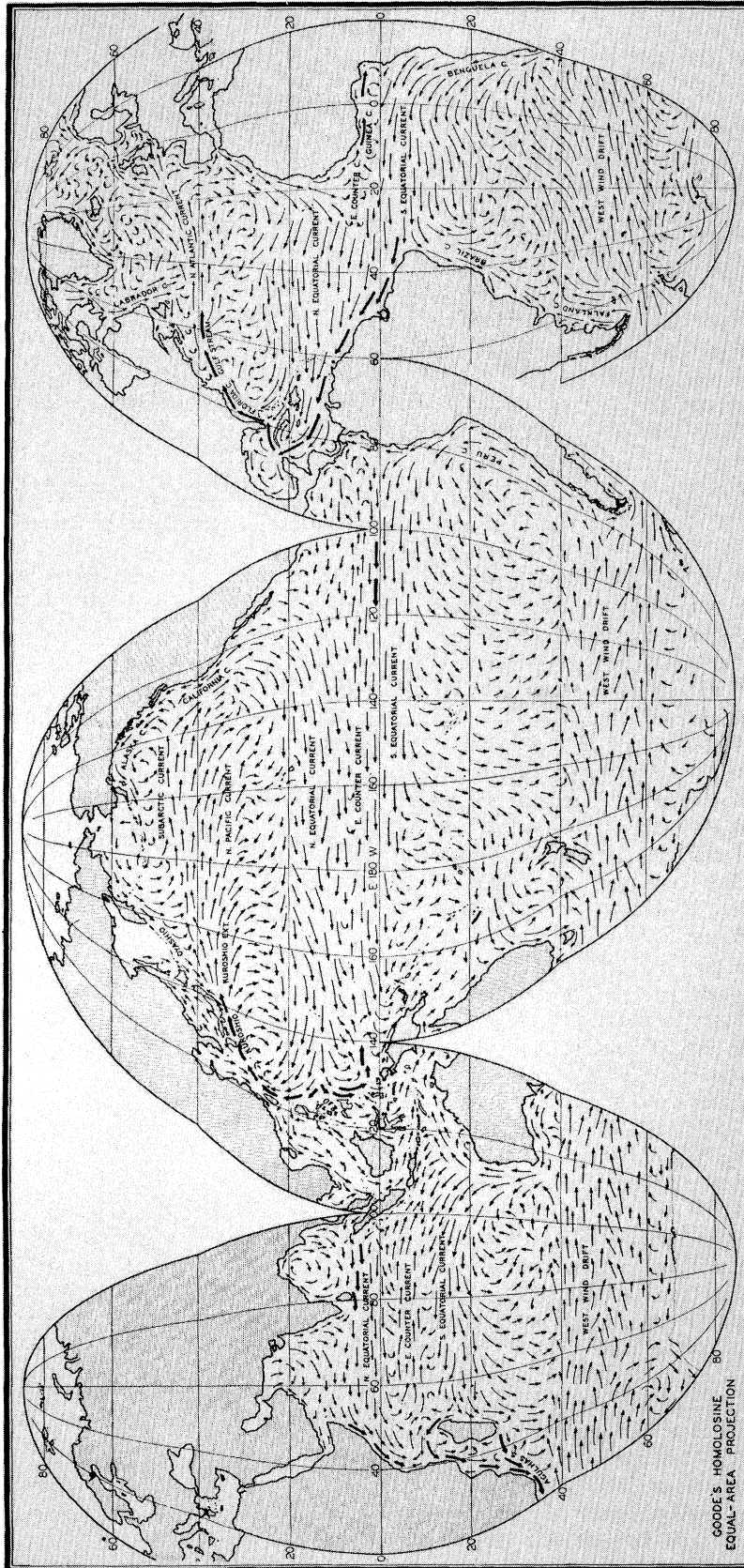


FIG. 19. Surface map of the major ocean currents during February through March from Sverdrup *et al.* (1962).

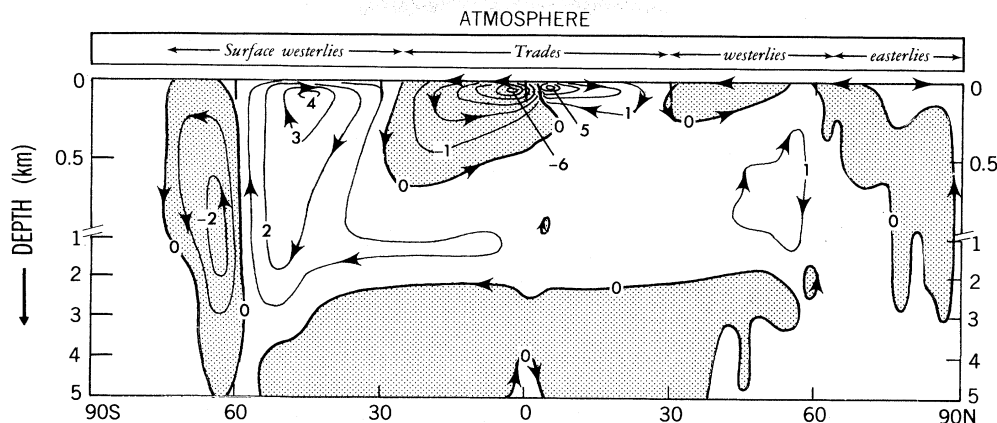


FIG. 20. Zonal mean cross section of the annual mean flow of mass (in  $10^{10} \text{ kg s}^{-1}$ ) for an ocean model constructed by Bryan and Lewis (1979). Their large-scale numerical model was driven mainly by observed wind stresses at the surface. The quantitative agreement in location and intensity of the mean meridional overturnings with those observed in the atmosphere [cf. Fig. 15(c)] is not accidental. In fact, the specification of observed wind stresses should induce a similar (but opposite) circulation as in the atmosphere. Note that the depth of penetration of the cells is determined largely by the model, and could therefore deviate appreciably from the (still) unknown real circulation.

tion torque, but smaller.

The observed oceanic currents resulting from the momentum exchange between the atmosphere and oceans are shown in Fig. 19. As expected, the currents tend to be in the same direction as the overlying mean atmospheric flow, shown before in Fig. 13. Striking exceptions to this general rule are found in the western boundary currents, such as the Gulf Stream, Kuroshio, Agulhas, and Brazil currents. Conservation of mass and planetary vorticity ( $=f + \text{curl}_2 \mathbf{v}$ ) require the existence of these very strong poleward boundary currents with maximum velocities on the order of  $1\text{--}2 \text{ m s}^{-1}$  (Stommel, 1960). We may mention that typical velocities in the interior of the ocean are on the order of  $10 \text{ cm s}^{-1}$  or less.

In order to show the vertical circulation of the oceans as a function of depth, we present in Fig. 20 a cross section of the zonal mean meridional flow derived by Bryan and Lewis (1979), using a three-dimensional world ocean model (see also Sec. VI.F). It is interesting to compare this ocean circulation with the corresponding meridional circulation in the atmosphere as given in Fig. 15(c). The patterns are similar in both media, showing the same magnitude but opposite sign.

### 3. Angular momentum exchange with the solid earth

In the preceding section we have mentioned the important role of the solid earth in what we may call the “terrestrial” branch of the angular momentum cycle, i.e., in returning eastward angular momentum from middle latitudes to the tropics. Here we want to highlight some of the global aspects of the problem.

Of course, as a whole, the atmosphere—ocean—solid

earth system has to conserve its absolute angular momentum in space when tidal torques and the comparatively small external torques exerted by, for example, the solar wind and meteor showers are neglected. However, this physical constraint does not hold for a subsystem of the total climatic system. In fact, there is observed to be a sizable seasonal cycle in the angular momentum of the global atmosphere with a stronger superrotation during northern winter. Since the oceans do not contain much relative angular momentum, the seasonal balance of the total climatic system has to be maintained by changes in the rotation rate of the earth. Astronomical observations of the length of day support this notion, and show a lengthening of the day by about  $0.7 \text{ ms}$  going from July to January, in remarkable agreement with the meteorologically inferred changes (Lambeck, 1981). The dynamic coupling between the solid earth and the atmosphere plus oceans has to take place almost instantaneously. The two mechanisms involved are the friction torque  $\mathcal{F}$  and the mountain torque  $\mathcal{P}$ , as shown by Eq. (3.31) and Fig. 18. Because the atmosphere and oceans are taken together, we should interpret  $\mathcal{F}$  as the east-west friction torque integrated globally over the land surfaces, and  $\mathcal{P}$  as the sum of the atmospheric pressure torque summed up globally for all mountain ranges and the corresponding oceanic pressure torque for all submarine ridges and the continents. (The friction stresses at the ocean bottom are negligible.)

Still more interesting than the seasonal effect is the close agreement at practically all time scales below the annual time scale, as illustrated in Fig. 21 taken from Rosen and Salstein (1983). This is, we feel, one of the most beautiful examples of a direct interaction between the various disciplines in geophysics, stressing the interdisciplinary nature of the subject.

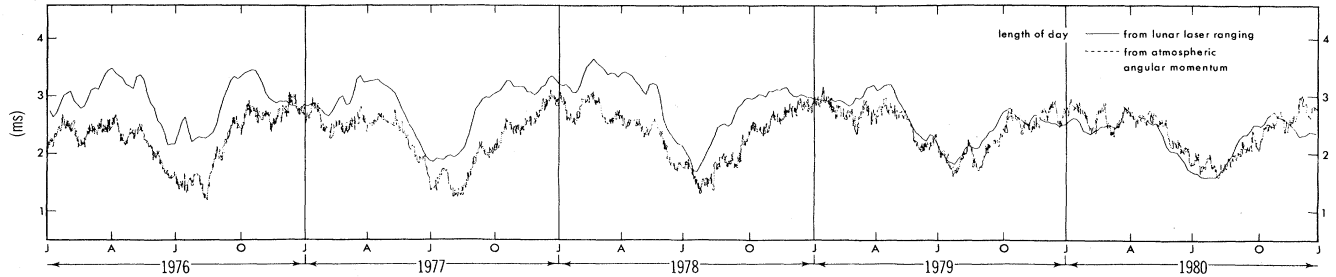


FIG. 21. Time series of the length of day for a 5-year period, January 1, 1976 through December 31, 1980, determined from lunar laser ranging observations (solid line) and also inferred from observed changes in the angular momentum of the global atmosphere (dashed line), after Rosen and Salstein (1983). The fortnightly and monthly tidal terms in the lunar laser ranging values were removed. The two curves are displaced relative to each other by an arbitrary constant amount. Markings on the abscissa indicate the first day of each midseason month ( $J$ =January 1,  $A$ =April 1,  $J$ =July 1,  $O$ =October 1).

#### D. Water balance

##### 1. Water vapor in the atmosphere

The water vapor in the atmosphere when condensed would form a layer of only about 0.025 m of liquid water over the surface of the earth. Masswise this water vapor is, of course, negligible compared with the oceanic water mass, with an average depth of about 4000 m. Nevertheless, water vapor plays a central role in the earth's climate. For example, next to direct radiational heating, latent heat release is the most important source of heat for the atmosphere. Furthermore, a substantial fraction of the total poleward flux of energy takes place in the form of latent heat [see Eq. (3.27)].

The global distribution of water vapor is shown in Fig. 22. As expected, more water vapor is found in the tropics and in general over the oceans, where the warmer air can

hold more water vapor. Less water is found over the desert regions and over mountains.

In a continuous sequence, evaporation supplies the atmospheric branch of the hydrological cycle with the needed water vapor, while precipitation removes water from the atmosphere and returns it to the terrestrial branch of the cycle. Evaporation is a very difficult quantity to measure directly from evaporimeters (open pans). Indeed, the surrounding atmospheric conditions are disturbed by the extra water vapor released by the evaporimeter. In other words, there is interference between the measuring instrument and the quantity to be measured. Usually evaporation is computed over the oceans using an empirical, bulk aerodynamical formula together with observed surface wind, temperature, and humidity data [see Fig. 23(a)]. Over land, evapotranspiration from plants and trees makes the problem even less tractable. On the other hand, precipitation [Fig. 23(b)] can be measured fairly

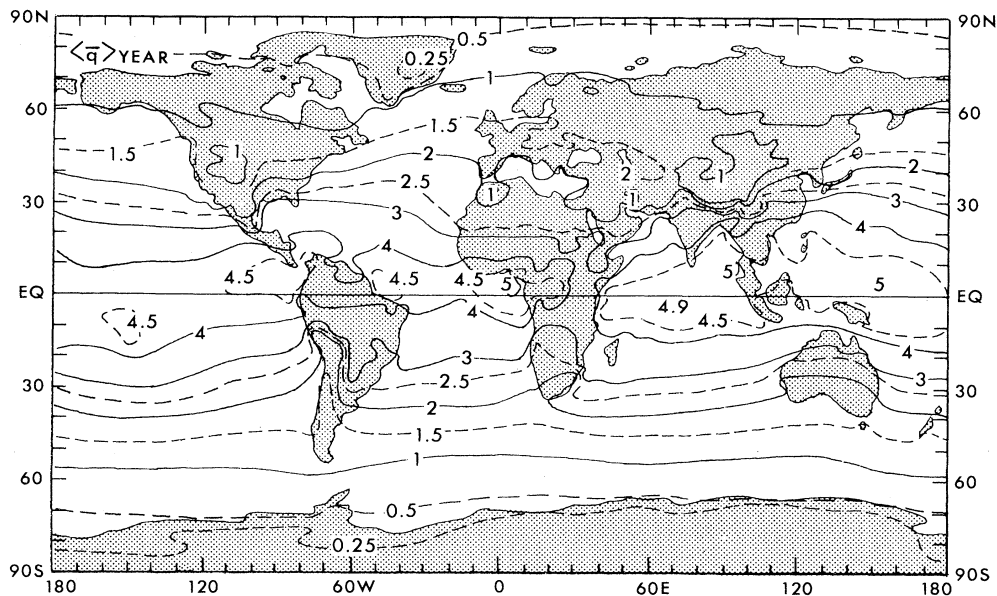


FIG. 22. Global distribution of the precipitable water in the atmosphere for annual mean conditions in units of  $10 \text{ kg m}^{-2}$  (Peixóto and Oort, 1983). Note that the global mean value is about  $25 \text{ kg m}^{-2}$ . When multiplied by  $L$  the isolines represent the latent energy.

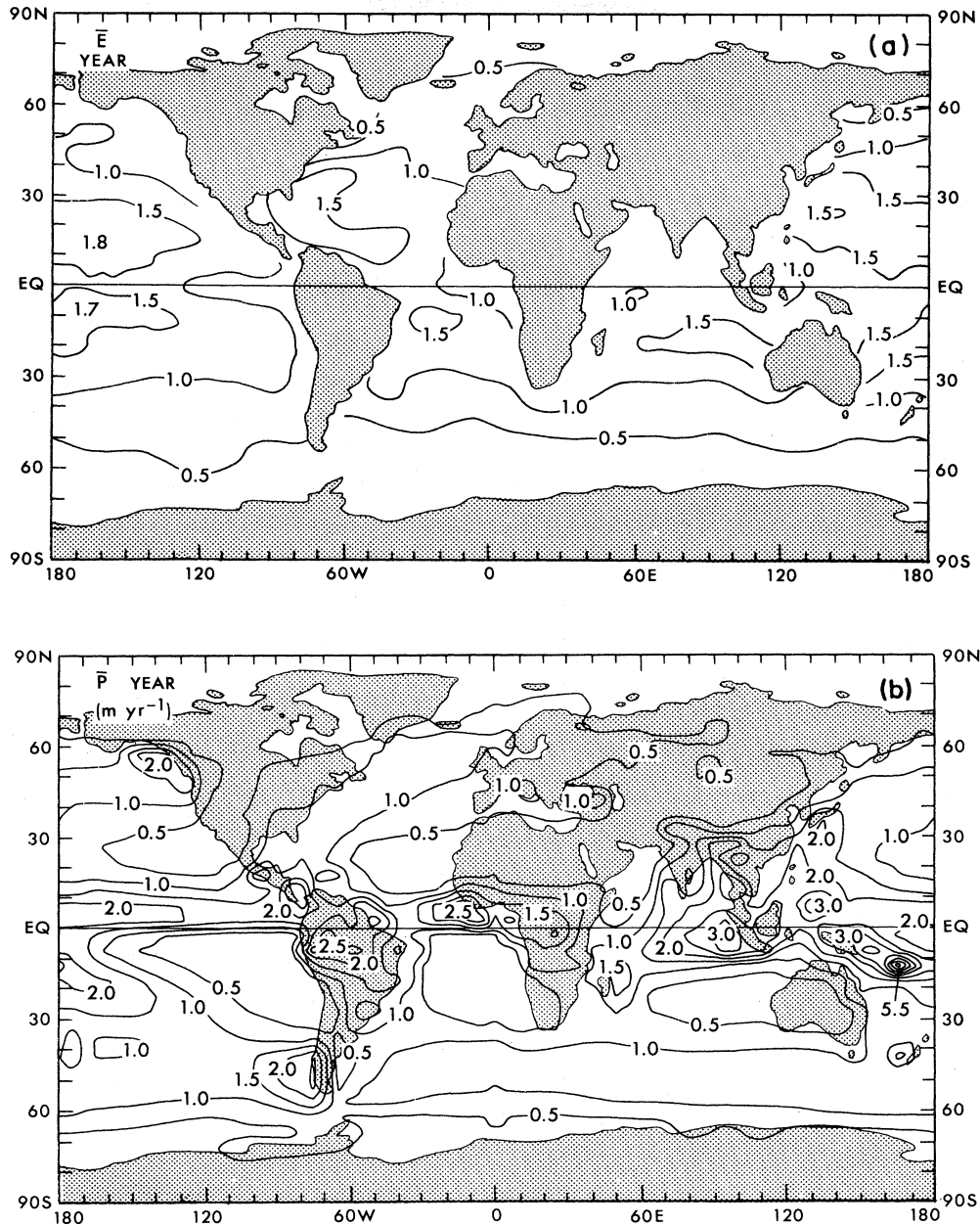


FIG. 23. (a) Global distribution of the estimated evaporation rate over the oceans in units of  $\text{m yr}^{-1}$ . The values are tentative; the uncertainties are estimated to be on the order of 50% (Peixóto and Oort, 1983). (b) Global distribution of the observed precipitation rate for annual mean conditions, after Jaeger (1976), in units of  $\text{m yr}^{-1}$ . Note that a precipitation rate of  $1 \text{ m yr}^{-1}$  corresponds to a release of latent heat in the atmosphere of about  $79 \text{ W m}^{-2}$ .

well over land, although a dense network of rain gauges is needed to capture the many local, topographically related anomalies. Over the oceans, quantitative estimates of precipitation are difficult to make from moving ships, while island data are often unrepresentative of open ocean conditions. Thus, unfortunately, two of the basic parameters of the hydrological cycle and climate, i.e., evaporation and precipitation, are poorly known over large portions of the globe. We will see later that the difference, evaporation minus precipitation,  $\bar{E} - \bar{P}$ , can be measured probably

much more accurately than either component itself using the aerological method [see later discussion of Eq. (4.4) and Fig. 25(b)].

The global mean evaporation and precipitation are estimated to be on the order of  $1 \text{ m/year}$ . Combining this estimate with the earlier estimate of  $0.025 \text{ m}$  water in the atmosphere, we may derive a recycling time of almost 10 days for the atmospheric water vapor.

The vertical distribution of water vapor in the atmosphere is presented in Fig. 24(a). It shows that the water



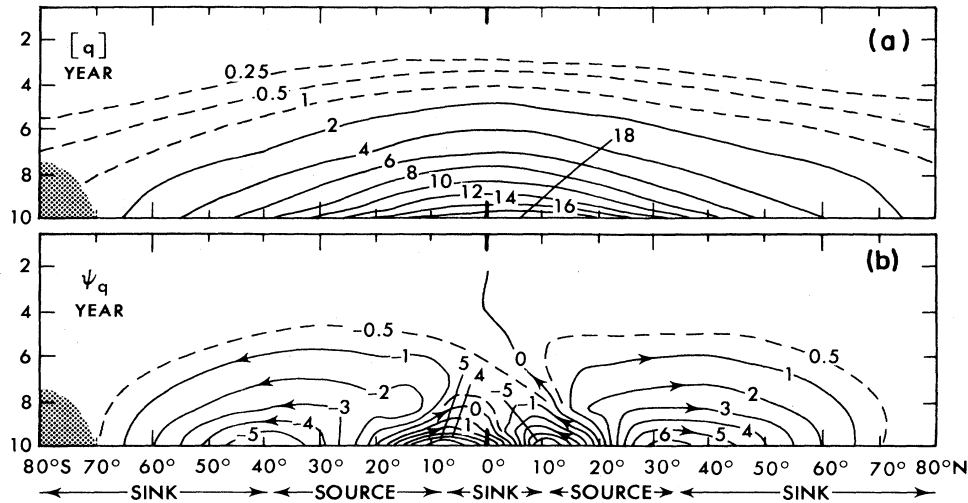


FIG. 24. Zonal mean cross sections of (a) the specific humidity in units of  $\text{g kg}^{-1}$  (i.e., g water vapor per kg moist air) and (b) the flow of water substance,  $\psi_q$  (vapor plus liquid plus solid), in the atmospheric branch of the hydrological cycle in units of  $10^8 \text{ kg s}^{-1}$  for annual mean conditions, from Peixóto and Oort (1983).

is strongly concentrated near the surface in the lower troposphere. In fact, more than 90% of the water vapor is found below the 500-mbars level, i.e., in the lower half of the atmosphere.

The zonal mean circulation of water substance (vapor plus liquid plus solid) in the atmospheric branch of the hydrological cycle can be computed from the basic rawinsonde observations of the meridional wind and the specific humidity using certain simplifying assumptions and a streamfunction,  $\psi_q$ , similar to the one defined by (4.1) (Peixóto and Oort, 1983). We present the resulting streamflow in Fig. 24(b), which shows a source region between about  $10^\circ$  and  $35^\circ$  latitude in each hemisphere. These are the climatic zones where most of the evaporation takes place from the ocean surface, and where the major deserts are located over land. Strong convergence is found in the equatorial sink region, with heavy precipitation occurring slightly north of the equator in the so-called Intertropical Convergence Zone, where the tropical cells of the northern and southern hemispheres meet [see Fig. 15(c)]. Finally, some of the water vapor is transported poleward from the subtropics to feed the midlatitude depressions, where precipitation dominates over evaporation.

The main features of the water vapor circulation in the atmosphere and its relation to the underlying surface are shown with more geographical detail in Figs. 25(a) and 25(b) in the form of global streamlines and water vapor divergence. These quantities were computed again with wind and moisture data from the rawinsonde network. In the annual mean (steady state) case, the divergence of the vertically integrated vapor transport,

$$\mathbf{W} \equiv \int_0^P \text{surface} \nabla \bar{q} dp / g,$$

is equal to the difference between surface evaporation and precipitation:

$$\text{div} \bar{\mathbf{W}} = \bar{E} - \bar{P}. \quad (4.4)$$

Thus negative values on the divergence map indicate areas where precipitation exceeds evaporation, and positive values where evaporation dominates. Although the map is rather patchy due to difficulties involved in computing the divergence from the sparse rawinsonde observations, we can recognize some important features. Convergence is found over the headwaters and drainage basins of the large river systems, such as the Amazon River in South America, the Ubangi, Congo, Senegal, and Blue Nile Rivers in Africa and the Indus, Ganges, Mekong, and Yangtze Rivers in southeastern Asia.

## 2. Exchange of water with oceans and land

As shown in Fig. 25(a), the main sources of water vapor for the atmosphere are located over the oceans in subtropical latitudes, whereas the main sinks occur in the confluence zones in the equatorial and midlatitude belts. The water vapor released from the oceanic sources is partly transported to the continents, where it precipitates, feeding the river runoff in the various drainage basins. Of course, the total import of water vapor over the continents is balanced in the long run by the runoff from the continents into the oceans.

A very interesting and still controversial issue is the divergence found over land in the major deserts of Africa, Arabia, and Australia. This effect was first discussed by Starr and Peixóto (1958). Since some river outflow does occur from the deserts, considerable amounts of underground flow have to occur from less arid regions to supply the necessary water and thereby counterbalance the observed atmospheric divergence.

Another important inference we can make from the divergence map in Fig. 25(b) concerns ocean salinity. In



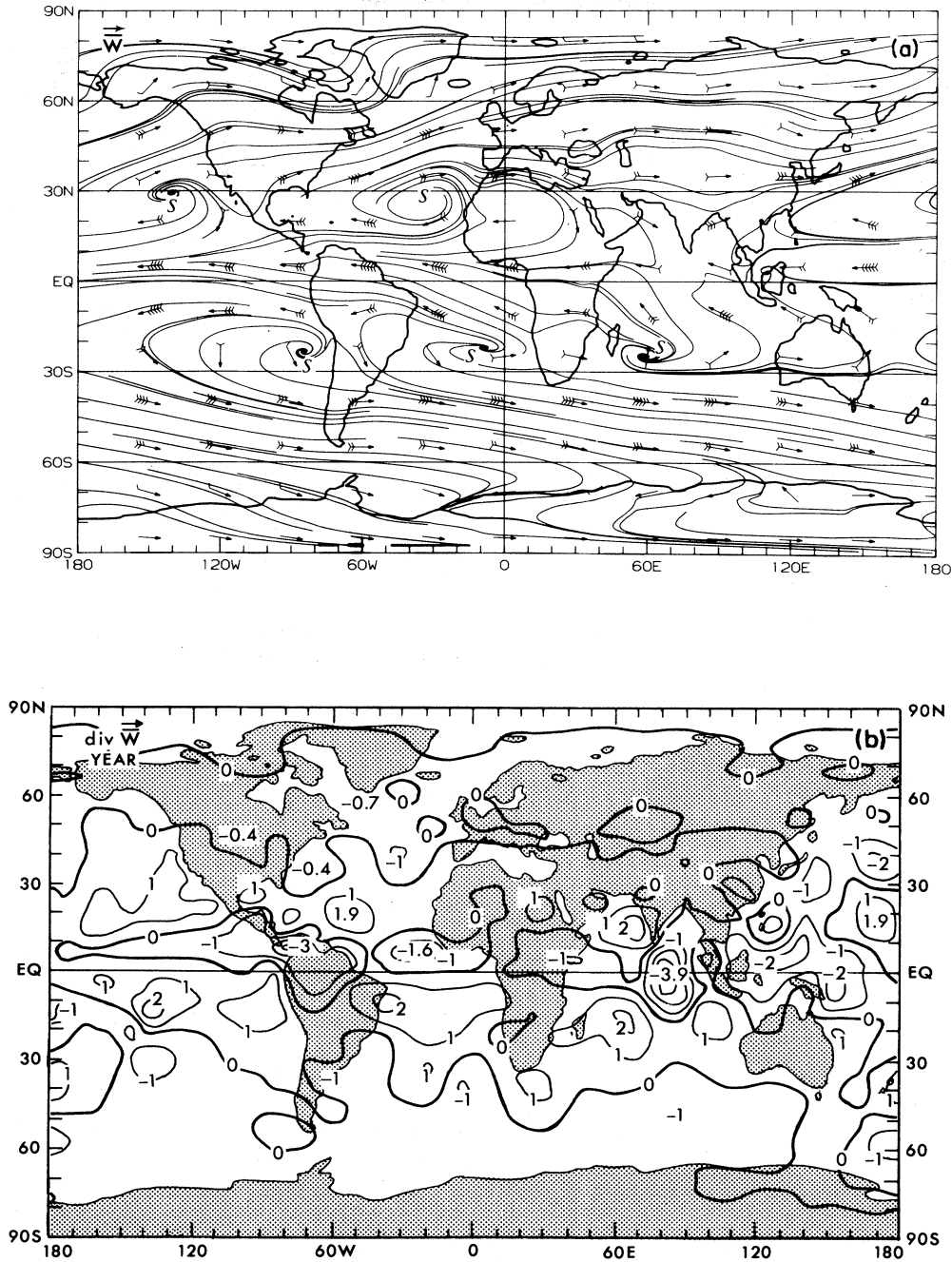


FIG. 25. (a) Global distribution of horizontal streamlines of the vertically integrated transport of water vapor,  $\bar{W}$ , for annual mean conditions. The source regions are indicated by *S*. The sink regions are mainly confined to the confluence zones near the equator and in midlatitudes. (b) Global distribution of the horizontal divergence of the vertically integrated transport of water vapor,  $\text{div } \bar{W}$ , for annual mean conditions in units of  $\text{m yr}^{-1}$ . Positive values indicate areas of divergence or source regions ( $\bar{E} - \bar{P} > 0$ ) for atmospheric water vapor, and negative value areas of convergence or sink regions ( $\bar{E} - \bar{P} < 0$ ).

the subtropical oceans, where evaporation much exceeds precipitation, one would expect, on the average, to find more saline water, but in the equatorial and middle and high latitudes more fresh water. Inspection of the map of observed surface salinity in Fig. 26 shows, indeed, a high

correlation with the divergence field. Although horizontal and vertical mixing connected with ocean currents and eddies will tend to smooth out some of these features, the atmospheric forcing is strong enough to impress its signature on the long-term mean salinity distribution in the

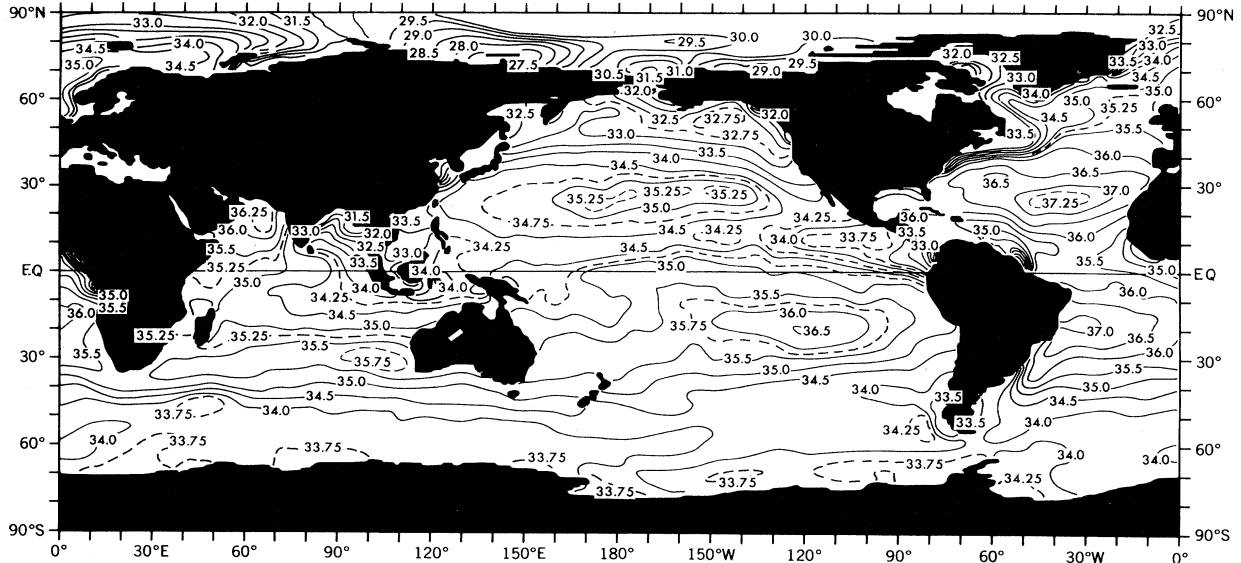


FIG. 26. Global distribution of annual mean salinity at the ocean surface in units of ‰ from Levitus (1983).

oceans. The annual mean latitudinal profiles of  $[\bar{E} - \bar{P}]$  and  $[\bar{S}_0]$  in Fig. 27 summarize well the previous discussion.

E. Energy balance

1. Energy in the atmosphere

As said before, energy in the atmosphere occurs in many different forms as shown in Eq. (3.14). Most im-

portant (Oort and Peixóto, 1983), are the internal energy (70.4%), potential energy (27.1%), latent heat (2.5%), and kinetic energy (0.05%). The horizontal distribution of the internal energy (and enthalpy) is presented in Fig. 28 in the form of a vertical-mean temperature map. The distribution of temperature closely resembles that of net radiation at the top of the atmosphere shown earlier in Fig. 10, where the  $-20^\circ\text{C}$  isotherm corresponds roughly with the zero isoline of net radiation. Of course, other factors, such as the release of latent heat [see precipitation map in Fig. 23(b)] and the redistribution of sensible heat by the highly turbulent atmospheric flow, are needed to maintain the observed thermal state of the atmosphere. The zonal anomalies in the midlatitude temperature field, with relatively low temperatures over the continents and high temperatures over the oceans, must be due to the differences in heat capacity of the underlying surface and to the greater release of latent heat over the oceans, where the precipitation is larger (mainly in winter).

It is not necessary to present a map of the geopotential energy, since such a map would be practically identical to the map of internal energy except for a constant multiplication factor (namely,  $R/c_v$ ).

The latent heat distribution was shown in the preceding section in terms of specific humidity (Fig. 22).

Finally, the kinetic energy is given in Fig. 29. The midlatitude maxima are associated with the rather steady subtropical jet streams as well as with the strongly meandering polar jets. There are two distinct peaks in the northern hemisphere winds just east of Japan and east of the North American continent, whereas an almost continuous belt of high winds is found between  $30^\circ\text{S}$  and  $60^\circ\text{S}$  in the southern hemisphere.

To summarize, the energy distributions in the atmosphere vertically integrated zonal-mean profiles of the various forms of energy are put together in Fig. 30. For easy comparison an equivalent energy scale is added at

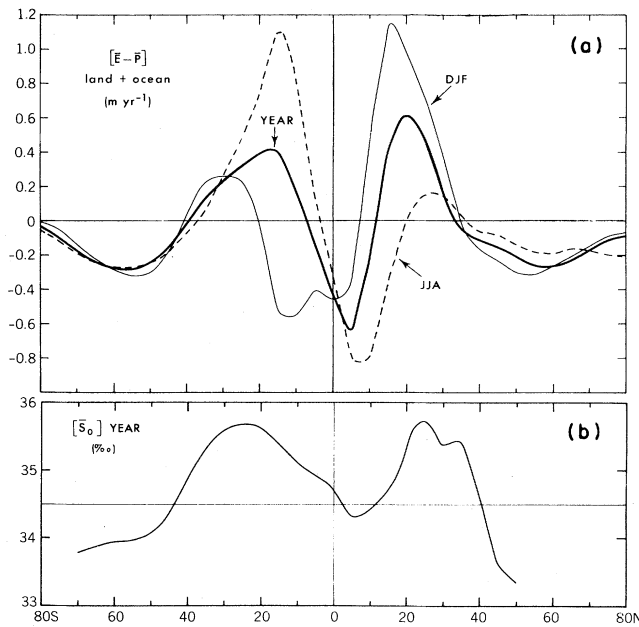


FIG. 27. Zonal mean profiles of (a) the evaporation minus precipitation rate,  $\bar{E} - \bar{P}$ , and (b) the surface salinity  $\bar{S}_0$  in the world oceans as computed by zonal averaging of the corresponding divergence and salinity maps in Figs. 25(b) and 26, respectively. Seasonal curves are also given for  $[\bar{E} - \bar{P}]$ .

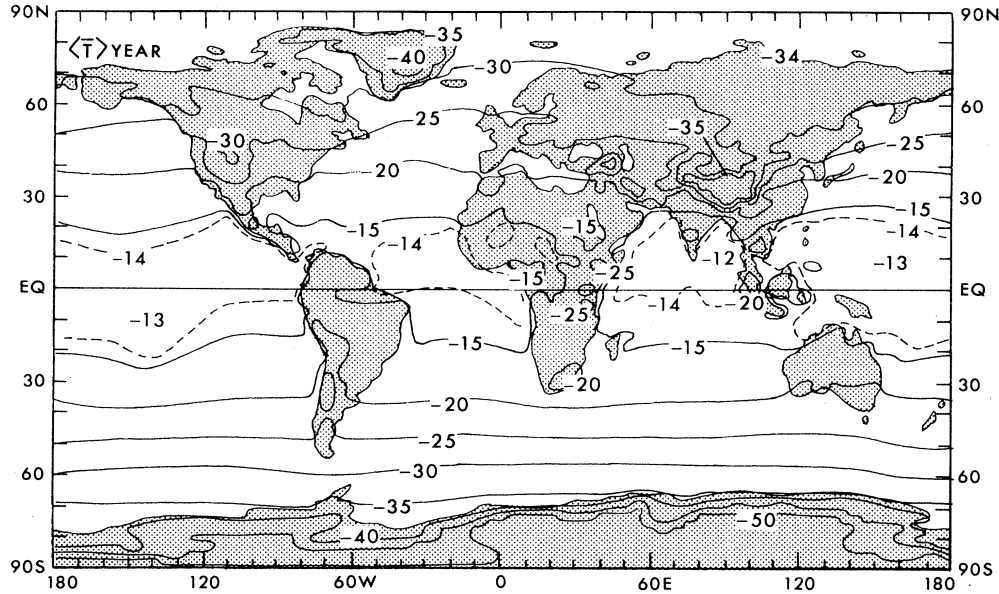


FIG. 28. Global distribution of the vertical mean temperature for annual mean conditions in  $^{\circ}\text{C}$ , from Oort and Peixóto (1983). When multiplied by  $c_v$  the isolines represent the internal energy, when multiplied by  $R$  the potential energy, and when multiplied by  $c_p$  the total enthalpy of the atmosphere.

the right-hand side of the figure. The values of the profiles in energy units indicate the relative magnitude of the various components, showing, for example, that the kinetic energy is 3 orders of magnitude smaller than the internal energy. They further reveal a greater energy in the summer hemisphere except for the kinetic energy, and some symmetry with respect to the equator between the northern and southern hemispheres. The two maxima in the kinetic energy profiles are associated with the jet streams.

To complete the description of the three-dimensional structure of the atmospheric energy vertical cross sections of the mean zonal temperature and kinetic energy are given in Fig. 31. The temperature (internal energy or enthalpy) distribution reveals the existence of the tropopause with an inversion of temperature. The vertical temperature gradient is quite pronounced over the entire globe. On the other hand, the horizontal gradient in temperature is most important in middle latitudes below the mean jet streams, where, in other words, the baroclinicity

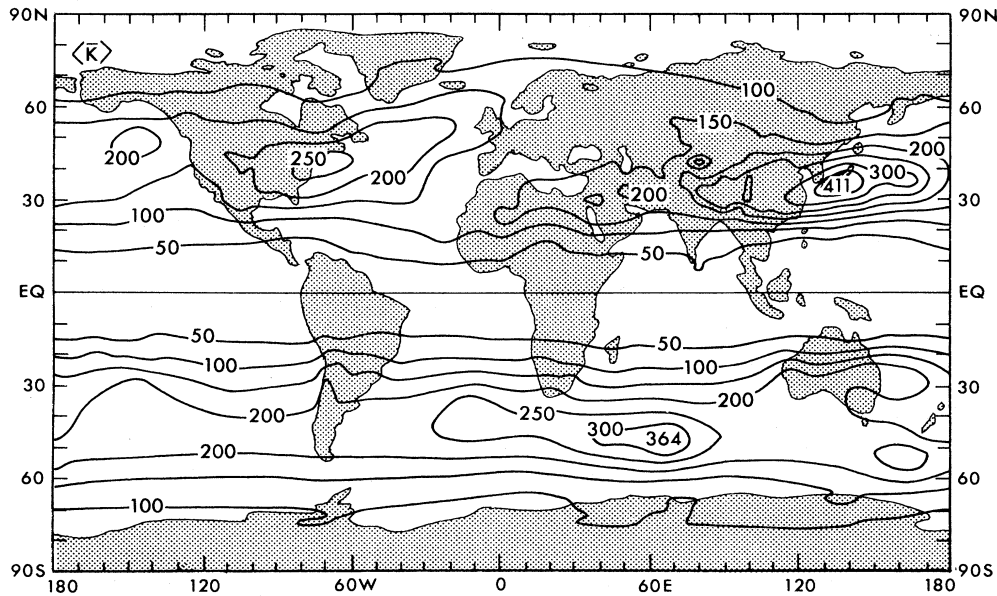


FIG. 29. Global distribution of the vertical mean kinetic energy for annual mean conditions in  $\text{m}^2 \text{s}^{-2}$ .

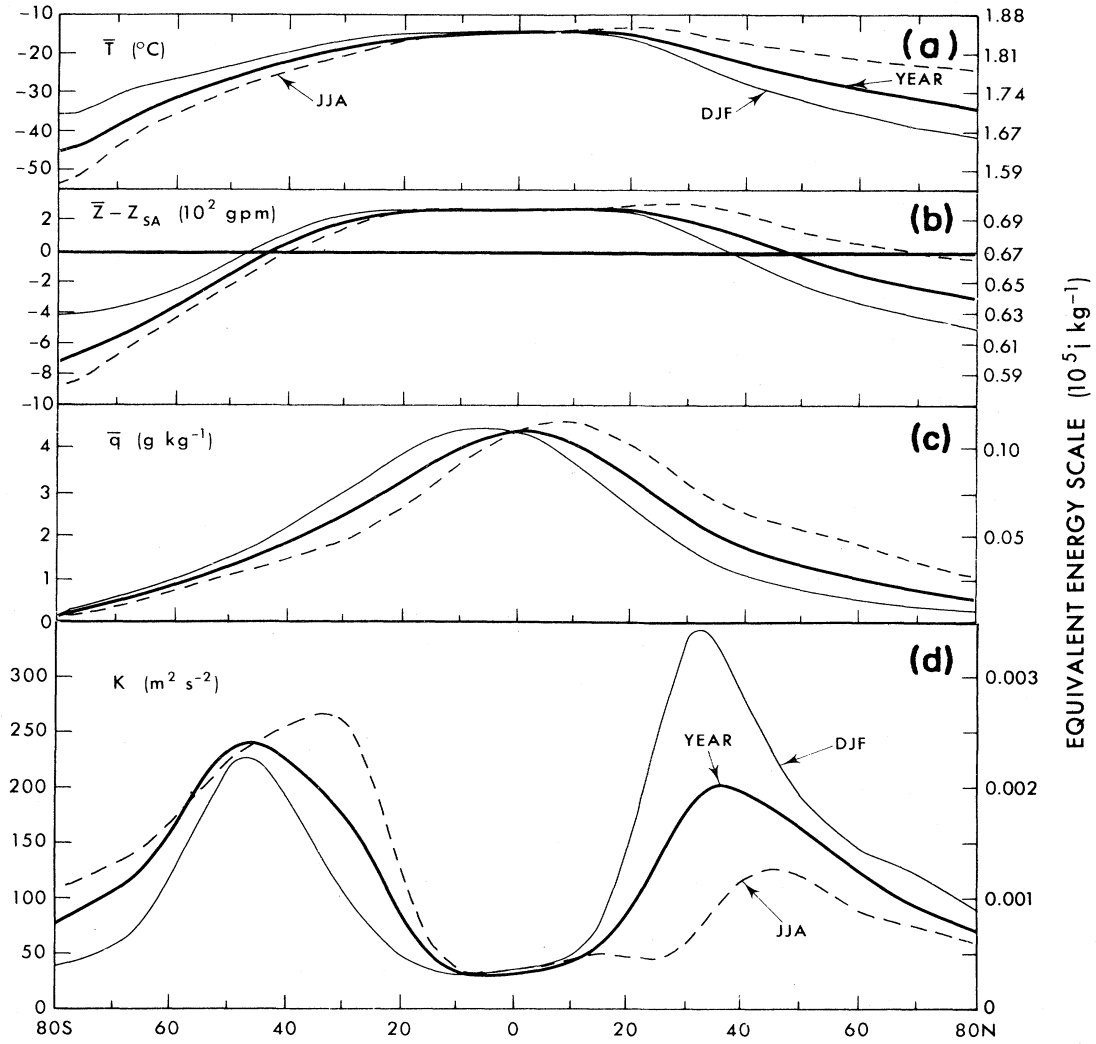


FIG. 30. Zonal mean profiles of the vertical mean (a) temperature in  $^{\circ}\text{C}$ , (b) geopotential height in gpm (with a standard atmospheric value,  $z_{SA}$ , subtracted), (c) specific humidity in  $\text{g kg}^{-1}$  and (d) kinetic energy in  $\text{m}^2 \text{s}^{-2}$ . An equivalent energy scale is given on the right-hand side margin of the figure.

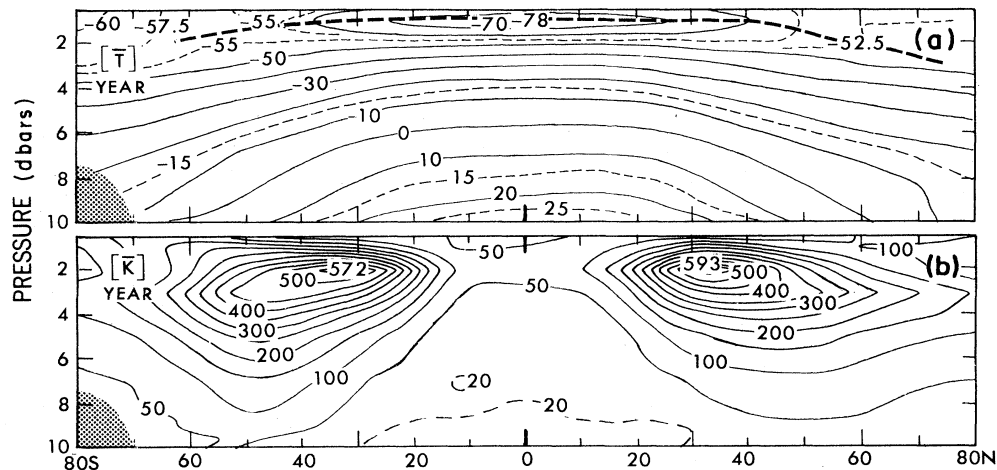


FIG. 31. Zonal mean cross sections of (a) temperature in  $^{\circ}\text{C}$  and (b) kinetic energy in  $\text{m}^2 \text{s}^{-2}$  for annual mean conditions. The temperature attains a minimum at the mean position of the tropopause (long-dashed line). The maxima in kinetic energy correspond to the average positions of the jet streams, centered above the latitude of maximum horizontal temperature gradient and just below the tropopause.

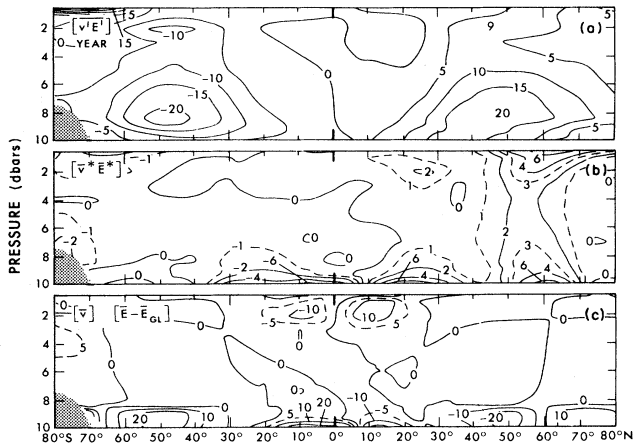


FIG. 32. Zonal mean cross sections of the northward transport of total energy by (a) transient eddies, (b) stationary eddies, and (c) mean meridional circulations for annual mean conditions in  $^{\circ}\text{C m s}^{-1}$ , from Oort and Peixóto (1983).

of the atmosphere is largest. The cross section of kinetic energy shows again two maxima associated with the jet streams in midlatitudes located just below the tropopause.

The poleward energy flux that (together with the vertical energy flux from the ocean surface) maintains the

temperature distribution against the continuous radiational heating in low latitudes and radiational cooling in high latitudes is given in Fig. 32 [see also Eq. (3.27)]. These graphs show clearly that the eddies are the dominant mechanism of transfer in middle and high latitudes, whereas the mean meridional circulations are more important at low latitudes. Associated with the observed stronger pole-to-equator temperature gradient, the transient eddies are found to be better developed in the southern than in the northern hemisphere, contrary to the behavior of the standing eddies. Thus, adding the stationary and transient eddies together, one finds the poleward transports of energy to be stronger in the northern hemisphere. The eddy transports are accomplished by disturbances along the polar front as shown on daily weather maps with a poleward flow of warm, humid air and an equatorward flow of cold, dry air, as shown schematically in Fig. 33(a). Thus the exchange of equal masses of air, but with different temperature and humidity, across a given latitude circle leads to a net poleward transport of heat and moisture like that which occurred in the case of the transfer of angular momentum (see Fig. 17). In fact, a strong positive correlation is observed between the meridional wind component  $v$ , and the temperature  $T$ , and moisture  $q$ .

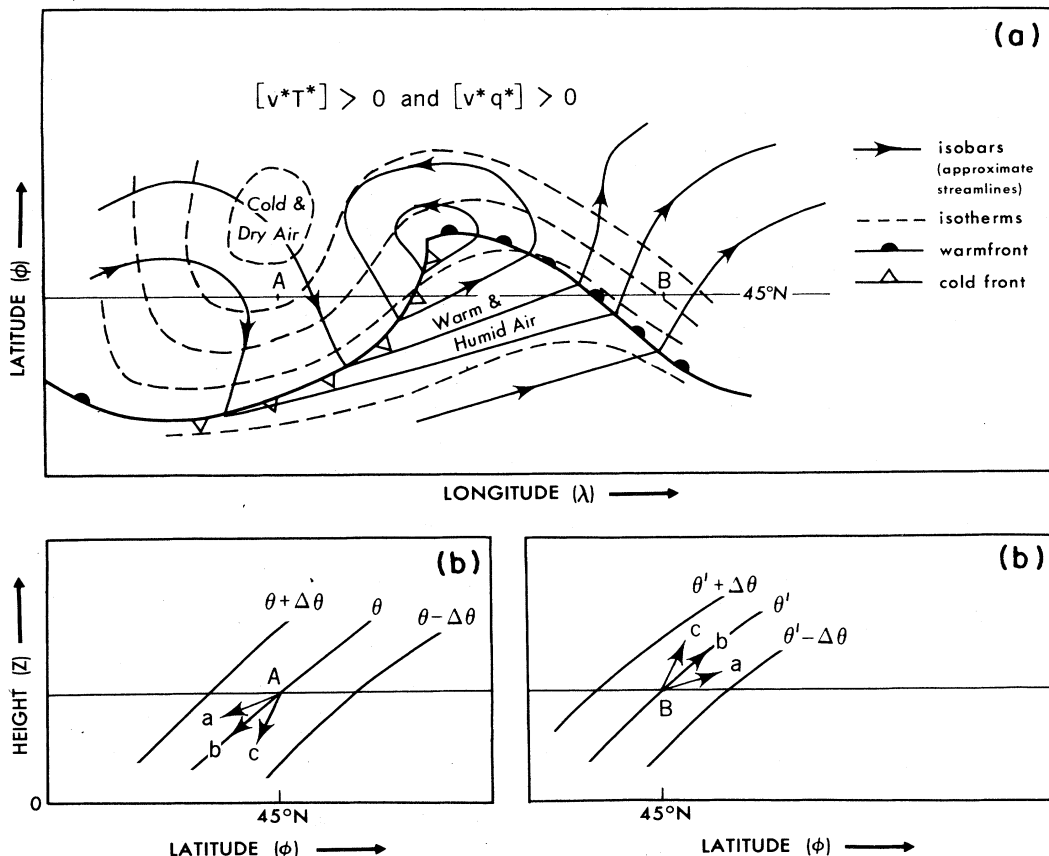


FIG. 33. Schematic picture of the dominant mechanism of northward transport of sensible and latent heat by eddies in midlatitudes of the northern hemisphere. The transport takes place mainly in the lower troposphere. Shown are (a) latitude-vs-longitude and (b) height-vs-latitude cross sections.

Let us now take a Lagrangian point of view. The poleward particle trajectories in the eddies must be slightly inclined with respect to the horizontal carrying warmer air poleward and upward, so that the necessary kinetic energy will be released and the general circulation be kept going [see Fig. 33(b)]. If the trajectories had the same slope as the isentropes (case *b*), the process would be adiabatic (isentropic) and no heat would be transported or kinetic energy released. If for point *B* the slope were greater than the slope of the isentropes (case *c*), cooler rather than warmer particles would be transported poleward, leading to a cooling instead of the required warming. On the other hand, for point *B* in case *a* the motions would become dynamically unstable, because in their new position the particles would be potentially warmer than their environment and would accelerate away from their original position. For point *A* to release kinetic energy the slope of the particle trajectories would again have to be smaller than the slope of the isentrope (case *a*), so that the temperature of the particle in its new position would become colder than its environment and the particle would continue to sink.

In order for this mechanism to operate, it is obvious that the isentropes have to be inclined with respect to the pressure surfaces, and that the atmosphere be baroclinic. We therefore find that the perturbations (eddies) grow, leading to what is called baroclinic instability (Charney, 1947; Eady, 1949). The perturbations are called baroclinic because the horizontal gradient of the mean temperature plays an essential role in their development. These processes are an essential element of the general circulation of the atmosphere, and thus of the climate. They may be regarded the result of macroscale slant convection.

Let us synthesize the present discussion on atmospheric energy with the aid of a vertical streamline section. Using the horizontal transports of energy in the atmosphere obtained from rawinsonde observations (Fig. 32) and the net radiation measured by satellite at the top of the atmosphere [Fig. 11(f)], we can calculate a zonal-mean streamfunction [similar to the mass streamfunction in (4.1)] for the flow of total energy which now includes radiation. The result is shown in Fig. 34. Striking is the large inflow of (short-wave solar) radiation in the tropics that largely penetrates through the atmosphere and is finally absorbed at the earth's surface mainly by the oceans. In fact, the continents with their vegetation absorb in the long run as much radiant energy as they lose in the form

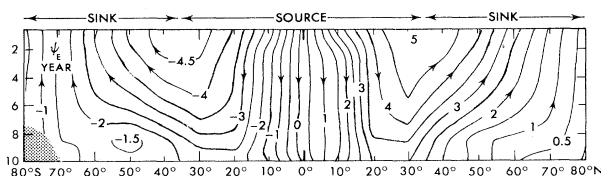


FIG. 34. Zonal mean cross section of the flow of energy in the atmospheric branch of the energy cycle for annual mean conditions in  $10^{15}$  W, from Oort and Peixóto (1983).

of latent heat, sensible heat, and infrared radiation, whereas the oceans, being fluid, can dispose of the excess of absorbed energy by the export of heat in ocean currents. Most of the energy absorbed by the climatic system returns to space in the form of infrared radiation at middle and high latitudes. The vertical tilt of the streamlines is a consequence of the atmospheric transports of energy, i.e., the symmetrical Hadley cells at low latitudes and the eddies in middle and high latitudes. The values of the streamlines that intersect the earth's surface represent the required oceanic heat transports that will be discussed in the next section.

## 2. Energy in the oceans

Even more so than for the atmosphere, the kinetic energy in the oceans constitutes only a minute fraction of the oceanic potential and internal energy. Therefore, it will be useful to introduce the notion of "available" total potential energy. Later, in Sec. V.A, we will try to separate the reservoir of potential plus internal energy into an available and an unavailable part. Only the first part would participate in the conversion to and from kinetic energy. As said before, typical ocean velocities are on the order of  $1\text{--}10\text{ cm s}^{-1}$  (except in the western boundary currents and near the surface), whereas typical wind speeds in the atmosphere were found to be about  $10\text{ m s}^{-1}$ .

The horizontal temperature (or internal energy) distribution at the ocean surface is shown in Fig. 35, while the vertical structure of temperature and salinity is given in the form of zonal mean depth versus latitude sections in Figs. 36 and 37. To first order the sea surface isotherms (Fig. 35) are zonal in character with some meridional distortion associated with the warm poleward currents (e.g., Gulf Stream and Kuroshio) and cold equatorward current systems (e.g., along the coasts of California and Peru).

The vertical sections in Figs. 36 and 37 show a prominent broad wedge of warm, saline water in each hemisphere penetrating downward near  $30^\circ$  latitude. As shown before by the meridional circulation in Fig. 20, these features are associated with convergence in the surface layers ("Ekman drift"). Similarly, the region of relatively cold and less saline water in between at equatorial latitudes is caused by upwelling from deeper layers associated with divergence in the surface layers. In spite of some spatial smoothing, this upwelling is also evident on the surface maps of temperature (Fig. 35) and salinity (Fig. 26), especially in the eastern parts of the equatorial Pacific and Atlantic Oceans.

As far as the energy transports are concerned, very little direct information is available for the oceans. One method of evaluating the transport, the so-called planetary energy balance method (Oort and Vonder Haar, 1976), infers the oceanic transport from a combination of satellite-derived net radiation values at the top of the atmosphere and global atmospheric transport data. Thus the oceanic heat transport was computed as the difference

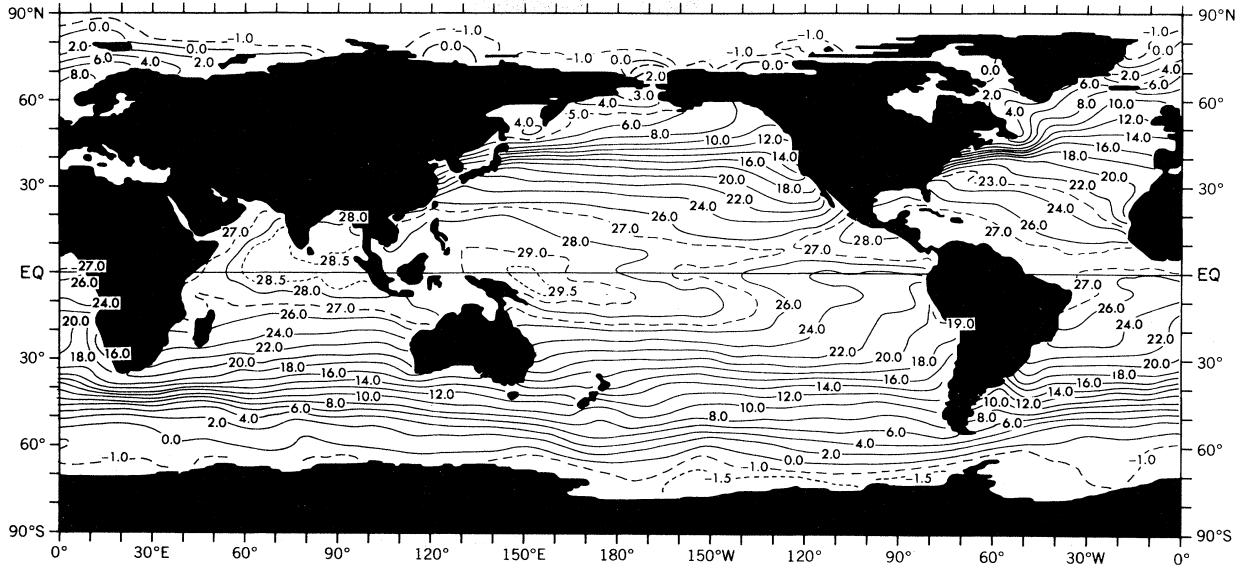


FIG. 35. Global distribution of sea surface temperature for annual mean conditions in °C, from Levitus (1982).

between the total energy transport required for radiative balance [Fig. 11(f)] and the observed atmospheric energy transport (Fig. 32). The three transport profiles are plotted in Fig. 38. This residual method suggests a strong poleward flow of heat by the oceans with a maximum of about  $3 \times 10^{15}$  W near 25° latitude. This value is about the same magnitude as the midlatitude maximum in atmospheric energy transport that occurs near 45° lati-

tude. However, many of the other, more classical methods of evaluating the oceanic heat transport (Hall and Bryden, 1981) lead to smaller maximum values on the order of  $(1-2) \times 10^{15}$  W, but located at about the same latitude in the tropics. The scientific debate on what the real transports are, is still going on, and extensive field programs are being planned to resolve this problem (Dobson *et al.*, 1982). The issue is an important one for cli-

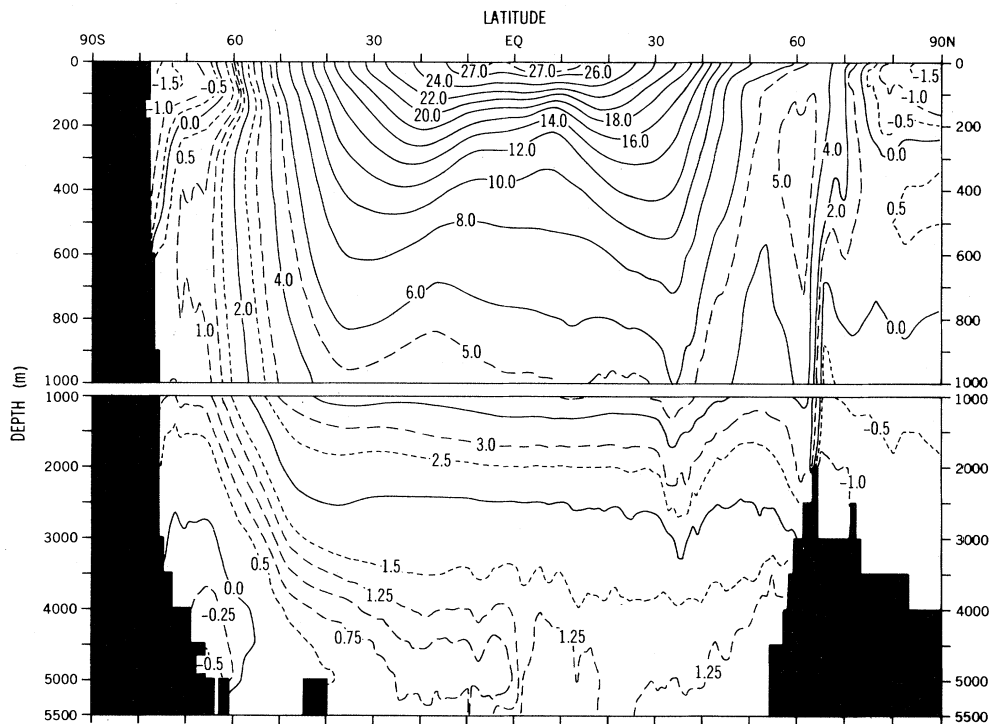


FIG. 36. Zonal mean cross sections of temperature for the top ocean layer 0–1000 m and the layer below 1000 m in °C for annual mean conditions, from Levitus (1982).

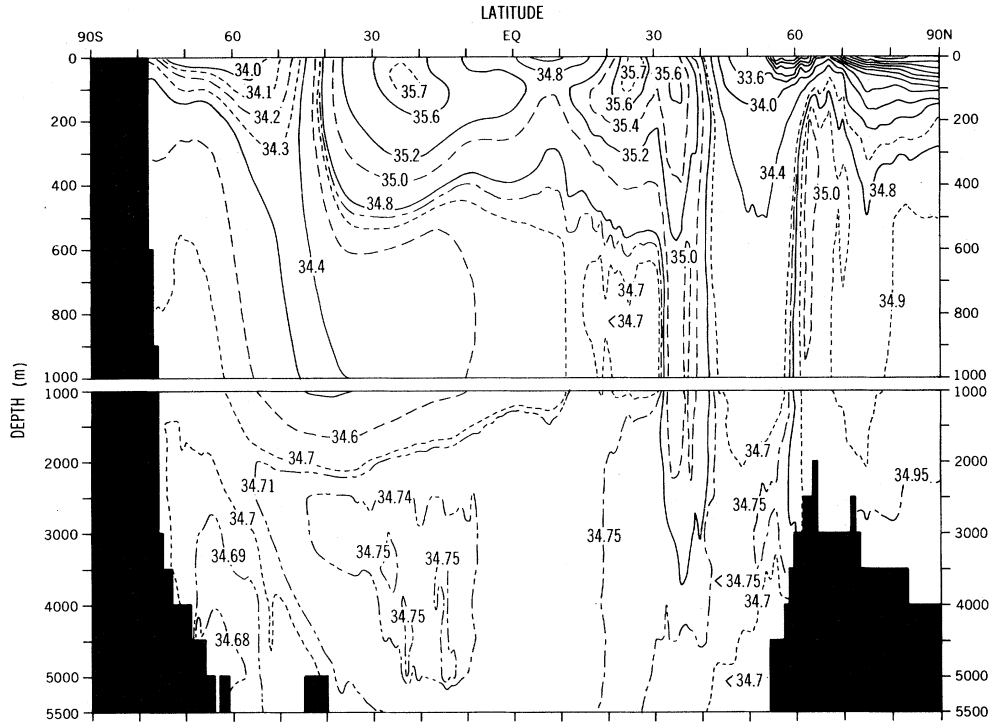


FIG. 37. As in Fig. 36, but for salinity in ‰.

mate, since it touches on the relative role of the atmosphere and oceans in shaping the present “normal” climate as well as its year-to-year variations.

Another indirect method frequently used is inferring

how large the regional oceanic heat convergence or divergence should be in order to balance the energy loss from or gain to the atmosphere as estimated from surface ship observations. A recent study by Hastenrath (1982) based

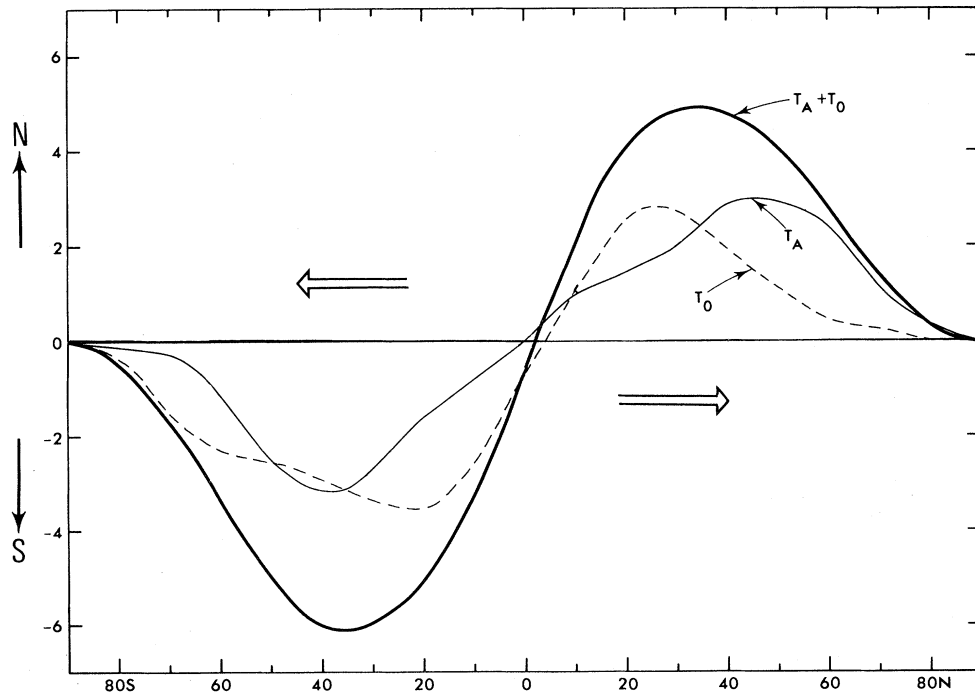


FIG. 38. Zonal mean profiles of the northward transports of energy in the atmosphere-ocean system ( $T_A + T_O$ ) based on radiation requirements, in the atmosphere ( $T_A$ ) obtained from rawinsonde data, and in the ocean ( $T_O$ ) inferred as a residual. All curves are for annual mean conditions in  $10^{15}$  W. Positive values indicate northward transports.



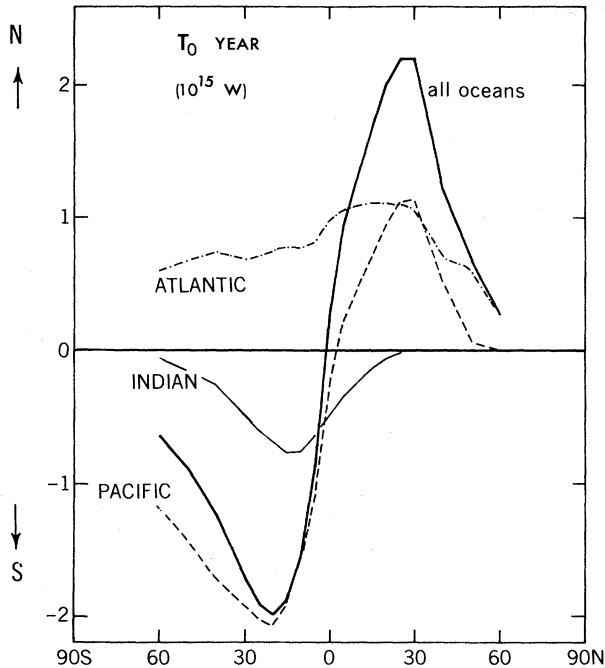


FIG. 39. Meridional profiles of the oceanic heat transport averaged zonally for the various oceans as computed indirectly from surface heat balance conditions by Hastenrath (1982) in units of  $10^{15}$  W.

on this approach leads to separate estimates for the transports in the three oceans, as shown in Fig. 39. Although very tentative, these curves give an intriguing picture of the possible large differences between the Atlantic and Pacific Oceans in transporting heat poleward. Hastenrath's total transport values agree reasonably well with those in Fig. 38, but the agreement may be fortuitous.

### 3. Energy storage

Up to now we have discussed mainly the long-term, annual mean balance of energy. If, instead, one is interested in the balance for shorter periods, such as for a season or for individual years, the storage of energy will play an important role. For example, Figs. 40(a) and 40(c) show meridional profiles of the observed rates of storage in the atmosphere  $S_A$  and in the oceans  $S_O$ , for normal winter and summer conditions. These storage terms,  $S_A$  and  $S_O$ , were evaluated at each latitude from the observed variations in the vertical mean atmospheric temperature and from those in the top layer of the oceans (0–275 m), respectively. In view of the large heat capacity of the oceans it is not surprising that the oceanic heat storage is about a factor 20 larger than the atmospheric one. In fact, the typical oceanic storage value of  $100 \text{ W m}^{-2}$  in middle latitudes is almost as large as the net seasonal radiation values at the top of the atmosphere [Fig. 11(f)]. Therefore, the oceans act as a huge buffer for the energy, damping the seasonal and interannual fluctuations in cli-

mate that otherwise would occur on an oceanless planet.

The relative importance of the oceanic heat storage and the transport of energy by oceanic motions can be assessed by comparing the storage in Fig. 40(c) with the computed flux of total energy across the earth's surface,  $F_{BA}$ , in Fig. 40(b). It is obvious that the oceanic transports are most important at low latitudes, and the oceanic storage at middle and high latitudes.

### F. Long-period fluctuations in the atmosphere-ocean system

On all time scales the meteorological and geological records show considerable variability in the climatic parameters. Overall, there seems to be the tendency for a red spectrum. In other words, longer-period phenomena tend to be associated with higher amplitudes of variability. Going back to the temperature spectrum shown earlier in Fig. 3, we find no strict periodicities in evidence besides the diurnal and annual periods and their harmonics. (We will not concern ourselves here with the peaks at periods between 10 000 and 100 000 years found in ice or sea floor cores that appear to be connected with variations in the orbital parameters.)

At the time scale of years to decades some large-scale oscillations in the atmospheric variables have been discovered. We may mention the oscillations in winter temperature (negative correlations—"sea saw") over Greenland and Northern Europe associated with north-south pressure anomalies over the Atlantic Ocean (van Loon and Rogers, 1978), and the North-Central Pacific and the Pacific-North American oscillations in temperature and surface pressure (Wallace and Gutzler, 1981). These anomalies are clearly related with variations in the general circulation of the atmosphere and its boundary conditions, namely, the sea surface temperatures and the snow and ice cover (see, e.g., Namias, 1983).

However, only one truly global-scale oscillation has been identified so far, the so-called Southern Oscillation. It was during the 1930s that Sir Gilbert Walker (Walker and Bliss, 1932, 1937) first documented this phenomenon, associating it with large east-west shifts of mass in the tropical atmosphere between the Indian and West Pacific Oceans on the one side and the Eastern Pacific Ocean on the other [for a recent review, see Rasmusson and Wallace (1983)]. This facet of the Southern Oscillation is illustrated in Fig. 41. It shows an analyzed map of the correlation coefficients between all available station pressures in the tropics and the surface pressure in Djakarta ( $6^\circ\text{S}, 107^\circ\text{E}$ ). A plot of the actual time series of the east-west pressure difference between Easter Island ( $27^\circ\text{S}, 109^\circ\text{W}$ ) and Darwin, Australia ( $12^\circ\text{S}, 131^\circ\text{E}$ ), is presented in Fig. 42. The time series shows a variable period, but with an average value of about 38 months.

Besides surface pressure, many other climate parameters both in the tropical atmosphere and oceans show remarkable fluctuations at the same frequency. We may mention in the atmosphere the strength of the easterly

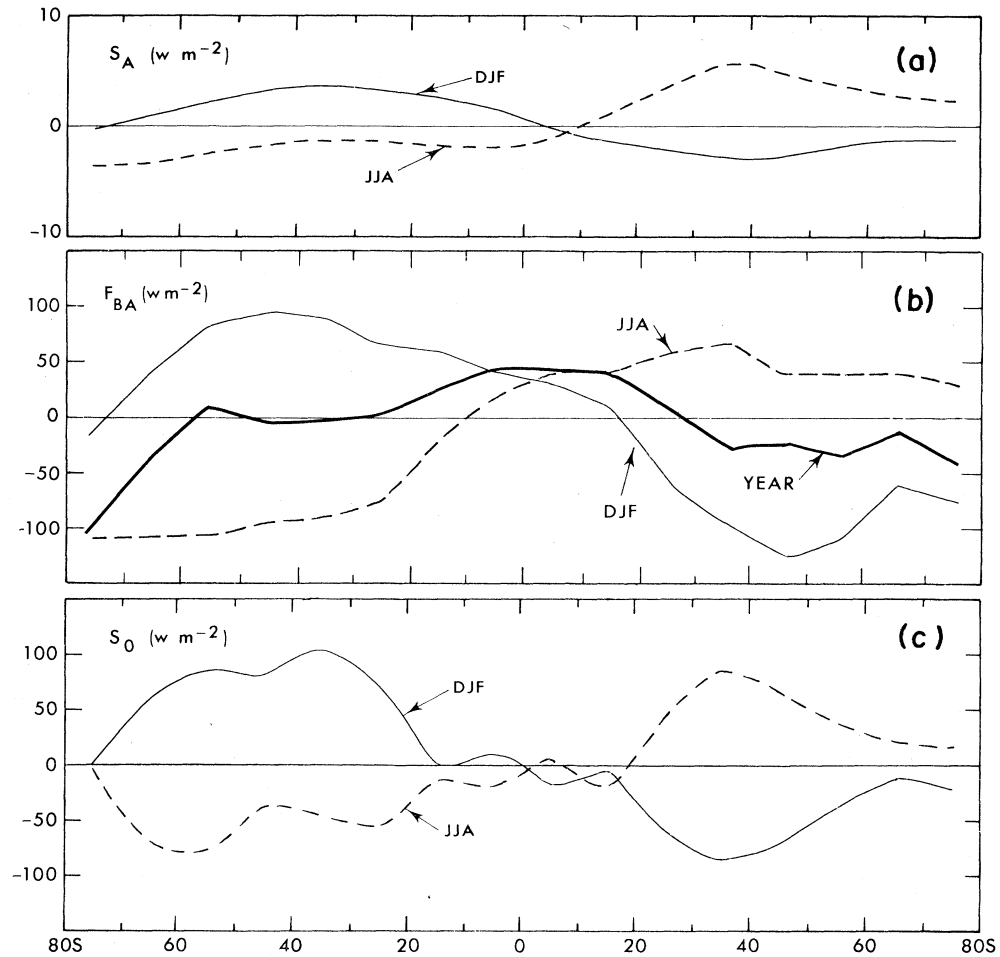


FIG. 40. Zonal mean profiles of (a) the observed rate of heat storage in the atmosphere ( $S_A$ ), (b) the flux of energy across the earth's surface ( $F_{BA}$ ) due to radiation, sensible heat and latent heat exchange, and (c) the observed rate of heat storage in the oceans ( $S_O$ ) from mean annual, winter, and summer conditions after Oort and Peixóto (1983).

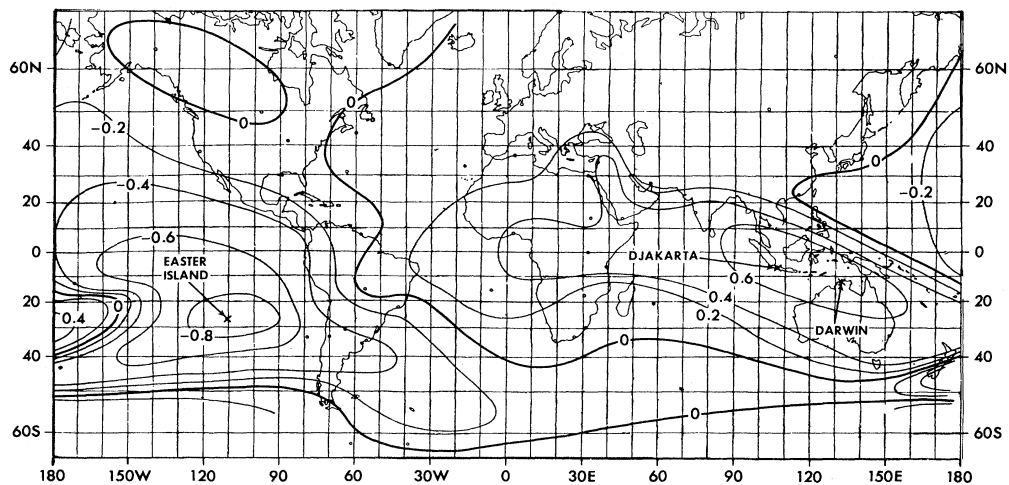


FIG. 41. Global shifts of atmospheric mass during the El Niño–Southern Oscillation phenomenon. Map of the correlation coefficient of monthly mean pressure anomalies over the world with those in Djakarta, Indonesia, for northern summer after Berlage (1966).

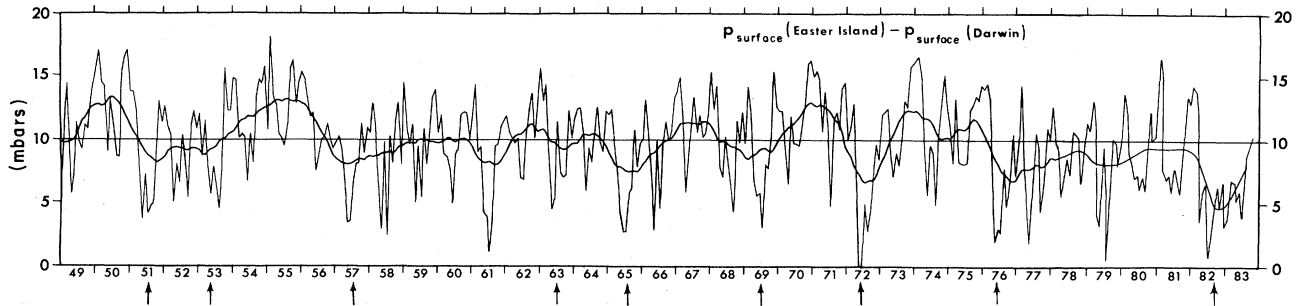


FIG. 42. Time series of the pressure difference between Easter Island and Darwin, after Wyrski (1982), and updated using data from Rasmusson and Carpenter (1983, personal communication). The thicker solid line indicates a 12-month running mean. The most important El Niño events (i.e., when warm water covers the entire eastern equatorial Pacific Ocean), according to Rasmusson and Carpenter (1982), are indicated by arrows.

trade winds, the zonal “Walker” oscillation with rising motions over Indonesia and sinking motions over the eastern tropical Pacific, the meridional Hadley circulations, and in the ocean the sea surface temperatures and associated ocean currents in the equatorial Pacific Ocean (Rasmusson and Carpenter, 1982). In fact, these last changes in the surface temperature play a crucial role in the Southern Oscillation. They are part of a very intense local phenomenon along the coasts of Peru and Ecuador, the so-called El Niño. This phenomenon is said to occur when warm waters replace the cold waters of the Peru current, usually starting around Christmas time. The El Niño may be the key for transmitting the Southern Oscillation signal from the oceans back to the atmosphere. This air-sea interaction seems to occur through increased convection and precipitation over the abnormally warm waters in the eastern Equatorial Pacific. The occurrence of warm water is, in turn, connected with the weakening of the cold equatorward current along the coast of Peru. In this phase of the Southern Oscillation, otherwise “desertlike” regions over the central and eastern equatorial Pacific Ocean receive torrential rains when El Niño conditions prevail. At the same time, pressures are high over India, the Indian Ocean, Australia, and Indonesia, where (relative) drought conditions occur.

It may be of interest to note that in 1982–1983 an exceptionally strong El Niño–Southern Oscillation (ENSO) has been observed, and that a return to more normal cold equatorial waters in the eastern Pacific only recently took place in the early summer of 1983. As presented very clearly in Fig. 42, the last two years show the largest pressure anomalies observed during the past 35 years. Some correlations have been found between ENSO and midlatitude weather, although they are weak and of doubtful use for prediction purposes. On the other hand, in the tropics once the ENSO phenomenon sets in there is considerable skill in forecasting the climatic anomalies more than six months later.

An explanation of what actually happens during ENSO must include the very complex feedback processes between oceans and atmosphere [see review article by Philander (1983)]. In the highly interactive ocean-atmosphere system it may prove practically impossible to

determine cause and effect, and we may have to be satisfied with only a knowledge of how the particular sequence of events occurs.

The global nature of the ENSO phenomenon is further demonstrated in Fig. 43. Here the atmospheric temperature averaged vertically and horizontally over the entire northern hemispheric mass is shown to be highly correlated ( $r=0.63$ ) with the local (but representative for the area  $20^{\circ}\text{S}-20^{\circ}\text{N}$ ,  $80^{\circ}\text{W}-180^{\circ}\text{W}$ ) sea surface temperature in the eastern equatorial Pacific Ocean with six months’ lag. It is clear that a large part of the observed variability in the global atmosphere must be connected with the variations in sea surface temperature in the eastern equatorial Pacific.

A cross section of the typical temperature difference in the atmosphere between periods of El Niño (warm) and normal (cold) sea surface conditions in Fig. 44 shows that the strongest heating occurs at low latitudes in the upper troposphere rather than near the ocean surface. The

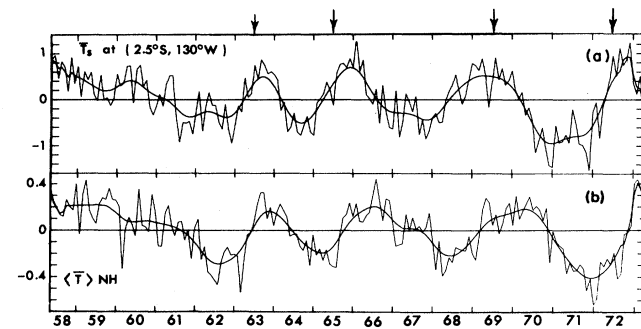


FIG. 43. Time series of (a) the monthly mean sea surface temperature in a key region ( $2.5^{\circ}\text{S}, 130^{\circ}\text{W}$ ) in the eastern equatorial Pacific Ocean and (b) the air temperature averaged vertically and horizontally over the entire mass of the northern hemisphere for a 15-year period, after Pan and Oort (1983). (The mean annual cycle has been removed.) The correlation coefficient between the two time series reaches a maximum value of 0.62 when the atmosphere lags the ocean by 6 months. The smoothed lines were obtained by applying a Gaussian filter in time. The arrows at the top of the figure indicate the El Niño events during the 15-year period, according to Rasmusson and Carpenter (1982).

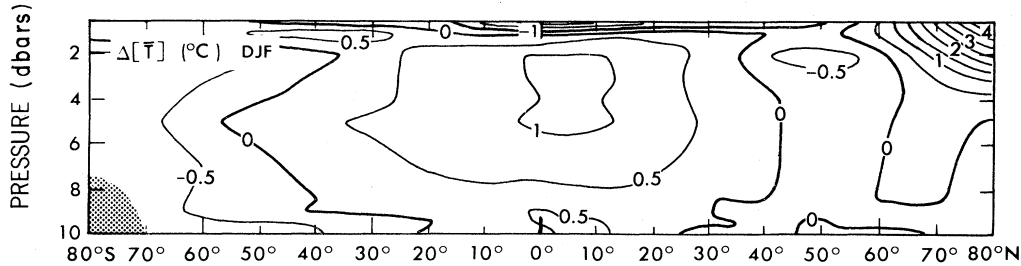


FIG. 44. Zonal mean cross section of the average temperature difference in the atmosphere for the cases when the sea surface temperature in the key region ( $2.5^{\circ}\text{S}, 130^{\circ}\text{W}$ ) was relatively warm (El Niño) and for those cases when it was relatively cold, from Pan and Oort (1983).

reason for this response may be the increased vertical convection and upper level release of latent heat that takes place during ENSO especially over the central and eastern Pacific Ocean. An intense effort in climate research is presently being made to obtain a deeper understanding of this oscillation (Rasmusson and Wallace, 1983). The ENSO phenomenon may be an ideal testing ground for the improvement of our present ocean-atmosphere coupled models.

Upper-air records of the kind shown in Fig. 43(b) are available only since the development of the rawinsonde network following World War II. For longer time series we have to rely on surface records alone, which have been available since about the 1880s. The 100-year time series of average atmospheric surface temperatures in Fig. 45 shows the well-known general heating until 1940, and the decrease in surface temperature since that time. The decrease since the 1940s is intriguing, since it took place in spite of the atmospheric heating which one would expect due to the (largely man-made) increase in atmospheric  $\text{CO}_2$  (see Fig. 56 and discussion in Sec. VII.B). We have to accept that we do not understand as yet how climatic variations as shown in Fig. 45 come about. An unanswered question is how important external factors, such as changes in solar input,  $\text{CO}_2$  concentration, volcanic activity, or particulate matter in the atmosphere (aerosols), are. We may have to include these effects in our climate models in addition to purely internal factors connected with atmosphere-ocean-cryosphere-lithosphere interactions.

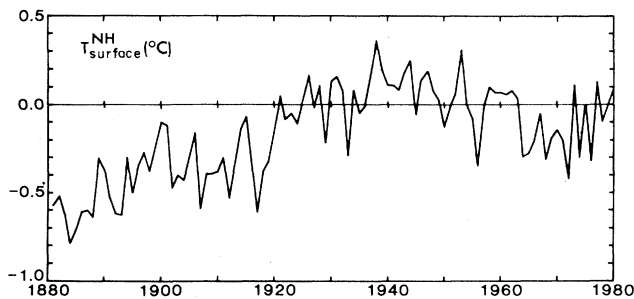


FIG. 45. Time series of the annual mean surface air temperature (in  $^{\circ}\text{C}$ ) averaged over the northern hemisphere, using the available historical records, after Jones *et al.* (1982).

## V. THE ATMOSPHERIC HEAT ENGINE

### A. Availability of energy in the atmosphere

We have already seen that the highest temperatures occur at low latitudes near the earth's surface and the lowest temperatures at high latitudes in the upper atmosphere. Furthermore, the atmosphere was found to act as a vehicle to transport heat poleward and upward. Thus the atmosphere may be regarded as a heat engine with heat flowing from the warm sources to the cold sinks. The work performed by the atmospheric engine is used to maintain the kinetic energy of the circulations against a continuous drain of energy by frictional dissipation.

Even for the ideal case of a Carnot machine, the efficiency  $\eta$  of the heat machine would be low, since the difference between the temperature of the warm source  $T_W$  and that of the cold sink  $T_c$  is relatively small compared with the temperature of the warm source.

$$\eta = (T_W - T_c) / T_W \lesssim 10\% .$$

Later in this discussion we will present other estimates of the efficiency, which, as expected, lead to lower values than the limiting ideal case. Thus the amount of kinetic energy generated by the atmospheric heat engine has to be small compared with the total potential plus internal energy (see Sec. IV.E.1).

In our preliminary analysis of the generation of kinetic energy we concluded that the source for kinetic energy was the total potential energy as discussed in conjunction with Fig. 6. However, only a fraction of the total potential plus internal energy in the atmosphere is available to be converted into kinetic energy, whereas most of the total potential energy is unusable. This same fact was already realized by Margules (1903). It is therefore necessary to refine our previous analysis of the problem when we discussed the balance equations for the energy components and their interrelations in Sec. III.C. Lorenz (1955, 1967) obtained a numerical expression for the energy available for conversion into kinetic energy. He coined this quantity "available potential energy." The availability functions in thermodynamics (Keenan, 1947; Hatzopoulos and Keenan, 1965) can be used as an alternative method to derive the expressions found by Lorenz. In

fact, this last theory shows that there is some ambiguity in the definition of the reference or dead state of the atmosphere. Lorenz (1955) was able to express the available potential energy in terms of the variance of pressure on a constant potential temperature or isentropic surface. In addition, he derived an approximate formula involving the variance of temperature on a constant pressure level and the mean static stability.

The amount of mean available potential energy  $P$  depends on the choice of the reference state of the atmosphere. However, when global distributions are considered, the uncertainties are much reduced. According to Lorenz (1955),

$$P = c_p \frac{\gamma}{2} \int \int \int (T^2 - \bar{T}^2) \rho dV, \quad (5.1)$$

where  $\gamma$  is a measure of the global mean static stability [see Eq. (3.6)], and the tilde indicates the global average over a constant pressure surface.

Because of the zonal character of the general circulation it is useful to partition the kinetic energy into the kinetic energy of the mean zonal flow  $K_M$  and the kinetic energy of the perturbations  $K_E$ . Henceforth we will call these components mean and eddy kinetic energy, respectively. Similarly, the available potential energy may be partitioned into the components  $P_M$  and  $P_E$ . This can be done using the expansion

$$[\bar{u}^2] = [\bar{u}]^2 + [\bar{u}'^2] + [\bar{u}^*2]$$

and similar expansions for  $[\bar{v}^2]$  and  $[\bar{T}^2]$ . Therefore, we have

(1) for kinetic energy

$$K_M = \frac{1}{2} \int \int \int ([\bar{u}]^2 + [\bar{v}]^2) \rho dV, \quad (5.2)$$

$$K_E = K_{TE} + K_{SE}$$

$$= \frac{1}{2} \int \int \int ([\bar{u}'^2 + \bar{v}'^2] + [\bar{u}^*2 + \bar{v}^*2]) \rho dV, \quad (5.3)$$

(2) for available potential energy

$$P_M = c_p \frac{\gamma}{2} \int \int \int ([\bar{T}]^2 - \bar{T}^2) \rho dV, \quad (5.4)$$

$$P_E = P_{TE} + P_{SE} = c_p \frac{\gamma}{2} \int \int \int ([\bar{T}'^2] + [\bar{T}^*2]) \rho dV. \quad (5.5)$$

The balance equations for these basic forms of energy permit a clearer interpretation than our previous analyses (see Figs. 6 and 7) of the mechanisms involved in the generation and dissipation of energy, as well as the transformations between the various forms of energy.

As an example we will indicate how to derive the balance equations for the zonal mean kinetic energy  $K_M$  and the eddy kinetic energy  $K_E$ . Taking the Eqs. (3.9a) and (3.9b), we first expand the total derivatives  $du/dt$  and  $dv/dt$ . Next we multiply the resulting equations by  $[\bar{u}]$  and  $[\bar{v}]$ , respectively. After some mathematical manipulations and noting that  $u = [\bar{u}] + \bar{u}^* + u'$  and  $v = [\bar{v}] + \bar{v}^* + v'$ , we obtain the equations for

$\partial([\bar{u}]^2/2)/\partial t$  and  $\partial([\bar{v}]^2/2)/\partial t$ . Addition of these two equations and integration over the total atmospheric mass leads to the required balance equation for the mean kinetic energy. If we multiply the initial equations (3.9a) and (3.9b) by  $u'$  (or  $\bar{u}^*$ ) and  $v'$  (or  $\bar{v}^*$ ), respectively, and apply the same procedure as above, we obtain the balance equation for the eddy kinetic energy.

Using similar procedures with the temperature equation (3.3), we can derive equivalent balance equations for the mean and eddy available potential energy,  $P_M$  and  $P_E$ .

The balance equations for the four basic forms of energy can be written in a symbolic form, where  $G(x)$  indicates the rate of generation of  $x$ ,  $C(x,y)$  the rate of conversion from  $x$  into  $y$ , and  $D(y)$  the rate of dissipation of  $y$ :

$$\frac{\partial P_M}{\partial t} = G(P_M) - C(P_M, K_M) - C(P_M, P_E), \quad (5.6)$$

$$\frac{\partial P_E}{\partial t} = G(P_E) - C(P_E, K_E) + C(P_M, P_E), \quad (5.7)$$

$$\frac{\partial K_M}{\partial t} = C(P_M, K_M) + C(K_E, K_M) - D(K_M), \quad (5.8)$$

$$\frac{\partial K_E}{\partial t} = C(P_E, K_E) - C(K_E, K_M) - D(K_E). \quad (5.9)$$

The connecting links between the various energy forms as given by the previous equations are illustrated in a box diagram in Fig. 46. The generation of available potential energy is proportional to the covariance of diabatic heating and temperature. Therefore, when regions of high temperature are heated and/or regions of low temperature are cooled, available potential energy will be generated, since the center of gravity of the atmosphere is raised. The generation of available potential energy parallels the behavior of a heat engine, where fuel has to be added to maintain the warm furnace and cooling has to be provided to maintain the required temperature difference. Basically, heating and cooling, in this sense, amount to decreasing the entropy of the system. Obviously, the opposite processes would lead to an increase of entropy and a destruction of available potential energy:

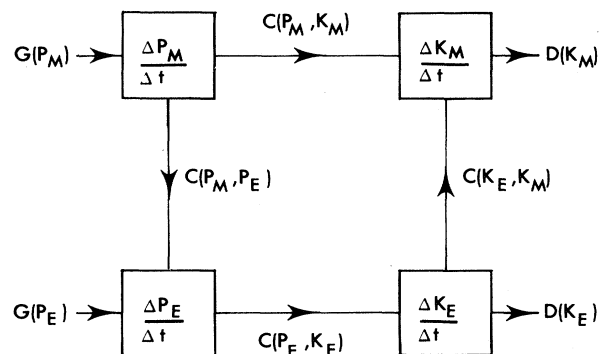


FIG. 46. Schematic box diagram for the energy cycle in the atmosphere, showing the rates of generation, conversion, and dissipation of the various forms of energy.

$$G(P) = \int \int \int \overline{\gamma(Q - \tilde{Q})(T - \tilde{T})} \rho dV .$$

The conversion of available potential energy into kinetic energy is given by

$$C(P, K) = - \int \int \int \overline{\mathbf{v} \cdot \text{grad} p \rho} dV ,$$

showing that only the ageostrophic component of the flow contributes to the conversion. This expression is actually the same as the one given in Eq. (3.18a) and Fig. 6 for the conversion from total potential to kinetic energy.

The conversion between mean and eddy potential energy is given by the product of the eddy transport of heat and the north-south gradient of the mean temperature

$$C(P_M, P_E) = -c_p \int \int \int \gamma [\overline{v'T'} + \bar{v}^* \bar{T}^*] \times (\partial[\bar{T}]/a \partial \phi) \rho dV .$$

In fact, the transport of heat by the eddies from the warmer tropics into the cooler high latitudes reduces the mean north-south gradient of temperature (see Fig. 33), resulting in a decrease of mean available potential energy.

Similarly, the rate of conversion of eddy into mean kinetic energy is given by

$$C(K_E, K_M) = \int \int \int [\overline{v'u'} + \bar{v}^* \bar{u}^*] \times \cos \phi \frac{\partial([\bar{u}]/\cos \phi)}{R \partial \phi} \rho dV .$$

In transporting angular momentum poleward the eddies tend to intensify the mean zonal current, thus increasing the mean kinetic energy at the cost of the eddy kinetic energy (Starr, 1968).

**B. The observed energy cycle**

Using the previous results from a ten-year data set we evaluated the various terms in Eqs. (5.6)–(5.9). The final results of these extensive computations are given in Fig. 47 for mean annual conditions for the entire globe.

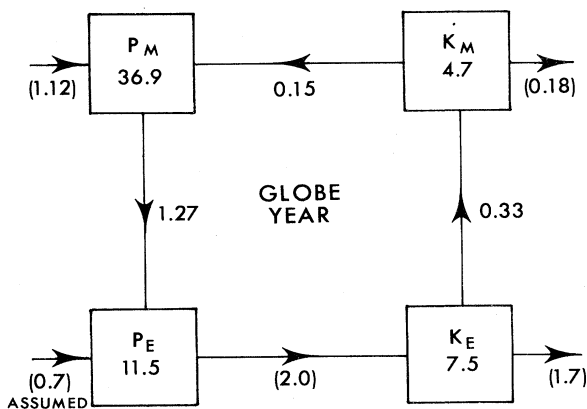


FIG. 47. The observed energy cycle for the global atmosphere. Energy amounts inside each box are given in  $10^5 \text{ J m}^{-2}$ , and rates of generation, conversion, and dissipation in  $\text{W m}^{-2}$ , from Oort and Peixóto (1983). Not directly measured terms are shown in parentheses.

We have now reached the point where we can describe the mechanisms by which the incoming solar radiation maintains the kinetic energy of the atmosphere and oceans against dissipation. Thus the radiation balance of the atmosphere tends to generate an almost zonally symmetric distribution of temperature in both hemispheres with a strong north-south gradient which is most intense in middle latitudes. The north-south variance of the zonal mean temperature at each level is a measure of the mean zonal available potential energy  $P_M$ . However, the meridional transport of enthalpy by the eddies in midlatitudes deforms the ideal zonally symmetric distribution of temperature, leading to an additional variance in the east-west direction which is proportional to the eddy available potential energy  $P_E$ . Through the mechanisms described in Sec. IV.E, i.e., by baroclinic instability, some of the eddy available potential energy is transformed into kinetic energy of the growing disturbances  $K_E$ . The eddies also transport momentum poleward, increasing the zonal motion, and thus generating zonal mean kinetic energy  $K_M$ . A large part of the eddy kinetic energy is directly dissipated by friction or cascades into smaller and smaller eddies (turbulence) until it is finally converted back into heat by molecular viscosity. This is a consequence of the second law of thermodynamics. In the absence of external forcing the system tends to evolve to states of larger and larger disorder. Of course, the maximum disorder or entropy is obtained when the ordered energy is converted into random molecular motions. The dissipation is most intense in the eddy kinetic energy. The direct mean meridional circulation (Hadley cell) generates zonal angular momentum in its upper branch [see Eq. (3.9a),  $f v$  term] and thereby, mean zonal kinetic energy. However, the indirect circulation in midlatitudes consumes mean zonal kinetic energy at a rate slightly exceeding the production in the Hadley cell and therefore converts some of the mean zonal kinetic energy back into mean zonal available potential energy.

Considering presently the actual numerical estimates shown in Fig. 47, we are led to the following scheme for the energy cycle. Net radiational heating by the sun and release of latent heat in the tropics, and net infrared cooling in high latitudes all result in a generation of zonal available potential energy. This energy is converted into eddy available potential energy by the growing baroclinic disturbances ( $1.3 \text{ W m}^{-2}$ ). The fastest-growing eddies are in the range of wave numbers 5–8 about the pole. Some of the eddy available potential energy may be dissipated by more loss of infrared radiation to space in warm than in cold air and by a similar heat exchange with the earth's surface. However, condensational heating is believed to surpass these effects leading to a small positive net generation of  $P_E$  ( $0.7 \text{ W m}^{-2}$ ). The eddy available potential energy is next converted into eddy kinetic energy ( $2.0 \text{ W m}^{-2}$ ) through the sinking of colder air and the rising of warmer air in the eddies (see Fig. 33). Some of the eddy kinetic energy is converted into kinetic energy of the mean flow in a barotropic process leading to a decascade of energy from the small into the larger scales ( $0.3$

$\text{W m}^{-2}$ ). As we have seen before, there is a prevalent countergradient flow of momentum up the gradient of zonal mean angular velocity. However, the bulk of the kinetic energy of the large-scale eddies is dissipated by friction in a normal cascade regime ( $1.7 \text{ W m}^{-2}$ ).

Finally, some of the mean zonal kinetic energy is dissipated by friction and turbulence ( $0.2 \text{ W m}^{-2}$ ), while a small residual is converted into zonal available potential energy ( $0.15 \text{ W m}^{-2}$ ) by the combined action of the direct and indirect mean meridional circulations. Comparing the total kinetic energy with the rate of dissipation, we come to the conclusion that it would take approximately one to three weeks to dissipate the kinetic energy.

Schematically we have found that the energy cycle in the atmosphere proceeds from  $P_M$  to  $K_M$  through the following scheme:

$$P_M \rightarrow P_E \rightarrow K_E \rightarrow K_M \rightarrow P_M .$$

It therefore appears that the eddies play a crucial role in regulating the general circulation of the atmosphere, as suggested by Starr (1948).

The intensity of the atmospheric energy cycle can be measured by estimating either the conversion of total available potential energy into kinetic energy,  $C(P,K)$ , the generation of available potential energy  $G(P)$ , or the total dissipation  $D(K)$ , since in a steady state all three terms must balance. Regarded again as a heat engine, the efficiency  $\eta$  of the atmosphere can be now taken as the ratio of the kinetic energy dissipated by friction ( $2.0 \text{ W m}^{-2}$ ) and the mean incoming solar radiation ( $238 \text{ W m}^{-2}$ ), which leads to a value  $\eta = 0.8\%$ . Alternatively, we may define the efficiency, according to Darrieux, as the ratio  $D(K)/P$  giving a value of 4%. These values of the efficiency are, of course, much more realistic than the Carnot efficiency found previously to be on the order of 10%.

Let us consider now the gross aspects of the energetics of the oceans using a tentative box diagram for the ocean circulation presented in Fig. 48. The heating or cooling together with the evaporation-minus-precipitation at the interface with the atmosphere generate spatial variations in the ocean temperature and salinity. These variations

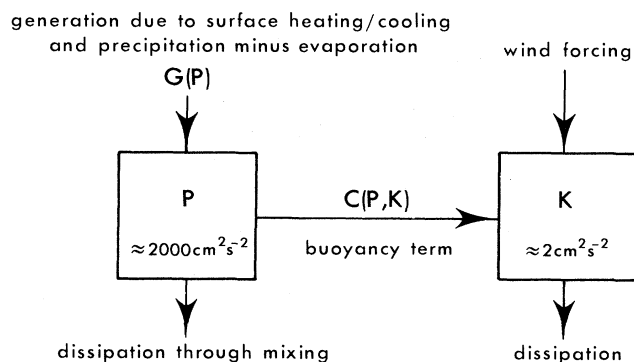


FIG. 48. Schematic box diagram for the energy balance of the oceans, after the numerical model estimates by Bryan and Lewis (1979).

lead, in turn, to variations in density (i.e., baroclinicity) and therefore generate available potential energy. This available potential energy is partly dissipated through mixing inside the oceans and partly converted into kinetic energy through direct thermohaline circulations. At the same time the atmosphere through tangential wind stresses transfers angular momentum into the oceans thus reinforcing the generation of kinetic energy in the oceans. There is some debate on the relative importance of the wind and thermohaline forcings in the maintenance of the oceanic general circulation against dissipation through friction and turbulence. It seems, however, that the currents in the top layer are mainly maintained by the wind stresses, whereas there is some evidence that the deep ocean circulation is due to thermohaline effects.

The magnitude of the available potential energy compared to that of the kinetic energy is striking. This shows that the rate of conversion from  $P$  into  $K$  must be very small, and that the time scales of oceanic phenomena must be very much larger than those in the atmosphere, namely, on the order of months to years in the surface layers and centuries in the deep ocean.

## VI. MATHEMATICAL SIMULATION OF CLIMATE

### A. Necessity of using numerical integrations

As discussed before, the physical laws that govern the dynamics of the atmosphere and climate constitute a complete set of mathematical equations [see Eqs. (3.1)–(3.5)]. However, these equations are highly nonlinear in nature, and no general analytical methods are available to solve them. It suffices to say that, for example,

$$\frac{du}{dt} = \frac{\partial u}{\partial t} + u \frac{\partial u}{\partial x} + v \frac{\partial u}{\partial y} + w \frac{\partial u}{\partial z} ,$$

where, of course, the last three terms are nonlinear. We have then to rely on numerical analyses to procure the desired solutions.

Thus the partial differential equations have to be replaced by equivalent finite difference equations. Even so, the primitive equations contain all scales of motion from sound and gravity waves up to planetary waves. Some of these scales of motion do not influence the weather processes significantly, but may produce a noise level during integration, obscuring the real meteorological signal. Such appears to be the case for the sound and gravity waves. These must then be filtered. This is accomplished by using the hydrostatic equilibrium hypothesis and in some models by using quasigeostrophic approximations in middle and high latitudes (see discussion in Sec. III.A).

The utilization of numerical methods brings, however, problems of a mathematical nature, such as the convergence of the solutions and their stability. Basically, we are forced to substitute a discretum  $x_i, y_j, z_k, t_l$  for a continuum  $x, y, z, t$ , where  $i=1,2,3, \dots, m, j=1,2, \dots, n, k=1,2, \dots, K$ , and  $l=1,2, \dots, L$ . The computational resolution is given by the increments  $\Delta x, \Delta y, \Delta z$ , and  $\Delta t$  and must be fixed in agreement with the nature of the problem to be studied. However, in the case of the atmo-

sphere and oceans the number of levels  $K$  in the vertical is on the order of 10–20, whereas the number of grid points in the horizontal to cover the globe must be several orders of magnitude higher. This last number may be given by  $A/\Delta^2$ , where  $A$  is the area of the globe and  $\Delta$  the average horizontal grid size. If  $n$  is the number of variables necessary to define the state of the atmosphere at each point, then at a given time the total number of variables is  $nKA/\Delta^2$ , which gives the number of degrees of freedom for the system we are dealing with. The increment of time,  $\Delta t$ , cannot be chosen arbitrarily, since it must obey the Courant-Friedrichs-Lewy (1928) condition in order to secure the stability and convergence of the integration

$$c \Delta t / \Delta x \leq 1,$$

where  $c$  denotes the speed of the fastest wave. Implicit methods to solve the equations do not require a pre-established time step, but their calculation is more complex (Richtmeyer and Morton, 1967).

We approximate the spatial derivatives of a variable  $\psi$  at a given point  $(i, j, k)$  as a centered difference between the values of  $\psi$  at the neighboring grid points of the discretum:

$$\frac{\partial \psi}{\partial x} = \frac{\psi_{i+l, j, k} - \psi_{i-l, j, k}}{2\Delta x},$$

$$\frac{\partial \psi}{\partial y} = \frac{\psi_{i, j+l, k} - \psi_{i, j-l, k}}{2\Delta y},$$

$$\frac{\partial \psi}{\partial z} = \frac{\psi_{i, j, k+l} - \psi_{i, j, k-l}}{2\Delta z}.$$

This centered differences scheme has to be modified at the boundaries using one-sided differences, forward or backward.

Using the prediction equations, we can compute the time rate of change at each grid point for a given instant  $\tau$ ,  $(\partial\psi/\partial t)_\tau$ , from the instantaneous distribution of the variables appearing on the right-hand side of the equations, so that at each point  $(i, j, k)$

$$\psi^{\tau+1} = \psi^\tau + \Delta t \left[ \frac{\partial \psi}{\partial t} \right]_\tau$$

or

$$\psi^{\tau+1} = \psi^{\tau-1} + 2\Delta t \left[ \frac{\partial \psi}{\partial t} \right]_\tau.$$

This last scheme is known as the leapfrog method.

By repeated application of the leapfrog method we can evaluate the state of the atmosphere, in principle, through any desired period.

The dimensions of the basic grid determine the minimum scale of phenomena that can be resolved. For numerical weather prediction purposes and short-range forecasts typical values are  $\Delta x \approx 150$  km,  $\Delta y \approx 150$  km,  $\Delta t \approx 5$  min, whereas  $\Delta z$  ranges from about 50 m in the boundary layer to several km in the free atmosphere (corresponding to about ten levels in the vertical). However, for climatic studies the typical values are usually larger because of computational restrictions (see Fig. 49).

Subgrid scale phenomena, such as cumulus convection, sharp fronts, and turbulence, cannot be resolved explicit-

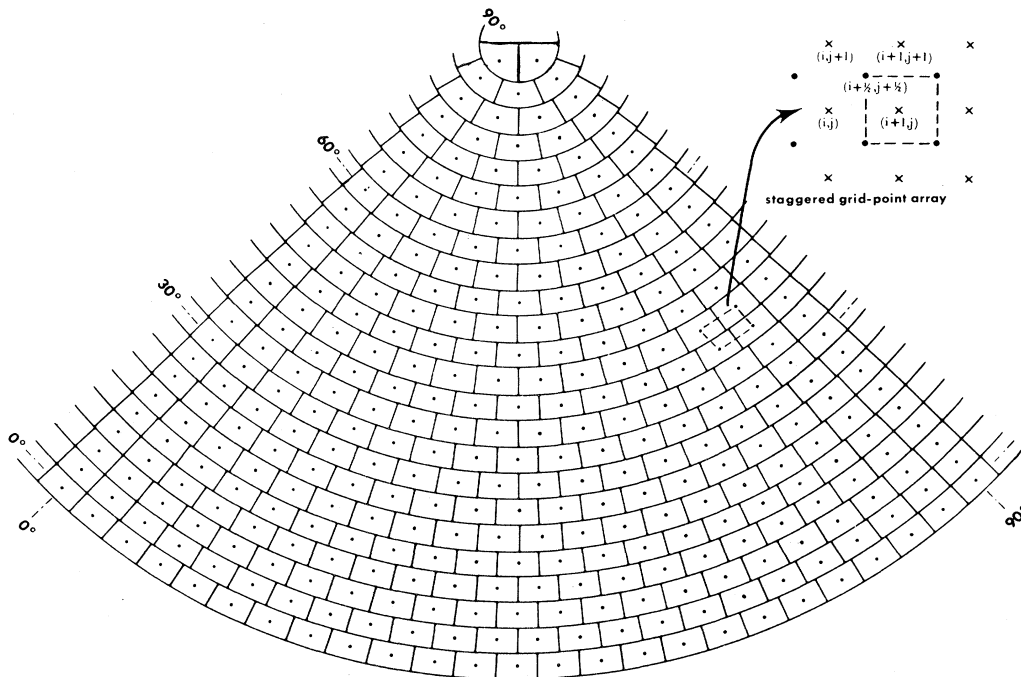


FIG. 49. An example of a horizontal grid system (the so-called Kurihara grid) with 24 grid points between the pole and equator, used in general circulation model experiments (only  $\frac{1}{8}$  of globe is shown). A staggered grid-point array for performing the needed finite difference computations is shown as an inset in the top right-hand corner. Other systems in use are regular latitude-longitude grids and various spherical harmonic systems.



ly. However, they are very important for the atmospheric circulation, and their effects must be included. The subgrid scales are commonly expressed in terms of the resolved macroscale parameters. This process is called parameterization. With this technique it is possible to describe the effects of subgrid-scale eddies on the large-scale phenomena both in the horizontal and vertical directions, using, in general, a diffusion scheme. However, there is no guarantee that this approach is the correct way of incorporating the subgrid-scale processes in the general circulation.

When we consider the number of degrees of freedom of the system, the number of operations required at each grid point, and the number of time steps to cover the forecast or simulation period, it is obvious that the integration requires very powerful computers to perform the calculations (Smagorinsky, 1974).

### B. Limits of predictability

In dealing with such a complex set of equations as those presented in Sec. III and with such complex initial and boundary conditions there are bound to be serious limitations due to various sources of errors in applying the numerical integration. These include simplifications imposed on the equations and on their transcription into numerical form, truncation errors, and errors inherent in the observations used to define the initial and boundary conditions. Because of the nonlinear and unstable characteristics of the atmosphere, an initial error can grow at such a high rate that it can mask the real meteorological signal, thus limiting the predictability by the model. The rate of error growth depends on the scales of motion considered. The smaller the scale, the shorter is the range of predictability in the model. As discussed before, for synoptic-scale weather patterns the limit of predictability is estimated to be on the order of two to three weeks (see Fig. 50), which means that no individual, instantaneous state of the atmosphere can be predicted beyond three weeks in spite of further perfections in the equations and in the accuracy of the initial data. A possible exception may be when blocking situations prevail. A blocking condition is usually formed by a persistent high-pressure system (anticyclone) near the western sides of the continents in middle latitudes. With this type of situation the trajectories of low-level disturbances and of the upper air jets are split into two branches as if they were blocked by the high-pressure system. This situation may persist for several weeks.

There are, of course (Sec. II), some intrinsic limitations in applying a finite-difference scheme repetitively in order to simulate the long-term climate. However, in studying climate we are not interested in an individual instantaneous state *per se* but only in an ensemble of states. This is very similar to the situation that occurs in statistical mechanics. Therefore, we may study instead the statistical moments of various orders for the atmospheric variables as well as their evolution in time when the external

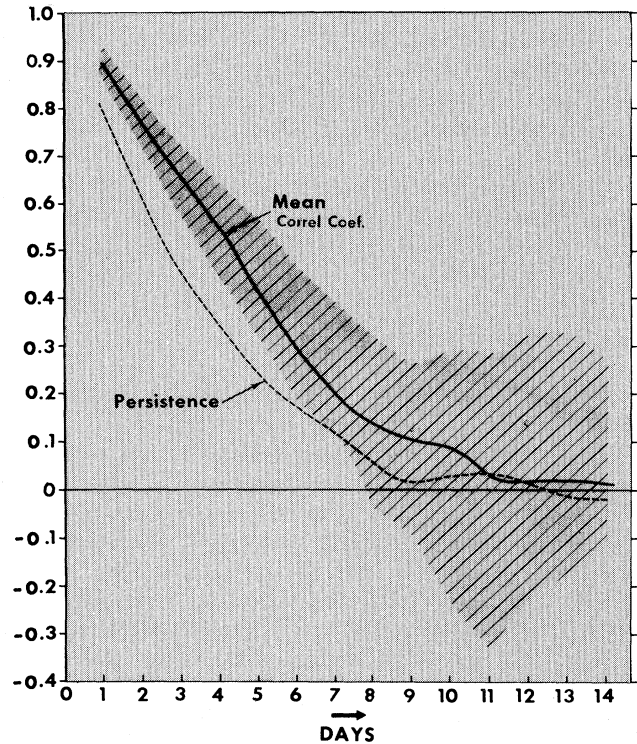


FIG. 50. An example of the predictive skill in numerical weather prediction. Plot of the decrease of the correlation coefficient in time between predicted and observed 500-mbars geopotential height anomalies for the mean of 12 winter cases from Miyakoda *et al.* (1972). The correlation coefficients were computed using all grid point values in the northern hemisphere. The shaded area shows the range for the individual winters. For comparison, the persistence curve (dashed) indicates the no-skill forecast. No skill is shown after about one week.

boundary conditions are given. These conditions determine the type of circulation regime and, in principle, the statistical behavior of the atmosphere. For example, in spite of difficulties in predicting the exact location and trajectory of a particular depression or other perturbation it is possible to obtain a statistical distribution function for the positions and trajectories of the entire class of perturbations.

In an early conference to study the potential of climate forecasting von Neumann (1960) defined three classes of predictions. The first class includes short-range predictions of day-to-day weather events, the second class medium-to-long-range weather or climate predictions from weeks to months and possibly years, and finally the third class, the climatic equilibrium simulation. As envisioned by von Neumann, much progress has been made since the 1950s in the first and third class of problems. However, in the second class of problems progress has been more limited, because both initial conditions and imposed boundary conditions are important in determining the final solution. We will be mainly concerned with climatic simulations where neither initial conditions nor the prediction of the specific phase of a disturbance is important, provided the overall statistics of the disturbances

are well simulated in a meteorologically reasonable way.

As we have mentioned before, the important question of uniqueness of the statistical equilibrium solution has been dealt with by Lorenz (1969). He concluded that for certain hydrodynamical systems more than one equilibrium state may exist that will satisfy the same governing equations and same boundary conditions. This point is very important, and raises the problem of climate determinism [see also Monin (1972)].

### C. Climate modeling

We will consider now in a more precise manner what constitutes a physical-mathematical model of climate. We assume that climate represents a statistical, quasisteady state of the atmosphere that depends only on the boundary conditions imposed by the external subsystems. A climate model is a set of specialized thermohydrodynamic equations with prescribed boundary and initial conditions, certain given values of the physical constants and specified schemes of parameterization of the subgrid-scale fluxes of matter, momentum, and energy. The physical constants include planetary data, such as the radius of the earth, the acceleration of gravity, the angular velocity of rotation, and internal constants, such as total mass, chemical composition of the air and oceans, specific heats, latent heats of phase transitions of water, albedos of clouds and the earth's surface, and radiative transfer parameters. The boundary conditions include the incoming solar energy, orbital parameters (ellipticity, obliquity, and longitude of perihelion), surface topography, surface roughness, heat capacity of the underlying surface, etc.

In studying climate, we must consider the behavior of each individual component of the climatic system and the strong interactions between the components. The characteristic phenomena in the various components of the climatic system have different time scales. Compared with the atmospheric time scale of  $10^{-3}$  to  $10^{-1}$  years, the internal time scale of the oceans ranges from  $10^{-1}$  to  $10^3$  years, whereas the time scales for the cryosphere (sea ice, snow cover, and glaciers) are still longer, namely, on the order of  $10^0$  to  $10^5$  years. We can then take the atmosphere as the main system with the continental surface topography, surface roughness, and sea surface temperatures as boundary conditions and using the basic thermohydrodynamic equations for the atmosphere.

Analogous considerations can be made for an ocean climate model with some minor adjustments concerning the boundary conditions (such as the surface wind stress and/or surface temperature), internal constants, and specified parameterization schemes. Since the atmosphere and oceans are strongly connected through the exchange of momentum, heat, and matter, it is obvious that a coupled atmosphere-ocean model is very desirable. However, the integration of a fully coupled model including the atmosphere, oceans, land, and cryosphere, with such different internal time scales poses almost insur-

mountable difficulties in reaching a final solution, even if all interacting processes were completely understood. The reason is that the model should ideally be run at time steps applicable to the fastest component of the system, i.e., the atmosphere. To circumvent this difficulty Manabe (1969) and Bryan (1969) have used a special technique for integration of their coupled ocean-atmosphere model. The details will be discussed later.

Another approach to modeling of the total climate system is to greatly simplify the basic thermohydrodynamic equations of the atmosphere through parameterization of all atmospheric eddies and to couple it to a more complete ocean model. Saltzman (1978) has suggested that the real atmosphere may operate in a statistically deterministic way described by a set of simplified climate equations. These parameterized equations would govern directly the atmospheric climatic statistics such as monthly or longer-term normals, variances, and higher moments of the probability distributions of climatic variables. The crucial point of this approach resides in the necessity of formulating physically sound parameterizations for the large-scale eddy processes in time and space. Such statistical-dynamical models are useful for the practical reason that they consume much less computer time than full general circulation models, and offer the possibility for integrating the model even over geological times.

To circumvent the time-scale difficulties in handling the atmosphere-ocean system we may regard the influence of the rapidly varying atmosphere on the slowly moving ocean as a stochastic process. In other words, the white-noise spectrum of the atmosphere tends to produce an oceanic response with a red spectrum, where most of the variance is confined to the long-period fluctuations (Hasselmann, 1976). During the long-period changes in the oceans new boundary conditions (e.g., new sea surface temperature and sea-ice distributions) are generated for the atmosphere, forcing the atmosphere into new quasiequilibrium states.

### D. Hierarchy of climate models

We will describe now the various types of mathematical models of climate following some kind of hierarchy in terms of the degree of their resolution and complexity, trying to give their physical foundation. For general reviews see Schneider and Dickinson (1974), Smagorinsky (1974), Saltzman (1978), Ramanathan and Coakley (1978), and North *et al.* (1981).

By and large we will divide the models into two main classes, namely, the deterministic and the stochastic models. We will include in the first class the statistical-dynamical models and the explicit dynamical models.

The statistical-dynamical models are based on averaged equations and the effects of large eddies are parameterized in terms of the mean quantities, as mentioned before. These models can yet be divided into thermodynamic (or energy-balance) models, which are based solely on the first law of thermodynamics, and into momentum

models, which are based on the same first law, completed with the parameterized meridional transports of momentum and heat.

The explicit dynamical models are three dimensional and based on the climate equations (3.23)–(3.29). They are commonly called general circulation models (GCM's). The evolution of the large-scale eddy circulations is followed on a day-to-day basis as in numerical weather forecasting practice. The equations can be solved in wave number space, using, e.g., spherical harmonics or in the actual space using a grid-point network. If in the wave-number models only a few components are included, they give a low resolution of the physical phenomena involved and require that the eddies be described by a small number of spectral components (Lorenz, 1960). The grid-point GCM's generally require a high resolution in space and an integration with relatively short time steps. In the general circulation models, the final climate statistics are evaluated from the daily simulations in the same manner as is done usually in climatological studies (see Sec. IV).

As mentioned before, the stochastic models were developed because the physical processes in some of the subsystems cannot be modeled or parameterized in a deterministic way due to, among other factors, the large differences in internal time scales; hours to weeks for the atmosphere, weeks to years for the mixed layer of the oceans and for sea ice and snow, and decades to millenia for the deep oceans and polar ice sheets (Hasselmann, 1976; Sutera, 1981). Any perturbation leads to very different response times in each of the subsystems due to the coupling between the fast and slow subsystems.

Many physical long-period signals can be regarded as the superposition of a large number of random, short-period signals. An analogy can be made with statistical mechanics, where certain macroscopic variables, such as temperature and pressure, can be determined by the statistics of the microscopic, molecular motions. The evolution of the slowly changing variables can be expressed in terms of the faster variables using stochastic differential equations, such as the Fokker-Planck equation.

Let us now go back to the internal system composed of the atmosphere and oceans (or cryosphere). The atmosphere acts in this system as a white-noise signal generator which leads to a low-frequency integral response in the oceans (or cryosphere). The random input is bounded by the prescribed variance of the fluctuations according to observations. The generating processes are assumed to be randomly distributed around their mean values, leading to probabilistic predictions for the entire system.

A different classification of climate models can be obtained by considering the modes of averaging in space. Let us consider the three-dimensional, climate fields, denoted by  $3-(\lambda, \phi, z)$ . They can be averaged in the vertical leading to two-dimensional  $2-(\lambda, \phi)$  models, or in the zonal direction leading to two-dimensional  $2-(\phi, z)$  models, which, of course, are axially symmetric. If these two-dimensional models are now averaged in one of the other dimensions, we obtain one-dimensional  $1-\lambda$ ,  $1-\phi$ , or  $1-z$  models. The integration of these last models with respect

to the remaining dimension will lead to global mean or zero-dimensional models.

The more averaging operations are performed, the lower the resolution needed, but the more eddy components have to be parameterized. Thus GCM's, being the models with highest resolution, where the synoptic weather systems are explicitly taken into account, require the least amount of parameterization. By the same token, global-mean models demand the most sophisticated parameterization schemes.

### E. Mathematical and physical structure of the models

Instead of our giving a detailed description of the wide range of models used and their individual features, it appears more appropriate for us to analyze some general points that apply to most of the models.

We shall start with the energy-balance models which are steady state or equilibrium solutions of the energy equation (3.27) when the boundary conditions and some internal parameters are prescribed. With these simple zonally averaged models we may compute the spatial distribution of the equilibrium temperature as a function of latitude and height in the atmosphere. Simple as they may seem, these models give valuable information about the sensitivity of the climatic system to changes in planetary albedo or in solar radiation input.

A decrease of the solar constant by as little as two percent (Budyko, 1969; Sellers, 1969) might lead to the glaciation of the earth, whereas an increase of less than one percent would lead to a melting of the polar ice caps. These conclusions came from  $1-\phi$ -dimensional models (only variations with latitude were taken into account) with a simple positive ice-albedo feedback mechanism. The models are again based on Eq. (3.27), prescribing, however, the infrared radiation emitted to space and the albedo as simple functions of the zonal-mean surface temperature. These one-dimensional models allowed Budyko and Sellers to estimate the influence of a change in radiation on the temperature in each latitudinal zone after adding the flux convergence of heat due to atmospheric motions. Budyko (1969) assumed the flux convergence to be proportional to the temperature departure from the global mean. With their choice of parameters the final latitudinal distribution of temperature was found to be very similar to the observed zonal mean distribution. In their models it was also possible to determine the extent of the polar ice caps, assuming that their boundaries coincided with the  $-9^\circ\text{C}$  isotherm.

A general review of the energy-balance climate models was published by North *et al.* (1981), covering this topic in great detail.

Another important contribution to the modeling of the atmosphere was given by the  $1-z$ -dimensional model of Manabe and Strickler (1964), which may be regarded as an asymptotic, boundary-value problem. This one-dimensional radiative-convective model is globally averaged and is particularly suitable for studying the influence

of the vertical exchange of heat on the temperature structure of the atmosphere. Global and annual mean vertical profiles of carbon dioxide, ozone, and, at times, water vapor, as well as cloudiness and surface parameters were specified, so that the infrared radiation emitted and the solar radiation absorbed could be evaluated. The model assumes a balance between the incoming solar and the emitted terrestrial radiation, leading to a condition of thermal equilibrium. It incorporates a convective adjustment to avoid superadiabatic stratification in the model atmosphere. Starting with isothermal initial conditions the system developed, within one year, a vertical temperature structure with a troposphere and a stratosphere separated by a well-defined tropopause. The temperature profile obtained was very close to the mean observed one in the atmosphere (see Fig. 51). For a review of the 1- $z$  radiative-convective models see Ramanathan and Coakley (1978).

The statistical-dynamical models are based on the time-averaged equations (3.23)–(3.28), where all source terms and eddy flux divergences are put on the right-hand side of the equations. The time-mean state of the atmosphere in these statistical-dynamical models may then be regarded as a regime forced not only by external processes, such as radiation, topography, surface friction, and evaporation, but also by the large-scale transient eddy transports of heat, water vapor, and momentum. These 2- $(\lambda, \phi)$ -dimensional models are designed to study the longitudinal variations of climate in the vertical mean or at the earth's surface, in order to take into account land-sea contrasts. Indeed, in some cases the observed variations from land to sea regimes are almost as pronounced as the latitudinal variations (see Figs. 10, 22, and 28). The main difficulty with this approach lies in the problem of formulating physically sound parameterizations of the transient eddy phenomena [see survey by Saltzman (1978)].

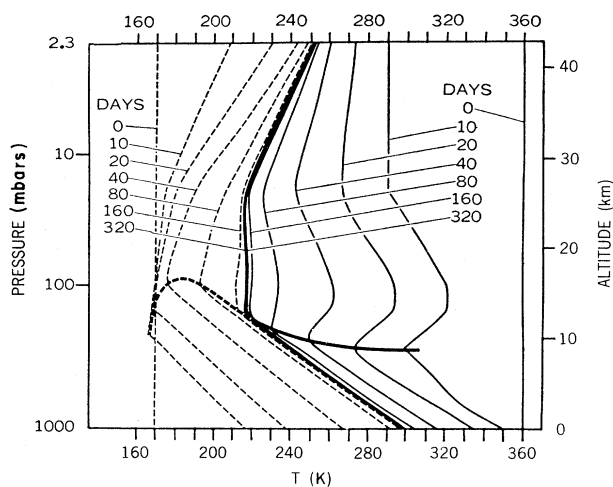


FIG. 51. The approach to the state of thermal equilibrium from a warm (solid lines) and a cold (dashed lines) isothermal atmosphere using a 1- $z$  model from Manabe and Strickler (1964).

Another parameterization approach has been used by Adem (1964). He assumes that latitudinal and longitudinal heat transports may be parameterized in terms of horizontal "Austausch" coefficients.

Other types of statistical-dynamical models, namely, 2- $(\phi, z)$ -dimensional ones (see cross sections in Figs. 15, 16, 31, and 32), have been used by, among others, Saltzman (1968), Green (1970), and Stone (1974). They parameterized the transient and stationary eddies in terms of the mean zonal parameters based on baroclinic instability theory.

## F. General circulation models

General circulation models are time-dependent hemispheric or global models. They simulate explicitly, with as much fidelity as possible, the various processes occurring in the atmosphere and, to some extent, in the oceans. The governing equations of the models are given essentially by Eqs. (3.1)–(3.10), which form a closed system of equations with specified boundary conditions.

A general view of the major components of the mathematic simulation of climate in the atmosphere is given in Fig. 52, complemented by Fig. 1, showing the basic conservation equations and the external factors, namely, radiation and other interactive processes, such as the transfers of momentum, heat, and water substance at the earth's surface.

These models have a huge number of degrees of freedom, because the equations must be solved at all grid points corresponding with the spatial resolution chosen. Actually, the resolution in the vertical is on the order of ten levels, while in the horizontal the grid resolution is about  $200 \times 200 \text{ km}^2$ . Thus these climate models are resolution bound in the sense that all processes occurring at smaller scales cannot be represented and resolved by the model grid. The subgrid-scale phenomena have to be parameterized, whenever and wherever possible, in terms of the resolved macroscale variables. This parameterization offers only a partial resolution of the problem. In fact, attempting to adjust the parameterization to better fit the observed subgrid-scale processes for one parameter sometimes leads to a worse simulation for some other parameters of the global system.

The simulation starts with a set of initial conditions that do not have to be realistic. The model is integrated in time over a very long ("infinite") time span until a statistical equilibrium is asymptotically reached (see, for example, Fig. 51).

Even starting with isothermal conditions and with solid rotation, a GCM will soon develop a convection circulation with a large, thermally direct, equator-to-pole cell in each hemisphere. In the course of months of integration, this symmetric circulation becomes baroclinically unstable and breaks down into large disturbances in middle latitudes. It then shows a well-defined macroturbulent regime with strong eddy motions in middle latitudes, while the thermally direct Hadley cell retreats into the tropics

## MATHEMATICAL SIMULATION OF THE ATMOSPHERE

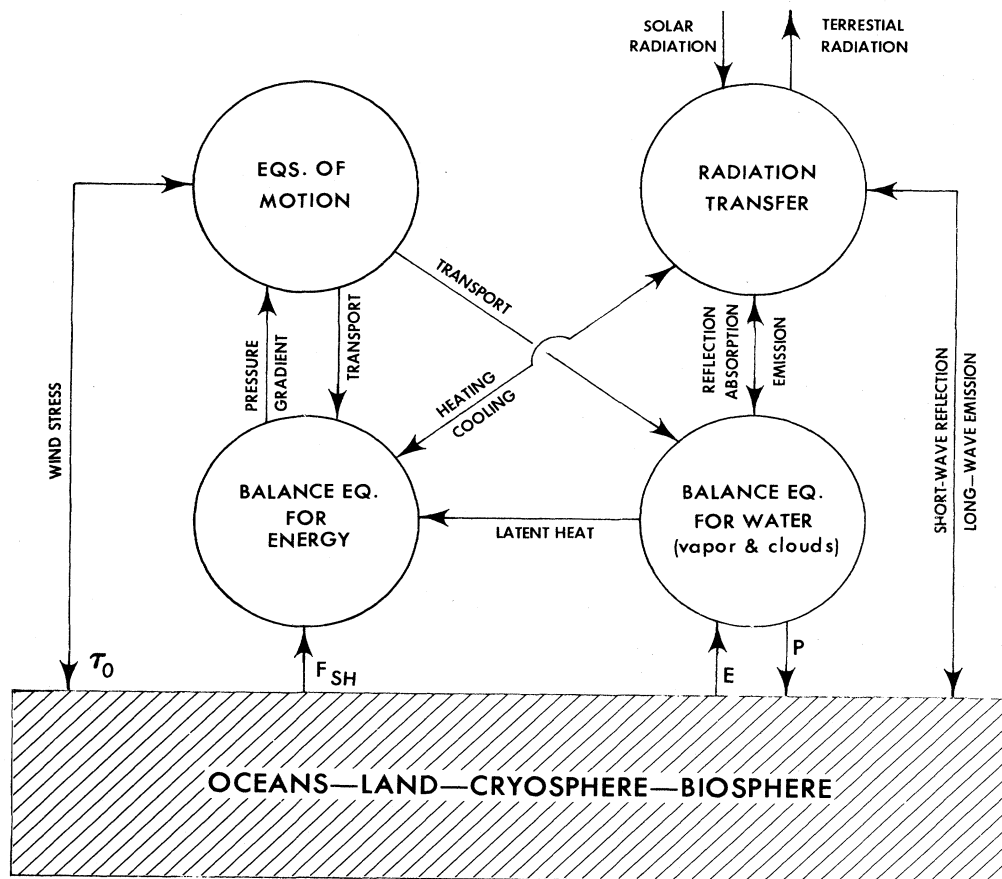


FIG. 52. Major components of the mathematical simulation of climate. (The equation of state has been left out of the diagram.)

and a weak indirect Ferrel cell develops in middle and high latitudes. These results agree with direct observations [see Fig. 15(c)]. We can also compare other large-scale statistics obtained through model simulations, such as mean fields and their variances and covariances, with those obtained for the real atmosphere (see Sec. IV).

With the use of GCM's an attempt is made to incorporate all relevant physical processes that are known to be important in the real atmosphere. In view of their high level of simulation capacity, they constitute a powerful tool for climate research studies. It is believed that these models have the potential to simulate the climate faithfully under a great variety of boundary conditions.

The first general circulation model of the atmosphere was developed by Phillips (1956). It was a quasigeostrophic, two-layer, hemispheric model which included friction and nonadiabatic heating effects in a simple manner. The model, although very simple, could develop a zonal flow with eddies in middle latitudes generated through the baroclinic instability mechanism. This experiment demonstrated the feasibility of simulating the global atmospheric circulation numerically.

An important next step in the development of the

GCM's was accomplished in a study by Smagorinsky (1963). In a two-layer model he solved the primitive equations numerically for an extended period of 60 days, clearly showing the development of baroclinic perturbations in middle latitudes. The motions were confined to a zone bound by the equator and  $64^\circ$  latitude, so that long planetary waves could develop. The kinematics of the motions on the sphere were taken into consideration using a Mercator projection.

Later many other GCM's were developed incorporating new features or using different types of parameterization, such as those of Mintz and Arakawa (Mintz, 1965), Smagorinsky *et al.* (1965), Manabe *et al.* (1965), Leith (1965), and Kasahara and Washington (1967). These were followed by even more sophisticated models (see survey by Smagorinsky, 1974).

The simulation of the general circulation in the world ocean was attempted first by Bryan and Cox (1967) using the basic thermohydrodynamic equations for the oceans with the hydrostatic assumption. The resolutions in the horizontal and vertical directions were higher than those used in atmospheric models. In fact, the small dimensions of the observed eddies in the ocean (a few hundred

km rather than thousands of km in the atmosphere) would require a grid distance on the order of tens of km, which is not yet feasible for global integrations. To minimize the effects of the unresolved eddies an unrealistically high viscosity had to be used to establish a steady circulation. In general, the ocean models are not yet as far advanced as the atmospheric models due to, among other factors, the wider range of time scales (see Fig. 2).

We will pass in review some of the important contributions in the evolution of the numerical models. With the improvement of computing facilities it was possible to increase the spatial and therefore the temporal resolution allowing a more detailed simulation of the atmospheric flow (Manabe *et al.*, 1970). This led to a better representation of the general circulation both in smaller and larger scales. It was also possible to improve the vertical structure of the atmosphere by, for example, including a surface boundary layer with several levels below 1 km height in order to better link the free atmosphere with the earth's surface through a turbulent boundary layer.

Due to its importance for hydrology, we will describe a recent atmospheric GCM with a hydrological cycle developed by Manabe and Holloway (1975). This model includes continents with mountains and soil that has a uniform "field capacity" of 15 cm water. In other words, the maximum amount of water the soil can retain without generating runoff is 15 cm. In the case of the oceans they assumed an infinite field capacity but no redistribution by ocean currents, i.e., a swamp-type ocean surface. The model computes basically the fields of temperature, wind, and water vapor for the atmosphere, and derives the rate of precipitation (rain or snow) minus evaporation from the convergence of moisture transport in the atmosphere (see Sec. IV.D). The evaporation is inferred through a simple scheme (Budyko, 1956) which assumes that evaporation is a function of soil moisture and potential evaporation

(maximum possible evaporation from a water-saturated soil). The rates of change of soil moisture and snow depth are then computed, keeping track of the water and heat budgets of the ground. Runoff occurs when the accumulated soil moisture exceeds the prescribed field capacity of 15 cm, and is assumed to flow directly into the surrounding seas without further infiltration. The total precipitation and other hydrological parameters compare well with those observed in the real atmosphere. The model also depicts the equatorial rain zone and major subtropical deserts (see Fig. 53). It is interesting to note that the climate obtained fits well with the famous climate classification given by Köppen (1931).

In the first global coupled ocean-atmosphere GCM constructed by Manabe (1969) and Bryan (1969) a special technique for integration was used to circumvent the difficulty of having two interacting subsystems with different time scales. They started with a horizontally uniform but vertically stratified ocean temperature distribution and an isothermal atmosphere at rest. After a short interval of time a mean wind stress and mean fluxes of heat and moisture obtained from the atmospheric model integration were used as new boundary conditions at the ocean surface for further integration of the ocean model. Then after a certain interval of time a new sea surface temperature distribution generated by integration of the ocean GCM was applied as a new forcing boundary condition to the atmosphere, and so on. Basically this technique constitutes an alternating, repetitive process. The results are synthesized in Fig. 54 from a later paper which includes the seasonal variations. It is clear that the model reproduces the gross features of the observed temperature distribution. These coupled models are still at a fairly primitive stage of development but will play a more and more important role in the future to evaluate possible climate predictions.

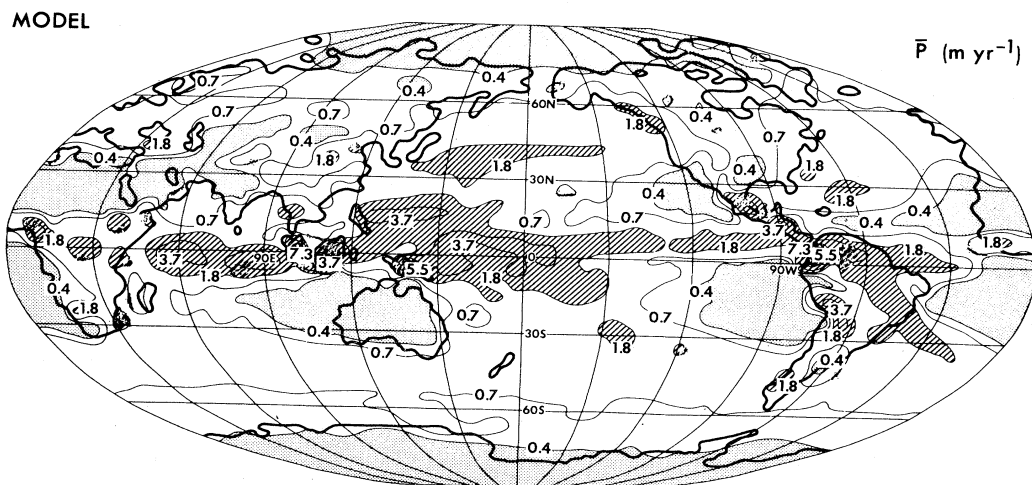


FIG. 53. Global distribution of the annual mean rate of precipitation ( $\text{m yr}^{-1}$ ) simulated by a general circulation model, after Manabe and Holloway (1975). [Compare with observed precipitation rates in Fig. 23(b).] Stippled areas indicate  $\bar{P} < 0.4 \text{ m yr}^{-1}$  and shaded areas  $\bar{P} > 1.8 \text{ m yr}^{-1}$ .



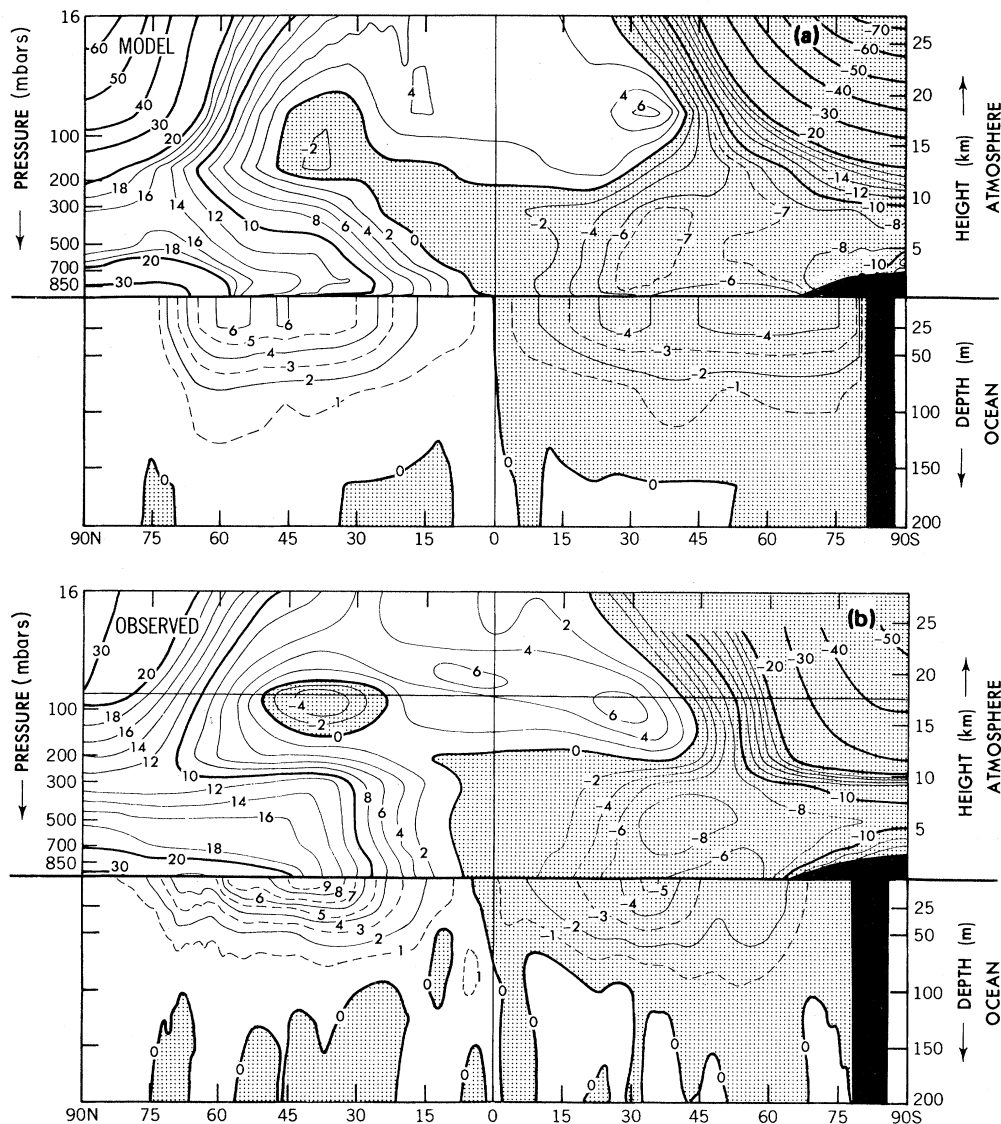


FIG. 54. Zonal mean cross sections of the seasonal range in temperature (August minus February) in the atmosphere-ocean system for both (a) simulated and (b) observed conditions, after Manabe *et al.* (1979). The units are  $^{\circ}\text{C}$ .

## VII. MATHEMATICAL SIMULATION AS AN EXPERIMENTAL TOOL

### A. Uses and applications of models

Mathematical simulation of climate has reached a level of development that can no longer be regarded as a purely academic exercise. It constitutes an indispensable tool for conducting indoor experiments of the natural climatic system. Indeed, through simulation it is possible to evaluate the sensitivity of the components of the climatic system to changes in external forcing, such as variations in solar radiation, surface topography, and composition of the atmosphere. The simulation is the only way of getting answers to important questions that now start to emerge (Peixóto, 1977). How would the temperature in the atmosphere respond to an increase in carbon dioxide? What would be the consequences if the solar constant

were subject to variations? What would be the critical decrease necessary in the solar constant to produce a new glaciation of the earth? How was the climate during the last glaciation? What is the influence of a change in the atmospheric heat balance on the intensity of the hydrological cycle? What are the effects of changing the surface albedo through overgrazing or deforestation? What are the impacts of other human activities, such as industrialization, changes in agricultural practices, and urbanization, on the climatic system?

Furthermore, simulation allows us to understand better the mechanisms involved in the nonlinear feedback processes operating almost simultaneously in the climatic system. Also, one can test different working hypotheses or ideas regarding the influence of clouds, aerosols, dust, ozone, tritium, and other tracer elements.

Tentative answers to some of the previous questions are

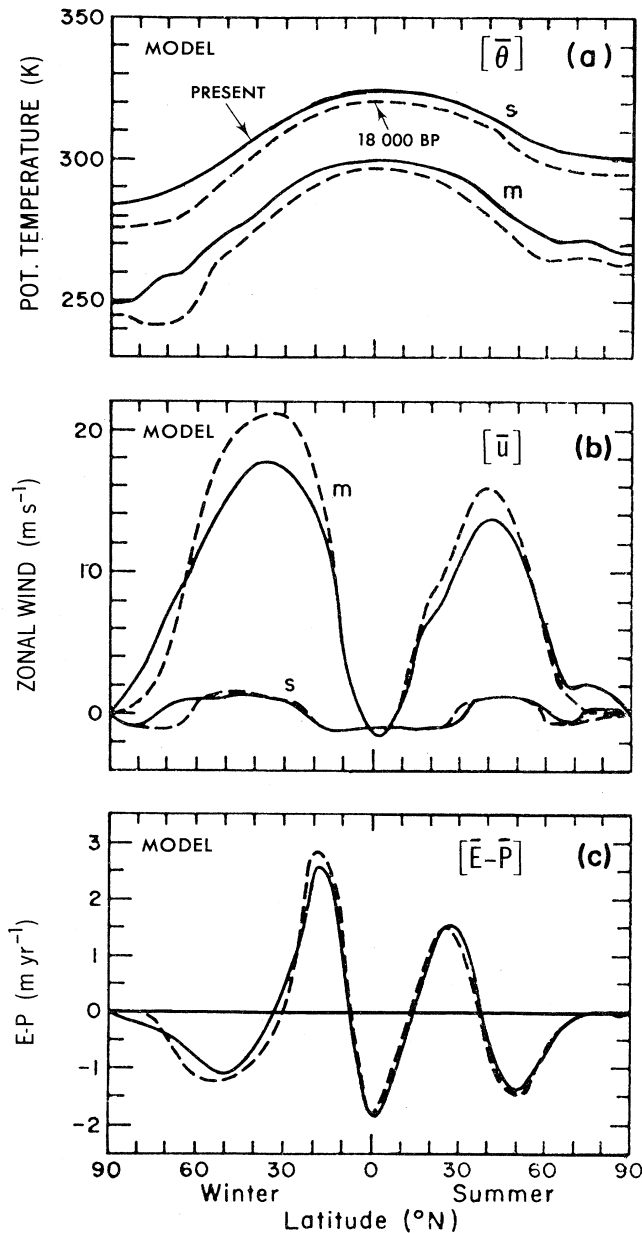


FIG. 55. Zonal mean profiles of (a) potential temperature, (b) zonal wind, and (c) evaporation minus precipitation, as simulated by a statistical-dynamical model for present (solid lines) and for glacial conditions about 18 000 BP (Before Present; dashed lines). The potential temperature is related to the real temperature by the Poisson equation (3.6). The subscripts  $s$  and  $m$  refer to surface and atmospheric (vertical mean) conditions, respectively, after Saltzman and Vernekar (1975).

starting to emerge. The effects of mountains on the general circulation of the atmosphere were studied by Manabe and Terpstra (1974) through a set of numerical experiments. The simulated circulation in a model with the actual topography was compared with the corresponding circulation in a model without mountains, keeping the land-sea distribution the same. The results show that the mountains are important in explaining many of the

quasistationary features of the general circulation, like the cyclogenesis on the leeside of the mountains, and the distribution of precipitation.

The effects of changing the solar constant on climate were already mentioned when we discussed the works of Budyko (1969) and Sellers (1969)—see Sec. VI.D. Later, using a GCM, Wetherald and Manabe (1975) attacked the same problem. Their results show a significant warming of the lower troposphere at high latitudes, resulting in a reduction of the baroclinic instability and of the sensible heat transport in middle latitudes; they also show a decrease in the oceanic heat transport. The computed increase in temperature with increasing solar constant is in qualitative agreement with the results of Budyko and Sellers. Another interesting result from the GCM is the large sensitivity of the intensity of the hydrological cycle to small changes in the solar constant.

Using various types of models there have been some attempts to model the ice-age climate. These models use boundary conditions at the earth's surface (extent of land and sea ice, sea surface temperature, and surface albedo) prescribed according to paleoclimatological evidence, and evaluate the atmospheric structure as an equilibrium solution. Among them we will refer to Saltzman and Vernekar (1975), who used a statistical-dynamical model, Gates (1976), who used a two-layer GCM, and Manabe and Hahn (1977), who used a multilayer GCM. The results of Saltzman and Vernekar (1975) are suggestive and are summarized in Fig. 55.

## B. Man's impact on climate

Human activities can interfere in the climate through changes in the composition and structure of the atmosphere, through the release of heat into the atmosphere, and through changes in the albedo and other properties of the earth's surface, thus changing the radiation balance. Human beings are inadvertently altering the composition of the atmosphere in a continuous manner because they change the concentration of some of the atmospheric constituents already in existence, and because they introduce new substances into the atmosphere that under normal natural conditions would not exist. We may mention the emission of gases, smoke, and particulate matter from the industrial complexes and urban centers and from agricultural practices such as the burning of trees, deforestation, and massive use of fertilizers, leading to the pollution of the atmosphere and waters. With deforestation and overgrazing, the soil is eroded and prevailing winds may remove large quantities of topsoil which later will be spread out into the atmosphere. These processes will produce substantial changes in the surface albedo, affecting then the radiation and moisture balances near the surface and eventually leading to desertification.

The gases and particles thrown into the atmosphere may affect the climate because (a) they alter the radiation balance of both the local and the global atmosphere, leading to modifications in the thermal and dynamical structure of the atmosphere, (b) they interfere in the photochemical equilibrium of the stratosphere and especially in



the balance of ozone (freons), and (c) they can form acids in either the gas phase or in the liquid phase as fog or cloud droplets which will lead to acid precipitation.

Aerosols consist of small liquid and solid particles dispersed inside the atmosphere. They interfere with the radiation balance through reflection, scattering and absorption of the short-wave solar radiation, leading likely to a slight, net cooling of the atmosphere (Bryson, 1972). Some of the particles may act as condensation nuclei for fog and cloud droplets or are picked up by existing drops. Those particles that contain sulfur or nitrogen oxides lead to the formation of acid rain.

Among the gases released into the atmosphere by human activities, the most important component is probably carbon dioxide ( $\text{CO}_2$ ). Carbon dioxide is well mixed in the atmosphere with an almost uniform concentration of, at present, about 340 parts per million (ppm). It is a small but essential component of the atmosphere, because, along with water vapor and ozone, it plays a very important role in heating the atmosphere. In fact, the  $\text{CO}_2$  molecules are transparent for short-wave solar radiation but are strong absorbers in the vibrational and rotational bands for infrared radiation emitted by the earth's surface. Thus through absorption  $\text{CO}_2$  prevents the radiation emitted by the surface from being lost into space. This mechanism is called the  $\text{CO}_2$ -greenhouse effect, although this is a misnomer, since heating in the usual greenhouse effect is due to the reduction of convection, whereas with  $\text{CO}_2$  the heating is due to the trapping of infrared radiation. The more  $\text{CO}_2$  there is in the atmosphere, the more radiation will be absorbed and the warmer the lower atmosphere will become. Thus the increase in  $\text{CO}_2$  will have profound and long-term effects on the climate.

The carbon in the climatic system is contained in four major reservoirs: the oceans, the biosphere, the atmosphere, and the lithosphere, including the fossil fuels.

The transfers of carbon between these reservoirs are complex and not very well known. They lead to the carbon cycle that has been the subject of much research (Keeling, 1982). In the atmosphere carbon exists mainly in the form of  $\text{CO}_2$  in much smaller amounts than in the other reservoirs. Recent computations give a residence time of  $\text{CO}_2$  in the atmosphere on the order of five to seven years (National Academy of Sciences, 1979), which is short compared to the residence times in the other reservoirs. Thus due to its large mobility the atmosphere plays an important role in the carbon cycle.

The amount of  $\text{CO}_2$  has been increasing mainly since the beginning of the industrial revolution (1850), when the concentration was about 290 ppm. Since then it has increased about 15%, with the largest increase between 1958 and 1983—see Fig. 56. This figure shows the general behavior of the evolution of  $\text{CO}_2$  in the atmosphere. Two effects can be seen clearly: first, a quasisinusoidal annual variation with a range of about 6 ppm, which is due to the annual cycle in photosynthesis, and, second, a steady increase in the annual mean on the order of 1 ppm/year. Although the general shape of the curves for the annual-mean  $\text{CO}_2$  concentration is the same at different geographical locations, the amplitude of the seasonal cycle may be quite different, as one would expect.

The increasing use of fossil fuels, such as natural gases, oil, and coal, has been a major factor in the observed increase in atmospheric  $\text{CO}_2$ . Deforestation and decay of organic matter may also constitute a small source of  $\text{CO}_2$  for the atmosphere. However, the idea proposed by Dyson (1977), that plants and trees would grow better in a richer  $\text{CO}_2$  environment and thereby would absorb some of the atmospheric  $\text{CO}_2$ , cannot be discounted. In any case, there has been a gross imbalance between the estimated input of  $\text{CO}_2$  and the observed change in atmospheric concentration. Thus the atmosphere retained at most only half of the amount produced by the burning of

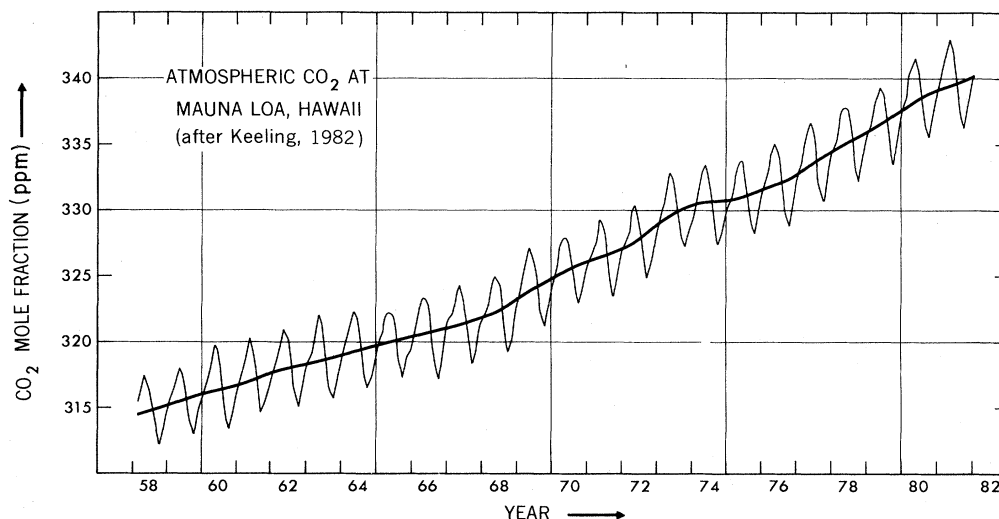


FIG. 56. Time series of the atmospheric  $\text{CO}_2$  concentration, as measured at Mauna Loa Observatory, Hawaii ( $19.5^\circ\text{N}, 155^\circ\text{W}$ ), after Keeling (1982). The thick solid curve is a spline fit to the monthly data showing the long-term trend. This trend is generally assumed to be representative for global mean conditions, because  $\text{CO}_2$  appears to be well mixed.

fuels during the past decades. It is now generally accepted that the oceans constitute the principal absorber for  $\text{CO}_2$  and that more than one-half of the newly released  $\text{CO}_2$  is removed from the atmosphere by absorption at the ocean surface. However, the detailed mechanisms are not yet well understood.

Accepting that the burning of fossil fuels will continue to be the dominant source of  $\text{CO}_2$  for the atmosphere and that the atmosphere can retain at most one-half of the  $\text{CO}_2$  produced, we can predict the atmospheric  $\text{CO}_2$  concentrations for various scenarios of the future consumption of fossil fuels. If we maintain the present rate of fuel consumption, the concentration of  $\text{CO}_2$  will double with respect to the preindustrial value ( $\sim 290$  ppm) by the year 2200. However, if instead the actual energy use will grow at a rate of 2.5% per year, doubling of  $\text{CO}_2$  will occur by the middle of the next century (National Academy of Sciences, 1979, 1982). With this increase in  $\text{CO}_2$  a sizable change in the surface temperature would be expected of about  $3^\circ\text{C} \pm 1.5^\circ\text{C}$  (Manabe, 1983)—a fact already noted by Arrhenius in 1896 and later by Callender (1938).

There is little empirical evidence to allow us to predict with confidence the effects of the increasing  $\text{CO}_2$  on climate. Therefore, we have to rely on mathematical simulations using a variety of climate models. Using a one-dimensional radiative-convective equilibrium model, Manabe and Wetherald (1967) computed the vertical distribution of the global-mean temperature for a  $\text{CO}_2$  concentration of 300 ppm, as well as twice and half this value (see Fig. 57). They computed a change in surface temperature of slightly more than  $2^\circ\text{C}$  when keeping relative humidity constant. Strong cooling was found in the stratosphere when the  $\text{CO}_2$  concentration was increased.

Later Manabe and Wetherald (1975) used a GCM to calculate the changes in the three-dimensional structure of the atmosphere resulting from a doubling of the  $\text{CO}_2$  concentration (see Fig. 58). They again obtained a general warming of the troposphere due to the increased greenhouse effect with an average global rise in surface temperature of  $3^\circ\text{C}$ . The largest warmings were computed in the polar regions as a result of the positive temperature—snow albedo feedback and due to the high static stability at those latitudes, which restricts the temperature changes to the lowest levels.

The resulting climatic changes would markedly affect the hydrological cycle, increasing both the overall evaporation and precipitation, and consequently the runoff. Furthermore, selective warming of the polar regions could lead to the melting of snow and ice, especially in the Antarctic, which might conceivably cause a 5-m rise in sea level during the next century with significant flooding of coastal regions (Hansen *et al.*, 1981). We might add that the consumption of energy by the melting of ice would possibly slow down the global atmospheric temperature increase, so that the rise in sea level might become the main signature of the  $\text{CO}_2$  effect.

Agricultural productivity depends critically on the incoming radiation, temperature, precipitation and cloudiness, and, of course, the soil fertility. Thus any climatic

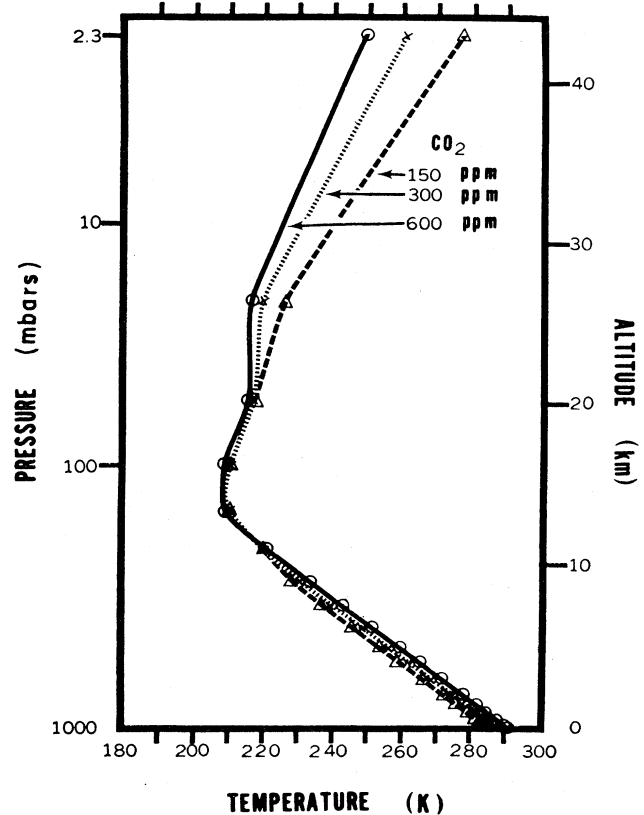


FIG. 57. Vertical distribution of temperature simulated in a 1-z radiative equilibrium model for  $\text{CO}_2$  concentrations of 300 ppm (the atmospheric value estimated for the year 1860), 600 ppm, and 150 ppm, from Manabe and Wetherald (1967). A doubling of  $\text{CO}_2$  concentration to 600 ppm may be expected during the latter half of the next century.

change, such as the change implied by a  $\text{CO}_2$  increase, would affect this productivity. The changes in  $\text{CO}_2$  would further influence other segments of the biosphere, such as the forests and fisheries. These last ones would be

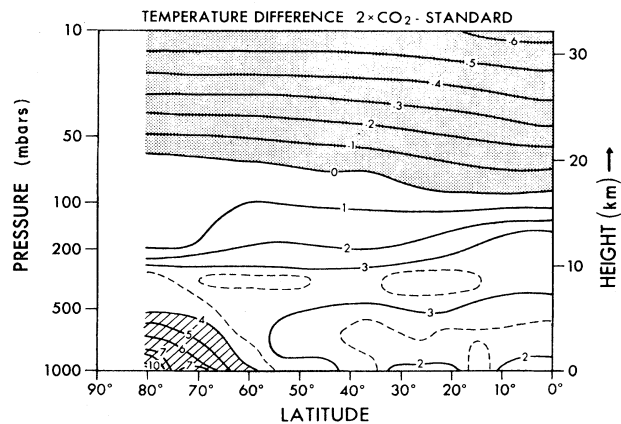


FIG. 58. Zonal mean cross section of the temperature change in  $^\circ\text{C}$  resulting from a doubling of the  $\text{CO}_2$  concentration from 300 to 600 ppm, as simulated in a three-dimensional general circulation model by Manabe and Wetherald (1975).

affected through changes in the upwelling of nutrient waters.

Lately many different model calculations have been performed, leading to approximately the same results as mentioned above for the global heating. However, we should stress the general premise in all these studies that all factors besides the CO<sub>2</sub> concentration should remain the same. For example, most models have not taken into account possible changes in cloud cover, which could affect the temperature response in the atmosphere. In a global assessment of the CO<sub>2</sub> problem the National Academy of Sciences (1979,1982) concluded that if carbon dioxide continues to increase, there is no reason to doubt that climatic changes will result and no reason to believe that these changes will be negligible.

## VIII. SUMMARY

### A. Nature of the problem

After defining the climatic system we passed in review the main characteristics of the various components of the earth's climate, namely, the atmosphere, the oceans, the cryosphere, the lithosphere, and the biosphere. Taking the atmosphere and oceans as the central subsystem, we analyzed the main interactions and feedbacks between the various coupled subsystems. Using an approach similar to that of statistical mechanics, we defined the climate state, or simply the "climate," as an ensemble average over the instantaneous states of the climatic system.

As we analyzed the nature of the climate problem, some questions came up as to the behavior of the atmosphere in time. The possibility that the atmosphere does not behave as a transitive (ergodic) system could not be excluded. Actually, it could behave as an almost intransitive system as manifested by the existence of glacial and interglacial periods in the climatic records.

### B. The climate equations

The climate was studied using some of the basic laws of physics, which are a consequence of the conservation principles of angular momentum, energy, and mass [see Starr (1951)]. These equations are nonlinear, and, in general, a linearization approach cannot be used. The climate variables are physical quantities defined in a space-time domain. Thus the thermohydrodynamical equations had to be prepared through adequate averaging in time and space, leading to what may be called the climate equations. We are faced with a mixed initial value-boundary condition problem that leads to a unique solution if the system is ergodic. Under this hypothesis the climate system behaves as if it has forgotten its initial conditions. The external factors, such as solar radiation input, rotation rate of the earth, composition of the atmosphere, and surface boundary conditions, would then determine the climate.

The predominance of zonal symmetry of the various

climatic quantities with respect to the rotation axis of the earth made it desirable to introduce the zonal averaging operator. The resulting climatic equations allowed us to analyze the maintenance of the zonal-mean conditions. The departures from zonal symmetry, the "eddies," are due not only to anomalies in the thermal and mechanical surface boundary conditions but also to inherent hydrodynamic instabilities in the atmosphere associated with the earth's rotation rate and the equator-to-pole heating gradient.

Finally, for analyzing the observed climate the climatic equations were averaged over the entire atmospheric mass. The resulting equations bring out the importance of the interactions between the atmosphere and the underlying surface through the transfers of mass (water vapor), angular momentum (friction and mountain torques), and energy (sensible heat, latent heat, and radiation).

### C. The observed climate

The observed climate was presented in the form of pole-to-pole horizontal maps for the various climatic variables, as well as in vertical-meridional cross sections and vertically integrated meridional profiles. Shown were not only the mean linear fields but also statistics of higher order. The results were obtained from a fifteen-year global data set for the atmosphere, all available historical data for the oceans, and recent satellite observations for the radiation balance at the top of the atmosphere.

Radiation, being the main external forcing, was thoroughly analyzed. The global net radiation balance required a poleward transport of energy in the atmosphere and oceans away from the equatorial region to maintain thermal equilibrium.

The zonal circulation showed the existence of two maxima of eastward winds in the upper troposphere at mid-latitudes, corresponding to the jet streams. In the tropical regions the lower-level winds are mainly from the east. The meridional circulation revealed a three-cell regime in each hemisphere with two thermally direct cells (the Hadley and polar cells) and in between a thermally indirect cell (the Ferrel cell).

The atmosphere was found to gain westerly angular momentum from the underlying surface in the tropics and to return it to the earth at middle and high latitudes. The angular momentum exchanged with the oceans generates the main ocean surface currents, whereas the exchange with the solid earth takes place through friction, mountain and continental torques. It was further shown that variations in the total angular momentum of the atmosphere have important implications for the length of the day.

The main sources of water vapor for the atmosphere are observed to be in the subtropics, predominantly over the oceans. The water vapor in the atmosphere is transported from the surface source to the sink regions by the general circulation, leading to the atmospheric branch of the hydrological cycle. The vapor will condense and precipitate in the equatorial convergence zone and in the

middle-to-high latitude zones associated with the polar fronts. The cycle is closed by the terrestrial branch through surface runoff (rivers) and subterranean runoff. Over the oceans in regions where evaporation exceeds precipitation the salinity (density) of the surface waters increases and thereby affects the dynamics of the ocean circulations.

The main forms of energy for the climate system, besides radiant energy, are potential, internal, latent heat, and kinetic energy. The oceans with their high thermal inertia are an important heat reservoir for the system, thereby acting as a moderator of the climate in the atmosphere.

The atmosphere was regarded as a heat engine with heat flowing from the tropics to the polar and upper regions. The work performed is used to maintain the kinetic energy of the circulations against the continuous drain by friction. Only a very small fraction of the total potential energy, the available potential energy, is usable for conversion into kinetic energy.

We found that the energy flows in a cycle from mean zonal available potential energy into eddy-available potential energy and then into eddy kinetic energy. Available potential energy is generated by the differential heating of the atmosphere. The efficiency of the atmospheric heat engine was determined to be less than 1%.

One of the most pronounced climatic variations on the scale of a few years is the El Niño phenomenon. It occurs every three to four years along the coasts of Peru and Ecuador, when the warm surface waters spread over the cold waters in the Eastern Pacific Ocean. This phenomenon is associated with the Southern Oscillation and has world-wide repercussions in the climate.

#### D. Mathematical simulation of climate

The mathematical models of climate are based on a set of specialized thermohydrodynamic equations with prescribed boundary conditions. The integration of a fully coupled model including the atmosphere, oceans, land, and cryosphere poses almost insurmountable difficulties in reaching a final solution even if all processes involved were completely understood.

The models were classified into deterministic and stochastic models. The first class includes the explicit dynamical models and the statistical-dynamical models. The explicit dynamical models are three-dimensional and use the complete climate equations. The evolution of the large-scale circulations is followed on a day-to-day basis. Among these models the general circulation models (GCM's) have been the most successful. They require a high resolution in space and an integration with relatively short time steps.

Stochastic models were developed because many of the physical processes in the climate system cannot be modeled or parameterized in a deterministic way, due to the large differences in internal time scales: hours to weeks for the atmosphere, weeks to months for the mixed layer of the oceans, months to years for sea ice and snow,

and decades to millenia for the deep oceans and polar ice. Using such a stochastic approach the evolution of the slowly changing variables in one subsystem can be expressed in terms of the faster variables in another subsystem.

Mathematical simulation has become an essential tool for the study of climate as well as for conducting experiments on the climatic system. Through simulations it is possible to assess the sensitivity of climate to variations in external forcing, such as an increase in carbon dioxide in the atmosphere and changes in the surface albedo. Mathematical simulations also lead to a better understanding of the nonlinear feedback processes operating in the climatic system.

#### E. Man's impact on climate

Human beings are interfering with climate through the release into the atmosphere of heat, smoke, particles, dust, and chemicals, and through changes in the earth's surface albedo due to deforestation, overgrazing, urbanization, etc.

From all these effects the increase of carbon dioxide (CO<sub>2</sub>) in the atmosphere during the last few decades seems to be most relevant for potential changes of climate. Before the industrial revolution (around 1850) the concentration of CO<sub>2</sub> was about 290 ppm, whereas the present observed value is about fifteen percent higher. Theoretical calculations show that, other things being equal, a doubling of CO<sub>2</sub> concentration in the atmosphere would lead to a significant warming of the earth's surface, but that the resulting temperature changes would not be uniformly distributed over the globe.

The increase of atmospheric CO<sub>2</sub> would tend to intensify the hydrological cycle and change the regional patterns of evaporation and precipitation. Furthermore, the expected increase in temperature might lead to the partial melting of the continental ice sheets and a rise in sea level. The increase of carbon dioxide would also have an important impact on the ecosystems.

#### IX. EPILOGUE

So far we have discussed mainly what we know about the physics of climate. We have seen how the total climate system operates as a gigantic machine—each part being connected with all other parts in, at times, very subtle ways. In analyzing this complex but beautiful machine we followed the pathways of water, angular momentum, and energy as they are cycled and recycled through the climate system in an apparent quasisteady manner. However, besides these largely resolved questions there are many more unresolved issues, and it is on some of these issues that we want to concentrate in this epilogue.

(1) Do the atmosphere, oceans, and cryosphere as a whole form a stable system, or are other states besides the present climatic state possible with the same external

boundary conditions as today? Could we go into a major glaciation of the earth with only a few percent decrease in solar radiation input, or could the ice sheets melt with only a minor increase in solar input? Simple energy balance models discussed earlier in Secs. VI and VII have given us some hints, but full-scale general circulation models are needed (though perhaps not sufficient) in conjunction with the analysis of actual geological records to resolve these issues. Considerable progress may be expected in the coming decade.

(2) Of perhaps more direct practical interest are the issues of medium- and long-range weather and climate forecasts. If we would better know the initial conditions together with the external boundary conditions and would better tune our models, could we successfully predict the large-scale weather two weeks to perhaps, under blocking conditions, a month ahead? (For a first attempt, see Miyakoda *et al.*, 1983.) Given the rate of increase in CO<sub>2</sub> in the atmosphere, can we reliably predict the expected general rise in temperature over the earth and, even more importantly for human affairs, the changes in regional patterns of temperature, precipitation, and evaporation throughout the year? The first indications are that the answer to the last two questions is yes. On the other hand, we know very little about the role of the oceans and biosphere in the CO<sub>2</sub> issue apart from the now accepted notion that more than half of the released CO<sub>2</sub> is being absorbed by the oceans. It seems entirely possible that sometime in the future the oceans would give off rather than absorb CO<sub>2</sub> from the atmosphere, thereby accelerating the increase in atmospheric CO<sub>2</sub> and the resulting greenhouse effect. A major effort in developing more adequate ocean models is called for. The effects of the biosphere may further complicate the issue. Dyson (1977) has suggested that plants and trees may grow better in an atmosphere richer in CO<sub>2</sub>, and that they may therefore slow down the projected increase in atmospheric CO<sub>2</sub> associated with increased industrialization.

(3) As we have seen in Sec. IV.F, one clear global long-period fluctuation stands out in the historical records, the El Niño—Southern Oscillation (ENSO) phenomenon. The most spectacular event on record occurred very recently, during 1982—1983, upsetting the weather in the tropics (heavy rains over the eastern equatorial Pacific and the coasts of Ecuador and Peru, along with drought conditions in India, Indonesia, and Australia) and, to some extent, probably also affecting weather in middle latitudes (e.g., more hurricanes in the Pacific Ocean, unusually heavy storms along the coast of California, and fewer than normal hurricanes in the Atlantic). A reasonable description of the sequence of events is now available, but why things suddenly start to happen after three to seven years of normal weather is still a mystery. Do the oceans build up their reservoir of available potential energy by excess absorption of solar radiation during normal years? After a certain critical level of oceanic energy has been reached, would a small trigger then cause a major redistribution of the warm water masses in the Pacific Ocean followed by an increased release of heat into the atmosphere

and, eventually, out to space? Again, joint global atmosphere-ocean models are essential to come to grips with this issue, which is of major economic concern to the people in the tropics.

(4) As far as general circulation models are concerned, a central problem is the incorporation of subgrid-scale phenomena into the equations. It is not known whether in the real world the subgrid-scale effects can be expressed, as is now common practice, in terms of the resolved motions. For example, cumulus convection is clearly subgrid scale, but nevertheless represents the dominant vertical exchange mechanism in the troposphere. Innovative modeling work is clearly needed.

Finally, we want to mention some specific unknowns in the various climate subsystems.

(5) First of all, in the radiation balance we do not know if there are long-term variations in solar forcing or in the earth's response to it. Recent satellite measurements of the solar constant for a three-year period show rather small month-to-month variations of less than 0.5% (Smith *et al.*, 1983). However, longer-term records are necessary. Also, variations in the earth's response through changes in albedo associated with clouds and through changes in long-wave emission are not well documented. Stable multiyear measurement series from satellites are needed.

(6) Of all elements of the climate system most is known about the atmosphere. Nevertheless, there are uncertainties about the role of clouds in modifying the atmospheric response to changes in solar constant, CO<sub>2</sub> concentration, etc., and about the role of various chemical substances released into the atmosphere. During the last few decades much research has been done on the relative importance of the mountains, the land-sea contrast, and the interaction with transient waves in exciting the quasistationary waves in the atmosphere. The position and intensity of these quasistationary waves largely determine the regional abnormality or normality in climate during a specific month or season, since they define the storm tracks and the direction of the prevailing air flow.

(7) From our present perspective, the most important unknown component of the climate system is the world ocean. The oceans moderate the atmospheric climate through their enormous heat capacity and their poleward transport of heat. Large year-to-year anomalies in both quantities may occur but have not yet been measured because of technical problems of measuring at sea and also because of the large financial costs involved. However, without large-scale direct measuring programs of both heat storage and transport, many of the pressing climate problems will remain unsolved.

The oceanic general circulation models are still in a primitive stage of development compared with the status of the atmospheric models. Very high resolution and computerwise expensive models will be required to determine the importance of transient phenomena in the mean ocean circulation.

(8) Changes in the cryosphere directly reflect changes in the latent heat stored in the earth. They also affect the

radiation balance through changes in the albedo for solar radiation and diminish any heat exchange taking place between the atmosphere and the underlying ocean or land. The extent of snow and ice cover and their variability are now pretty well documented from satellite data. However, the net growth or decay of the snow and ice masses on earth are still largely unknown and should be monitored, probably using *in situ* observations.

(9) The land surfaces and more generally the lithosphere play an important role in the hydrological and angular momentum cycles, as shown before in Secs. IV.C and IV.D. One of the central dilemmas in hydrology concerns the observed atmospheric divergence of water vapor from the subtropical deserts, leading to the necessity of an excess of evaporation over precipitation and the need for river or subterranean inflow of water into the subtropical land masses. Aside from the possible, but unlikely, solution that the atmospheric data are systematically biased, speculation on the occurrence of extensive subterranean reservoirs and large subsurface flows of water seem warranted and should be further explored.

The earth's crust and mantle are an essential element in the angular momentum cycle to maintain the overall balance. The mechanisms of exchange between the atmosphere, oceans, and the solid earth have to take place through friction and mountain (continental) torques. Only limited factual information on these matters is presently available. Much will no doubt be learned about the earth and perhaps about its geological processes through more detailed studies of the angular momentum balance.

(10) Finally, we should mention the biosphere, including man. The central role of biospheric processes in the early development of the chemical composition of the atmosphere and oceans, as well as in the maintenance of their present composition, is obvious. Also, through evapotranspiration, plants and trees affect the hydrological cycle on both local and global scales. However, quantitative large-scale information on all these processes is largely missing. In the present generation of general circulation models biology is generally disregarded, but it should certainly take a prominent place in future model generations.

#### ACKNOWLEDGMENTS

The authors would like to thank Stephen B. Fels, Ngar-Cheung Lau, Syukuro Manabe, Richard D. Rosen, David M. Salstein, Joseph Smagorinsky, Alan R. Thomas, and the official reviewers for their constructive criticisms of the manuscript, Hiram Levy II, J. Murray Mitchell II, and Kikuro Miyakoda for helpful discussions, Sydney Levitus for supplying oceanic statistics, Mel Rosenstein for processing the basic data, Phil Tunison and his group for drafting, and Joyce Kennedy, Jim Byrne, and John Conner for general assistance. The visits of J. P. Peixóto to the Geophysical Fluid Dynamics Laboratory were supported through NOAA Grant No. 04-7-022-44017.

#### REFERENCES

- Adem, J., 1964, "On the physical basis for the numerical prediction of monthly and seasonal temperatures in the troposphere-ocean-continent system," *Mon. Weather Rev.* **92**, 91.
- Arrhenius, S., 1896, "On the influence of carbonic acid in the air upon the temperature of the ground," *Philos. Mag.* **41**, 236.
- Berlage, H. P., 1966, *The Southern Oscillation and World Weather*, Royal Netherlands Met. Inst., Communications and Transactions No. 88.
- Bryan, K., 1969, "Climate and the ocean circulation: 3. The ocean model," *Mon. Weather Rev.* **97**, 806.
- Bryan, K., and M. D. Cox, 1967, "A numerical investigation of the oceanic general circulation," *Tellus* **19**, 54.
- Bryan, K., and L. J. Lewis, 1979, "A water mass model of the world ocean," *J. Geophys. Res.* **84**, 2503.
- Bryson, R. A., 1972, "Climate modification by air pollution," in *The Environmental Future*, edited by N. Polunin (MacMillan, London), p. 133.
- Budyko, M. I., 1956, *Atlas eplovovo balansa zemnovo zhara* [The Heat Balance of the Earth's Surface] (Gidrometeorologicheskoe Izdatel'stvo, Leningrad) [translated from Russian by N. A. Stepanova, Office of Technical Services, U.S. Dept. of Commerce, Washington, D.C. (1958)].
- Budyko, M. I., 1969, "The effect of solar variation on the climate of the earth," *Tellus* **21**, 611.
- Callender, G. S., 1938, "The artificial production of carbon dioxide and its influence on temperature," *Q. J. R. Meteorol. Soc.* **64**, 223.
- Campbell, G. G., and T. H. Vonder Haar, 1980, *Climatology of radiation budget measurements from satellites*, Atmos. Sci. Paper No. 323, Dept. Atmos. Sci., Colorado State University, Fort Collins.
- Charney, J. G., 1947, "The dynamics of long waves in a baroclinic westerly current," *J. Meteorol.* **4**, 135.
- Charney, J. G., 1948, "On the scale of atmospheric motions," *Geophys. Publ.* **17**, 1.
- Courant, R., K. O. Friedrichs, and H. Lewy, 1928, "Ueber die partiellen Differenzgleichungen der mathematischen Physik," *Math. Ann.* **100**, 32.
- Crowley, T. J., 1983, "The geological record of climatic change," *Rev. Geophys. Space Phys.* **21**, 828.
- Dobson, F. W., F. P. Bretherton, D. M. Burridge, J. Crease, E. B. Kraus, and T. H. Vonder Haar, 1982, *The "CAGE" Experiment: A Feasibility Study*, World Climate Program **22**, World Meteor. Org., Geneva.
- Dyson, F. J., 1977, "Can we control the carbon dioxide in the atmosphere?" *Energy* **2**, 287.
- Eady, E. T., 1949, "Long waves and cyclone waves," *Tellus* **1**, 33.
- Gates, W. L., 1976, "The numerical simulation of ice-age climate with a global general circulation model," *J. Atmos. Sci.* **33**, 1844.
- Green, J. S. A., 1970, "Transfer properties of the large-scale eddies and the general circulation of the atmosphere," *Q. J. R. Meteorol. Soc.* **96**, 157.
- Hadley, G., 1735, "Concerning the cause of the general trade winds," *Philos. Trans. R. Soc. London* **39**, 58 [Reprinted *Smithsonian Misc. Coll.* **51**, (1910)].
- Hall, M. M., and H. L. Bryden, 1981, "Direct estimates and mechanisms of ocean heat transport," *Deep-Sea Res.* **29**, 339.
- Hansen, J., D. Johnson, A. Lacis, S. Lebedeff, P. Lee, D. Rind, and G. Russell, 1981, "Climate impact of increasing atmospheric carbon dioxide," *Science* **213**, 957.

- Hasselmann, K., 1976, "Stochastic climate models, Part 1. Theory," *Tellus* **28**, 473.
- Hasselmann, K., 1977, "The dynamical coupling between the atmosphere and the ocean," in *The influence of the ocean on climate*, World Meteorological Organization, No. 472, Report on Marine Science Affairs No. 11, p. 31.
- Hasselmann, K., 1978, "On the problem of multiple time scales in climate modeling," in *Man's Impact on Climate*, Proceedings of an International Conference, Berlin, June 14–16, 1978, p. 43.
- Hastenrath, S., 1982, "On meridional heat transports in the world ocean," *J. Phys. Ocean.* **12**, 922.
- Hatsopoulos, G., and J. H. Keenan, 1965, *Principles of General Thermodynamics* (Wiley, New York).
- Held, I. M., 1982, "Stationary and quasi-stationary eddies in the extratropical troposphere: Theory," in *Large-Scale Dynamical Processes in the Atmosphere*, edited by B. J. Hoskins and R. P. Pearce (Academic, New York), p. 127.
- Hunt, B. G., 1979, "The influence of the earth's rotation rate on the general circulation of the atmosphere," *J. Atmos. Sci.* **36**, 1392.
- Huschke, R. E., 1959, Ed., *Glossary of Meteorology* (American Meteorological Society, Boston).
- Imbrie, J., and K. P. Imbrie, 1979, *Ice Ages—Solving the Mystery* (Enslow Publishers, Hillside, New Jersey).
- Jaeger, L., 1976, "Monatskarten des Niederschlags für die ganze Erde" ["Monthly precipitation maps for the entire earth"], *Ber. Dtsch. Wetterdienstes* **18**, No. 139.
- Jones, P. D., T. M. L. Wigley, and P. M. Kelly, 1982, "Variations in surface air temperatures: Part 1. Northern hemisphere, 1881–1980," *Mon. Weather Rev.* **110**, 59.
- Kasahara, A., and W. M. Washington, 1967, "NCAR global general circulation model of the atmosphere," *Mon. Weather Rev.* **95**, 389.
- Keenan, J. H., 1941, *Thermodynamics* (Wiley, New York; reprinted in 1977 by MIT Press.)
- Köppen, W., 1931, *Grundriss der Klimakunde* [The Climates of the Earth] (Walter de Gruyter, Berlin).
- Lambeck, K., 1981, *The Earth's Variable Rotation* (Cambridge University Press, Cambridge, England).
- Lau, N. C., and J. M. Wallace, 1979, "On the distribution of horizontal transports by transient eddies in the Northern Hemisphere wintertime circulation," *J. Atmos. Sci.* **36**, 1844.
- Leith, C. E., 1965, "Numerical simulation of the earth's atmosphere," *Methods Comput. Phys.* **4**, 1.
- Leith, C. E., 1978, "Predictability of climate," *Nature* **276**, 352.
- Levitus, S., 1982, *Climatological Atlas of the World Ocean*, NOAA Professional Paper No. 13 (U.S. GPO, Washington, D.C.).
- Lorenz, E. N., 1955, "Available potential energy and the maintenance of the general circulation," *Tellus* **7**, 157.
- Lorenz, E. N., 1960, "Maximum simplification of the dynamic equations," *Tellus* **12**, 243.
- Lorenz, E. N., 1963, "Deterministic nonperiodic flow," *J. Atmos. Sci.* **20**, 130.
- Lorenz, E. N., 1967, *The Nature and Theory of the General Circulation of the Atmosphere*, WMO Publication No. 218, T.P. 115 (World Meteorological Organization, Geneva, Switzerland).
- Lorenz, E. N., 1968, "Climatic determinism," *Meteorol. Monogr.* **8**, No. 30, 1.
- Lorenz, E. N., 1969, "The predictability of a flow which possesses many scales of motion," *Tellus* **21**, 289.
- Manabe, S., 1969, "Climate and the ocean circulation: 2. The atmospheric circulation and the effect of heat transfer by ocean currents," *Mon. Weather Rev.* **97**, 775.
- Manabe, S., 1983, "Carbon dioxide and climatic change," in *Theory of Climate*, edited by B. Saltzman, Adv. Geophys. (Academic, New York), Vol. 25, p. 39.
- Manabe, S., K. Bryan, and M. J. Spelman, 1979, "A global ocean-atmosphere climate model with seasonal variation for future studies of climate sensitivity," *Dynamics Atmos. Oceans* **3**, 393.
- Manabe, S., and D. G. Hahn, 1977, "Simulation of the tropical climate of an ice age," *J. Geophys. Res.* **82**, 3889.
- Manabe, S., and J. L. Holloway, Jr., 1975, "The seasonal variation of the hydrological cycle as simulated by a global model of the atmosphere," *J. Geophys. Res.* **80**, 1617.
- Manabe, S., J. Smagorinsky, J. L. Holloway, and H. M. Stone, 1970, "Simulated climatology of a general circulation model with a hydrological cycle. 3. Effects of increased horizontal computational resolution," *Mon. Weather Rev.* **98**, 175.
- Manabe, S., J. Smagorinsky, and R. F. Strickler, 1965, "Simulated climatology of a general circulation model with a hydrological cycle," *Mon. Weather Rev.* **93**, 769.
- Manabe, S., and R. F. Strickler, 1964, "Thermal equilibrium of the atmosphere with a convective adjustment," *J. Atmos. Sci.* **21**, 361.
- Manabe, S., and T. Terpstra, 1974, "The effects of mountains on the general circulation of the atmosphere as identified by numerical experiments," *J. Atmos. Sci.* **31**, 3.
- Manabe, S., and R. T. Wetherald, 1967, "Thermal equilibrium of the atmosphere with a given distribution of relative humidity," *J. Atmos. Sci.* **24**, 241.
- Manabe, S., and R. T. Wetherald, 1975, "The effects of doubling the CO<sub>2</sub> concentration on the climate of a general circulation model," *J. Atmos. Sci.* **32**, 3.
- Margules, M., 1903, Über die Energie der Stürme, *Jahresber. Zentralanst. Meteor.* **40**, 1-26 *The Mechanics of the Earth's Atmosphere* [translated by C. Abbe (1910), *Smithson. Misc. Collect.* **51**, 553].
- Milankovitch, M., 1941, *Kanon der Erdbestrahlung und seine Anwendung am Eiszeit* [History of radiation on the earth and its use for the problem of the ice ages]. K. Serb. Akad. Beogr. Spec. Publ. 132 (translated by the Israel Program for Scientific Translation, Jerusalem, 1969).
- Mintz, Y., 1965, "Very long-term global integration of the primitive equations of atmospheric motion (an experiment in climate simulation)," W. M. O. Tech. Notes, No. 66, 119 [and *Am. Met. Soc. Meteorol. Monogr.* **8**, No. 30, 20 (1968)].
- Mitchell, J. M., 1976, "An overview of climatic variability and its causal mechanisms," *Quat. Res.* **6**, 481.
- Miyakoda, K., T. Gordon, R. Caverly, W. Stern, and J. Sirutis, 1983, "Simulation of a blocking event in January 1977," *Mon. Weather Rev.* **11**, 846.
- Miyakoda, K., G. D. Hembree, R. F. Strickler, and I. Shulman, 1972, "Cumulative results of extended forecast experiments. I. Model performance for winter cases," *Mon. Weather Rev.* **100**, 836.
- Monin, A. S., 1972, *Weather forecasting as a problem in physics* (MIT, Cambridge, Mass.).
- Namias, J., 1983, *Short Period Climatic Variations*, Collected Works of J. Namias 1975 through 1982 (University of California, San Diego), Vol. III.
- National Academy of Sciences, 1975, *Understanding Climatic Change: A Program for Action* (National Academy of Sciences, Washington, D.C.).
- National Academy of Sciences, Climate Research Board, 1979,



- Carbon dioxide and climate: a scientific assessment (National Academy of Sciences, Washington, D.C.).
- National Academy of Sciences, Climate Research Board, 1982, Carbon dioxide and climate: a second assessment (National Academy of Sciences, Washington, D.C.).
- Newton, C. W., 1971, "Mountain torques in the global angular momentum balance," *J. Atmos. Sci.* **28**, 623.
- North, G. R., R. F. Cahalan, and J. A. Coakley, Jr., 1981, "Energy-balance climate models," *Rev. Geophys. Space Phys.* **19**, 91.
- Oort, A. H., 1978, "Adequacy of the rawinsonde network for global circulation studies tested through numerical model output," *Mon. Weather Rev.* **106**, 174.
- Oort, A. H., 1983, *Global Atmospheric Circulation Statistics, 1958–1973*, NOAA Professional Paper No. 14 (U.S. GPO, Washington, D.C.).
- Oort, A. H., and J. P. Peixóto, 1983, "Global angular momentum and energy balance requirements from observations," in *Theory of Climate*, edited by B. Saltzman, Adv. Geophys. (Academic, New York), Vol. 25, p. 355.
- Oort, A. H., and E. M. Rasmusson, 1971, *Atmospheric Circulation Statistics*, NOAA Professional Paper 5 (U.S. GPO, Washington, D.C.).
- Oort, A. H., and T. H. Vonder Haar, 1976, "On the observed annual cycle in the ocean-atmosphere heat balance over the Northern Hemisphere," *J. Phys. Ocean* **6**, 781.
- Pan, Y. H., and A. H. Oort, 1983, "Global climate variations connected with sea surface temperature anomalies in the equatorial Pacific Ocean for the 1963–1973 period," *Mon. Weather Rev.* **111**, 1244.
- Peixóto, J. P., 1977, "Dinâmica do Clima" ["Dynamics of climate"], *Mem. Acad. Ciênc. Lisboa, Cl. Ciênc.* **22**, 195.
- Peixóto, J. P., and A. H. Oort, 1974, "The annual distribution of atmospheric energy on a planetary scale," *J. Geophys. Res.* **79**, 2149.
- Peixóto, J. P., and A. H. Oort, 1983, The atmospheric branch of the hydrological cycle and climate, in *Variations of the global water budget* (Reidel, London), p. 5.
- Philander, G. S., 1983, "El Niño Southern Oscillation phenomena," *Nature* **302**, 295.
- Phillips, N. A., 1956, "The general circulation of the atmosphere: A numerical experiment," *Q. J. R. Meteorol. Soc.* **82**, 123.
- Ramanathan, V., and J. A. Coakley, Jr., 1978, "Climate modeling through radiative-convective models," *Rev. Geophys. Space Phys.* **16**, 465.
- Rasmusson, E. M., and T. H. Carpenter, 1982, "Variations in tropical sea surface temperature and surface wind fields associated with the Southern Oscillation/El Niño," *Mon. Weather Rev.* **110**, 354.
- Rasmusson, E. M., and J. M. Wallace, 1983, "Meteorological aspects of the El Niño/Southern Oscillation," *Science* **222**, 1195.
- Richtmeyer, R. D., and K. W. Morton, 1967, *Difference Methods for Initial-Value Problems*, 2nd ed. (Interscience, New York).
- Rosen, R. D., and D. A. Salstein, 1983, "Variations in atmospheric angular momentum on global and regional scales, and the length of day," *J. Geophys. Res.* **88**, 5451.
- Saltzman, B., 1968, "Steady state solutions for axially-symmetric climatic variables," *Pure Appl. Geophys.* **69**, 237.
- Saltzman, B., 1977, "Global mass and energy requirements for glacial oscillations and their implications for mean ocean temperature oscillations," *Tellus* **29**, 205.
- Saltzman, B., 1978, "A survey of statistical-dynamical models of the terrestrial climate," *Adv. Geophys.* **20**, 183.
- Saltzman, B., and A. D. Vernekar, 1975, "A solution for the Northern Hemisphere climatic zonation during a glacial maximum," *Quat. Res.* **5**, 307.
- Schneider, S. H., and R. E. Dickinson, 1974, "Climate modeling," *Rev. Geophys. Space Phys.* **12**, 447.
- Sellers, W. D., 1969, "A global climate model based on the energy balance of the earth-atmosphere system," *J. Appl. Met.* **8**, 396.
- Shukla, J., and Y. Mintz, 1982, "Influence of land-surface evapotranspiration on the earth's climate," *Science* **215**, 1498.
- Smagorinsky, J., 1963, "General circulation experiments with the primitive equations. 1. The basic experiment," *Mon. Weather Rev.* **91**, 99.
- Smagorinsky, J., 1970, "Numerical simulation of the global atmosphere," in *The Global Circulation of the Atmosphere*, edited by G. A. Corby (Royal Meteorological Society, London), p. 24.
- Smagorinsky, J., 1974, "Global atmospheric modeling and the numerical simulation of climate," in *Weather and Climate Modification*, edited by W. N. Hess (Wiley, New York), p. 633.
- Smagorinsky, J., 1983, "The beginnings of numerical weather prediction and general circulation modeling: Early recollections," in *Theory of Climate*, edited by B. Saltzman, Adv. Geophys. (Academic, New York), Vol. 25, p. 3.
- Smagorinsky, J., S. Manabe, and J. L. Holloway, 1965, "Numerical results from a nine-level general circulation model of the atmosphere," *Mon. Weather Rev.* **93**, 727.
- Smith, E. A., T. H. Vonder Haar, J. R. Hickey, and R. Maschhoff, 1983, "The nature of the short-period fluctuations in solar irradiance received by the earth," *Climatic Change* **5**, 211.
- Starr, V. P., 1948, "An essay on the general circulation of the earth's atmosphere," *J. Meteorol.* **5**, 39.
- Starr, V. P., 1951, "Applications of Energy Principles to the General Circulation" in *Compendium of Meteorology* (American Meteorological Society, Boston, Mass.), p. 568.
- Starr, V. P., 1953, "Note concerning the nature of the large-scale eddies in the atmosphere," *Tellus* **5**, 494.
- Starr, V. P., 1968, *Physics of Negative Viscosity Phenomena* (McGraw-Hill, New York).
- Starr, V. P., and J. P. Peixóto, 1958, "On the global balance of water vapor and the hydrology of deserts," *Tellus* **10**, 189.
- Stommel, H., 1960, *The Gulf Stream: A physical and dynamical description* (University of California, Berkeley).
- Stone, P. H., 1974, "The meridional variation of the eddy heat fluxes by baroclinic waves and their parameterization," *J. Atmos. Sci.* **31**, 444.
- Sutera, A., 1981, "On stochastic perturbation and long-term climate behaviour," *Q. J. R. Meteorol. Soc.* **107**, 137.
- Sverdrup, H. U., M. W. Johnson, and R. H. Fleming, 1962, *The Oceans; their physics, chemistry and general biology*, 11th printing (Prentice Hall, Englewood Cliffs).
- Trenberth, K. E., 1981, "Seasonal variations in global sea level pressure and the total mass of the atmosphere," *J. Geophys. Res.* **86**, 5238.
- van Loon, H., and J. C. Rogers, 1978, "The seasaw in winter temperature between Greenland and Northern Europe. Part I: General description," *Mon. Weather Rev.* **106**, 296.
- Vinnichenko, N. K., 1970, "The kinetic energy spectrum in the free atmosphere—1 second to 5 years," *Tellus* **22**, 158.
- von Neuman, J., 1960, "Some remarks on the problem of forecasting climatic fluctuations," in *Dynamics of Climate*, edited by R. L. Pfeffer (Pergamon, New York), p. 9.



- Walker, G. T., and E. W. Bliss, 1932, "World Weather V," *Mem. R. Meteorol. Soc.* **4**, 53.
- Walker, G. T., and E. W. Bliss, 1937, "World Weather VI," *Mem. R. Meteorol. Soc.* **4**, 119.
- Wallace, J. M., and D. S. Gutzler, 1981, "Teleconnections in the geopotential height field during the Northern Hemisphere winter," *Mon. Weather Rev.* **109**, 784.
- Wetherald, R. T., and S. Manabe, 1975, "The effects of changing the solar constant on the climate of a general circulation model," *J. Atmos. Sci.* **32**, 2044.
- Williams, G. P., and J. L. Holloway, Jr., 1982, "The range and unity of planetary circulations," *Nature* **297**, 295.
- Wyrтки, K., 1982, "The Southern Oscillation, ocean-atmosphere interaction and El Niño," *Mar. Technol. Soc. J.* **16**, 3.

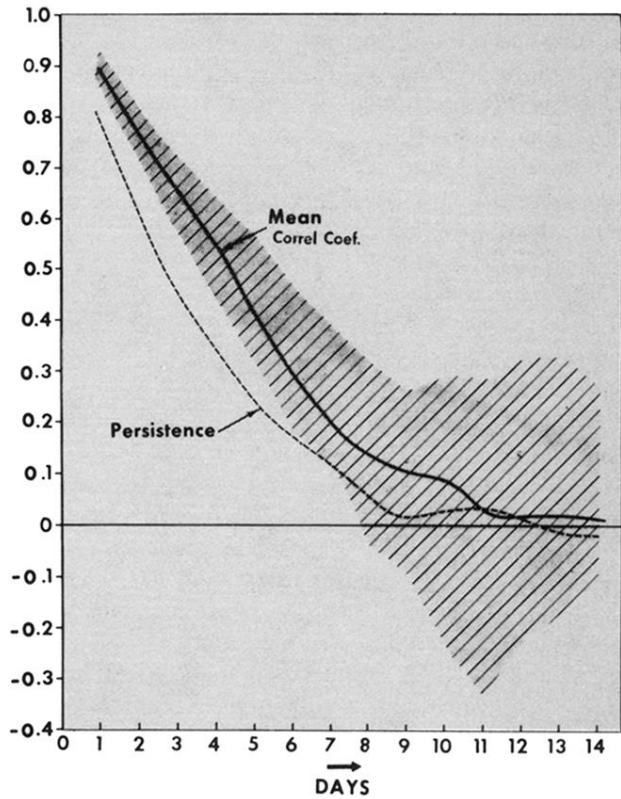


FIG. 50. An example of the predictive skill in numerical weather prediction. Plot of the decrease of the correlation coefficient in time between predicted and observed 500-mbars geopotential height anomalies for the mean of 12 winter cases from Miyakoda *et al.* (1972). The correlation coefficients were computed using all grid point values in the northern hemisphere. The shaded area shows the range for the individual winters. For comparison, the persistence curve (dashed) indicates the no-skill forecast. No skill is shown after about one week.

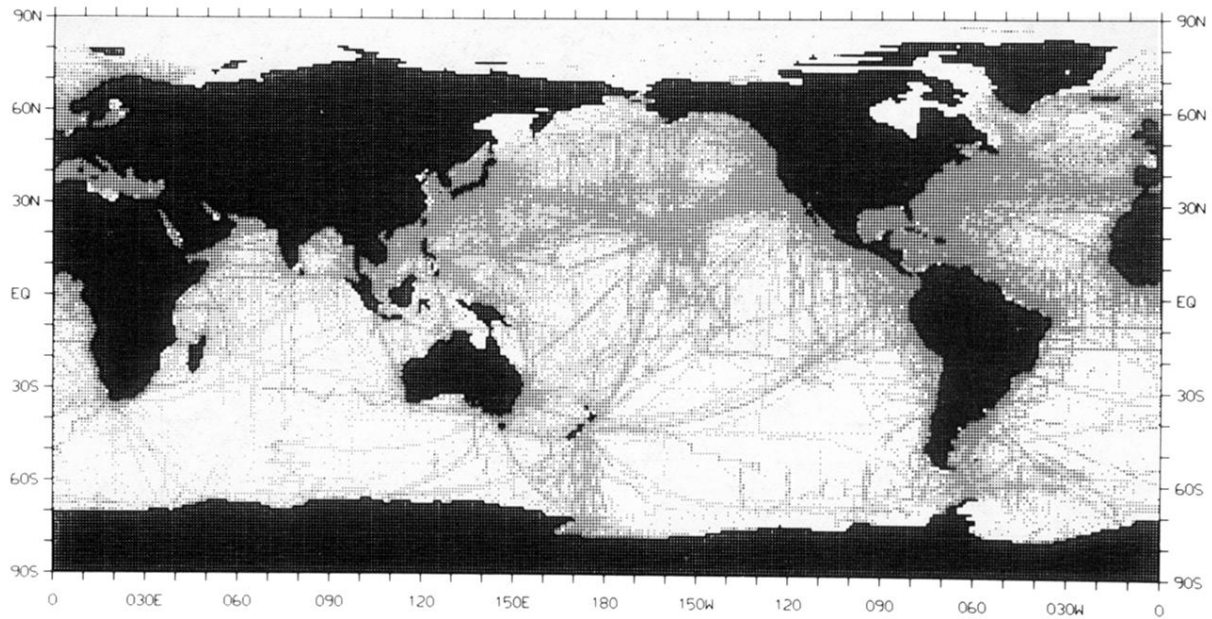


FIG. 9. Network of subsurface ocean data. Shown are those  $1^\circ$  latitude  $\times$   $1^\circ$  longitude squares that contain any historical temperature data taken by oceanographic research vessels during the 3-month period February to April, irrespective of year. A small dot indicates that a square contains 1–4 observations, and a large dot that it contains 5 or more observations (Levitus, 1982).